# TOWARDS THE UNBOUND STELLAR POPULATION IN THE SLOAN DIGITAL SKY SURVEY

By

Lauren Elizabeth Campbell

Dissertation

Submitted to the Faculty of the

Graduate School of Vanderbilt University

in partial fulfillment of the requirements

for the degree of

DOCTOR OF PHILOSOPHY

in

Physics

May 2015

Nashville, Tennessee

Approved:

Dr. Kelly Holley-Bockelmann

Dr. Andreas Berlind

Dr. David A. Weintraub

Dr. David Ernst

Dr. Shane Hutson

*To my family.*

## Table of Contents

# List of Tables

Table Page

## List of Figures

# Chapter I

# INTRODUCTION

In this dissertation, I present my work to identify and understand the unbound stellar population within our Milky Way using data from the Sloan Digital Sky Survey. This investigation is a single facet in the broader field of Galactic structure research. As I will elaborate on in this document, this unique population can help us understand the dynamics and stellar content of the Galactic center, the mass of the dark matter halo, and the evolution of the Milky Way.

The study of Galactic structure isn't simply compiling a map of the different components that comprise the Milky Way. While this is important in itself, it is only the first stepping stone to creating a complete understanding of galaxy formation, star formation, and the distribution of dark matter through the Universe (Rockosi et al., 2009). Studying the density, kinematics, and chemistry of stars and their preferred locations within the Galaxy introduces new possibilities for understanding the formation and evolutionary histories therein (e.g., Freeman & Bland-Hawthorn, 2002; Rockosi et al., 2009; Schönrich & Binney, 2009).

To place this work in the context of Galactic Astronomy, I need to first provide some background information. It is the goal of this chapter to paint a picture of our current understanding of the structure of the Milky Way and how that view has changed over time. To that end, I will begin, in Section 1.1, with a description of Galactic structure as it was roughly 20 years ago and then move to a presentation of our current perception in Section 1.2. In Section 1.3, I will discuss the Sloan Digital Sky Survey and how it has had a tremendous impact on our understanding of Milky Way structure. Finally, in Section 1.4, I will discuss ways in which understanding the unbound stellar population can provide further insight into the larger context of Galactic structure, formation, and evolution.

## 1.1 Historical Perspectives on Galactic Structure

Astronomical studies focusing on the evolutionary history of the Milky Way only became feasible during the 1950's when theoretical and observational advances were finally able to join structure, kinematics, chemistry, and age into a single context (Majewski, 1993). The first development linking these parameters into a single model of the Milky Way, and perhaps the most influential, came in the form of the Eggen, Lynden-Bell, and Sandage model, discussed in detail in Section 1.1.1 below (Eggen et al., 1962; Majewski, 1993). A very simplified view of the Milky Way consists of a bulge and disk surrounded by a diffuse halo. The following sections will elaborate on this picture.

### 1.1.1 Stellar Halo

Before the 1990's the Milky Way halo was believed to be spheroidal, slowly rotating, and comprised of metal weak[1] stars, $[Fe/H] < -1$ (Freeman, 1987). Its rotational velocity,

[1]The metallicity of stars, typically denoted as [Fe/H], is a measurement of the amount of heavy metals (that is, heavier than Helium) in a star's composition. Metallicity is reported with respect to that of our Sun. Therefore, stars are described as either having more (metal rich) or less (metal poor or weak) metals than the Sun. Metallicity is also a signature of age as higher metallicity implies a star was formed more recently.

$v_{rot}$, was measured to be roughly 40 km/s, with a velocity dispersion[2] of $\sigma \sim 100$ km/s (Freeman, 1987). This halo follows an $r^{-3.5}$ density profile (Freeman, 1987).

The globular clusters that are found in the halo are also metal weak with $[Fe/H] < -1$, and with similar velocities, $v_{rot} \sim 50$ km/s and $\sigma \sim 110$ km/s, to that of the halo (Freeman, 1987). In addition, about 30 globular clusters were known to lie on retrograde orbits with $v_{rot} \sim -70$ km/s (Freeman, 1987).

Globular clusters are believed to be some of the oldest objects in the Universe, and therefore provide an ideal test-bed for the earliest stages of galaxy formation (e.g., Binney & Merrifield, 1998; Freeman & Bland-Hawthorn, 2002). Figure 1.1 shows the color-magnitude diagram of the nearby globular cluster 47 Tuc. The sharp knee at a magnitude[3] of $\sim 17$ indicates the age of the cluster since the more luminous stars have evolved off the main sequence[4]. Because these clusters are the oldest observable stellar objects, they provide a lower limit on the age of the Universe and the timescale over which galaxies form.

The Eggen Lynden-Bell and Sandage (ELS) model of 1962 (Eggen et al., 1962) describes the formation of our Galaxy from a protogalactic cloud of intergalactic material. To summarize, a large cloud of rotating gas, about 100 kpc[5] in radius, began its collapse roughly $10^{10}$ years ago. From the collapsing gas the first stars formed into globular clusters, and as the material continued to collapse more stars formed in a rotating, thin disk.

[2]Velocity dispersion refers to the range of velocities about the mean. Therefore, a small velocity dispersion means all stars in the system have roughly the same velocity.

[3]Magnitude is a measure of brightness. Greater magnitude values correspond to fainter objects, and likewise smaller values correspond to brighter objects.

[4]The main sequence is a feature on color-magnitude diagrams running diagonally from bright and blue to faint and red. Stars that are fusing Hydrogen into Helium in their cores live along the main sequence.

[5]1 kpc $= 3 \times 10^{19}$ m.

After time enough for the first O and B type stars[6] to fuse their core gas into heavier elements and undergo supernovae eruptions that would enrich the remaining gas at the end of their lifetimes, a second generation of stars began forming in the disk of the Galaxy (Eggen et al., 1962).

This model was theorized in order to explain correlations between ultraviolet (UV) excess[7] and 1) orbital eccentricity, 2) W velocity (perpendicular to the plane of the Galaxy), or $z_{max}$ (height above or below the plane), and 3) angular momentum in a sample 221 dwarf stars in the solar neighborhood (Eggen et al., 1962; Majewski, 1993). Ultraviolet excess is a signature of very old, metal poor stars. A correlation between this and any other stellar property may provide information about how these stars, and therefore the Galaxy, formed.

The first correlation, between UV excess and orbital eccentricity, is shown here in the top-left panel of Figure 1.2. This figure shows stars with large UV excess have highly eccentric orbits although stars exhibiting less UV excess live in nearly circular orbits (Eggen et al., 1962).

The second correlation is between UV excess and maximum distance above or below the plane of the disk, $z_{max}$. Stars with little UV excess remain in or near the plane of the disk. However, stars with high UV excess have a wider variety of $z_{max}$ values, ranging from 0 to 10 kpc, shown in the top right panel of Figure 1.2. These two correlations,

[6] The spectral classification of stars follows the sequence: OBAFGKM. In general, the most massive, hottest, and bluest stars are denoted as O-type and transition down to the least massive, coolest, reddest M-type stars.

[7] The UV excess, $\delta(U-B)$, of a star is measured in the ultraviolet-blue wavelengths of a star's spectrum. It manifests itself in very metal poor stars that have few elemental absorption features in this region of the spectrum resulting in excess emission.

together, suggest that there is also a correlation between UV excess and the age of the stars– more UV excess in older stars, less UV excess in younger stars (Eggen et al., 1962).

Finally, the third correlation, between UV excess and angular momentum, shown in the bottom panel of Figure 1.2, suggests that older stars with more UV excess have smaller angular momenta than the stars with less UV excess (Eggen et al., 1962).

The combined results of these data leads to a concise description of the first stars in the Galaxy. These stars tend to live on highly eccentric orbits, can be observed at a wide range of heights above and below the plane, and generally have low angular momenta (Eggen et al., 1962). This new information made possible a complete theory of Galactic formation that describes how these stars came to have their observed properties.

In this model, the Galaxy forms from a smooth, hot cloud of rotating gas. As the gas begins to cool and collapse, stars begin forming in globular clusters. Then, with continued cooling, the remaining gas begins rotating faster to conserve angular momentum and collapses into a flat disk and central spheroidal component. Therefore, the stars formed during collapse have highly eccentric orbits, although the stars formed from the gas in the disk have more circular orbits. As those stars enrich the interstellar medium at the end of their lifetimes, the newly formed, younger stars will exhibit higher metallicities and lower UV excesses.

The stars used in this study were primarily chosen to be nearby, solar neighborhood, stars due to their high proper motions. Therefore, this sample, and this model, neglects metal poor stars on low eccentricity orbits (Majewski, 1993; Bond, 1970). Also, the ELS model neither accounts for nor explains the number of retrograde orbits seen in the halo of the Galaxy (e.g., Majewski, 1993; Larson, 1969; Yoshii & Saio, 1979). The ELS model was first challenged by Searle & Zinn in 1978 who noted a range in metal abundances in globular clusters independent of distances from the Galactic Center (Searle & Zinn, 1978) and suggested that the halo was built over an extended period of time from $\sim 10^8 M_\odot$ independent fragments (Searle & Zinn, 1978; Freeman & Bland-Hawthorn, 2002).

The subsequent Yoshii & Saio model (Yoshii & Saio, 1979) incorporated low metallicity, low eccentricity stars and retrograde orbits by allowing a slower collapse of a clumpy protogalaxy (e.g., Majewski, 1993; von Weizsäcker, 1951; Oort, 1958) over several gigayears. This model lends itself easily to the (perhaps, preferred) notion of a possible tumultuous Galactic evolution due to a series of hierarchical mergers (e.g., Majewski, 1993; Tinsley & Larson, 1979).

### 1.1.2 Disk

The Galactic disk is flat, rotating at 220 km/s with $\sigma \sim 20$ km/s, and comprised of the majority ($6 \times 10^{10} M_\odot$) of the stellar mass (Freeman, 1987). The disk also contains relatively high metallicity stars, with $[Fe/H] > -0.5$ (Freeman, 1987). It has an overall scale height 300-350 kpc and scale length 3.5-5.5 kpc (Freeman, 1987). A spiral arm pattern was also discovered in the Milky Way in the early 1960's. There are at least 4 arms beyond 3 kpc from the Galactic center, and each is roughly 2 kpc from the next (Rougoor & Oort, 1960). In addition, there is a thin layer of Hydrogen gas also rotating at roughly 220 km/s (Rougoor & Oort, 1960). This disk of gas is also known to "warp" at the edges, rising roughly 700 kpc above the Galactic plane on one side and similarly below the plane on the opposite side (Rougoor & Oort, 1960).

It was well known that the scale height of the disk varied with stellar population

(Mihalas & Binney, 1981). For example, young O and B stars lie very near the plane within $\sim 50$ pc, interstellar gas and dust have a scale height $\sim 100$ pc, and old M stars and white dwarfs have scale heights $\sim 500 - 1000$ pc (Mihalas & Binney, 1981).

In 1983 Gilmore & Reid used the photometric parallax of a sample of 12,500 stars complete to an I-band (near-infrared) magnitude of 18, and all within $\sim$18 degrees of the South Galactic Pole. With these data they applied exponential fits of varying scale heights.

They show, in Figure 1.3, the spatial density of two subsamples of their stars (in the magnitude range $4 \leq M_V \leq 5$ and in the range $5 < M_V \leq 6$, correlating to F-G type stars and G-K type stars, respectively) as a function of distance from the galactic plane. The solid line depicts an exponential decrease with a scale height of 300 pc. This single exponential no longer fits at distances greater than 1000 pc. Therefore, they fit a second exponential, the dashed line, for stars with $z > 1$ kpc, corresponding to a scale height of $\sim 1500$ kpc for both subsamples of stars (Gilmore & Reid, 1983; Freeman, 1987). Thus, Gilmore & Reid introduced an additional "thick disk" component, convincingly unique from the thin disk population, to the existing two-component, bulge-disk, model of the Milky Way.

They propose an explanation for this apparently distinct population of thick disk stars, comprising only $\sim$2% of the stars in the solar neighborhood, $\sim 10^9 M_\odot$, as being Galactic bulge stars that have felt the gravitational pull of the massive thin disk. This is largely due to the chemical similarities this population of stars has with the spheroidal component of our Galaxy (Gilmore & Reid, 1983).

This led to many models describing the formation of this "thick disk" population, also referred to as “extended disk,” “high velocity disk,” or “flattened spheroid” depending on the preferred formation criteria (Majewski, 1993). These thick disk models tend to fall into one of two camps– “top down” or pre-thin disk, or “bottom up” or post-thin disk (Majewski, 1993).

The “top down” models form the thick disk population prior to the formation of the thin disk (Majewski, 1993). In these pre-thin disk models the thick disk is often treated as a transitionary stage between the collapse of the halo and the formation of the thin disk (e.g., Majewski, 1993; Larson, 1976; Gilmore, 1984)

The “bottom up” models typically involve some interaction or evolution of the thin disk that results in the formation of the thick disk (Majewski, 1993). These models draw from the idea that processes that can increase the velocity dispersion of, or kinematically heat, the thin disk stars may contribute to the formation of a thick disk population that is smoothly linked to the thin disk (e.g., Majewski, 1993). Thus, we would expect to see gradients in age, metallicity, and kinematics within the disks, as older, metal poor stars would have undergone more heating events. Three main heating mechanisms considered in these post-thin disk models include 1) interactions with $\sim 10^6 M_\odot$ molecular clouds, 2) disk instabilities such as spiral arms, and 3) interactions with fast moving, massive objects like dwarf galaxies or supermassive black holes (Majewski, 1993).

The thick disk component contains stars with $[Fe/H] < -1$, and has a velocity dispersion roughly double that of the thin disk, $\sim 40$ km/s (Freeman, 1987).

### 1.1.3 Bulge

The central region of the Galaxy is comprised of a spheroidal stellar bulge. These stars are metal rich with $[Fe/H] > -1$ and rotate at $\sim 200$ km/s (Freeman, 1987; Rougoor & Oort, 1960). The bulge is slightly elongated and has a radius about 2.5 kpc (Freeman, 1987).

The idea of a central bar was first introduced in the early 1960's based on observations of non-circular stellar motions near the center of the Galaxy (Rougoor & Oort, 1960; de Vaucouleurs, 1964). It was suggested to be roughly 3 kpc in radius and oriented at about 30° from our line-of-sight (Rougoor & Oort, 1960; de Vaucouleurs, 1964). However, the bar wasn't studied in detail until the 1990's, and therefore refer to Section 1.2.1 for a more detailed discussion of its properties.

At this point, the generally adopted idea of what components make up our Galaxy can be described by the schematic shown in Figure 1.4. This cartoon representation shows a large dark halo extending out to about 100 kpc, in black, and smaller stellar halo, in yellow, each with the old, metal poor globular clusters distributed throughout, marked by the filled reddish dots. It also shows a thin disk, light blue, surrounded by a puffy thick disk, dark blue, with radii about 15 kpc. Finally, in the center of the Galaxy is a stellar bulge, shown in yellow (Freeman & Bland-Hawthorn, 2002).

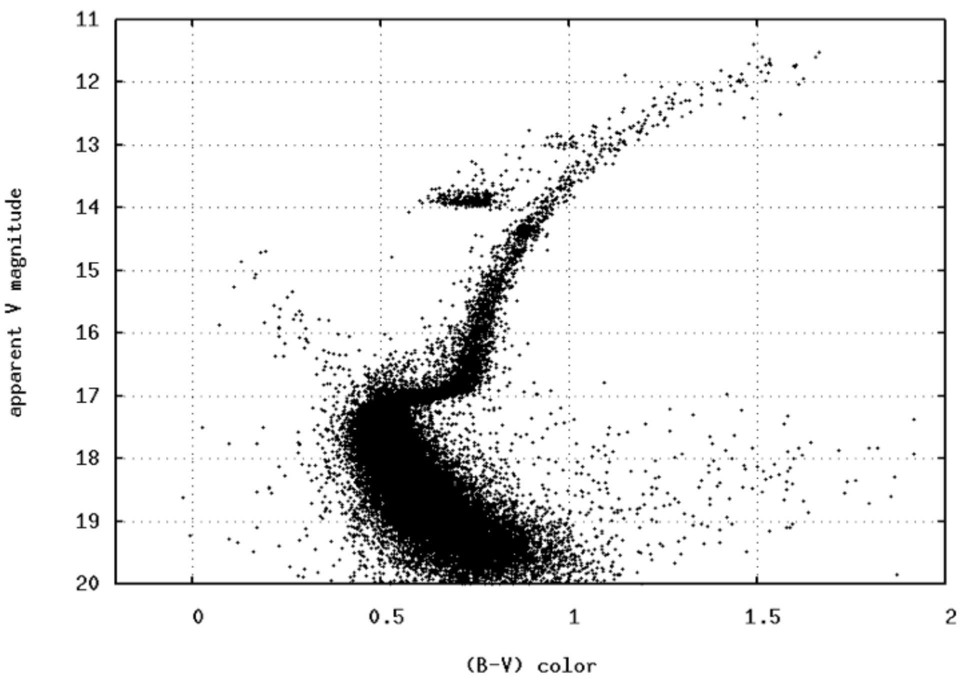


Figure 1.1: The color magnitude diagram of globular cluster 47 Tuc. The location of the knee directly corresponds to the age of the cluster, estimated to be approximately 12 Gyr. (Image courtesy of Michael Richmond at http://spiff.rit.edu/classes/phys301/lectures/mw_size/mw_size.html.)

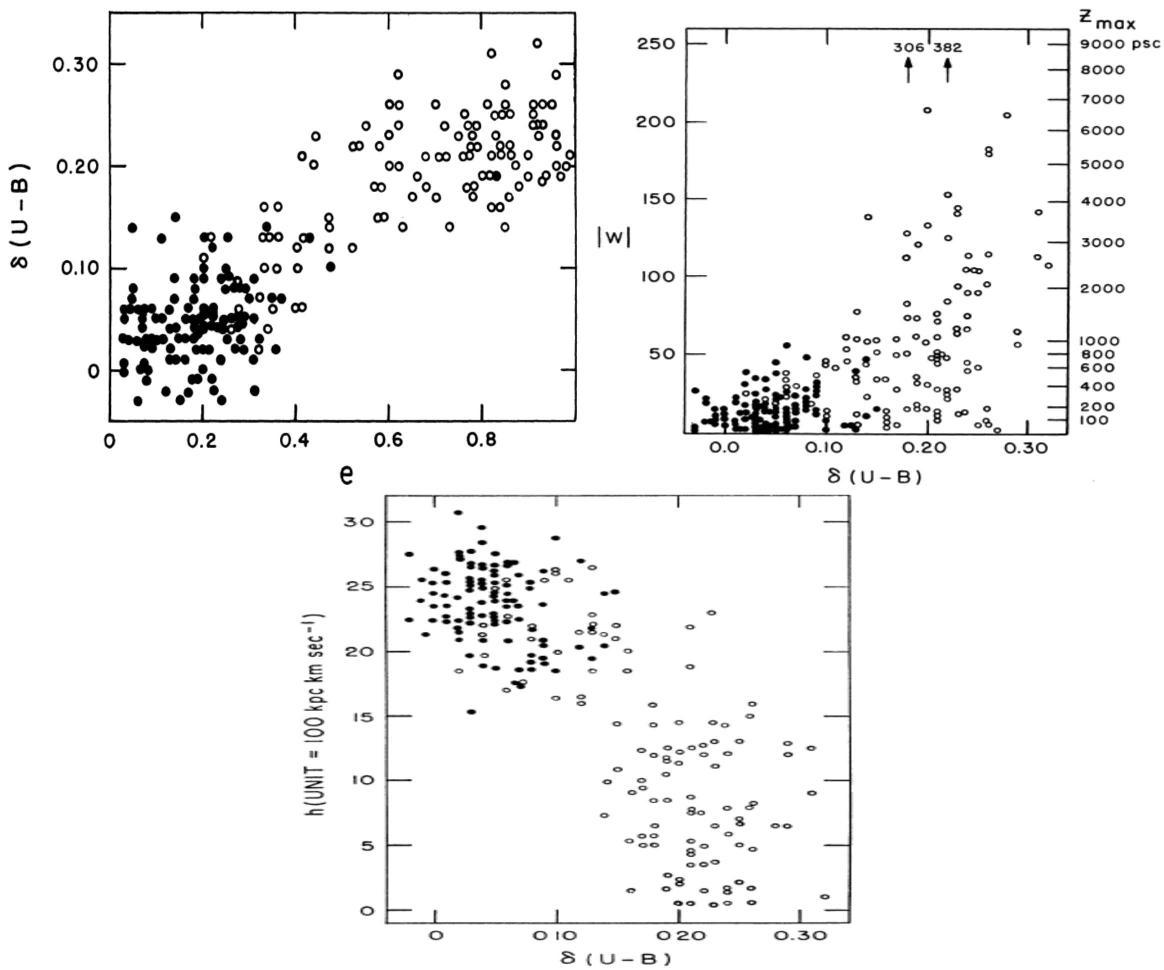


Figure 1.2: Top left: Ultraviolet excess as a function of orbital eccentricity. This shows stars with a greater UV excess tend to live on highly eccentric orbits, whereas stars with less UV emission have more circular orbits. Top right: W velocity as a function of UV excess. Also plotted on the right-hand vertical axis is $Z_{max}$ above the plane. Stars with greater UV excess exhibit a much larger range of possible W and $Z_{max}$ values. Bottom: Angular momentum as a function of UV excess, showing stars with more UV excess have little or no angular momentum. (Eggen et al., 1962)

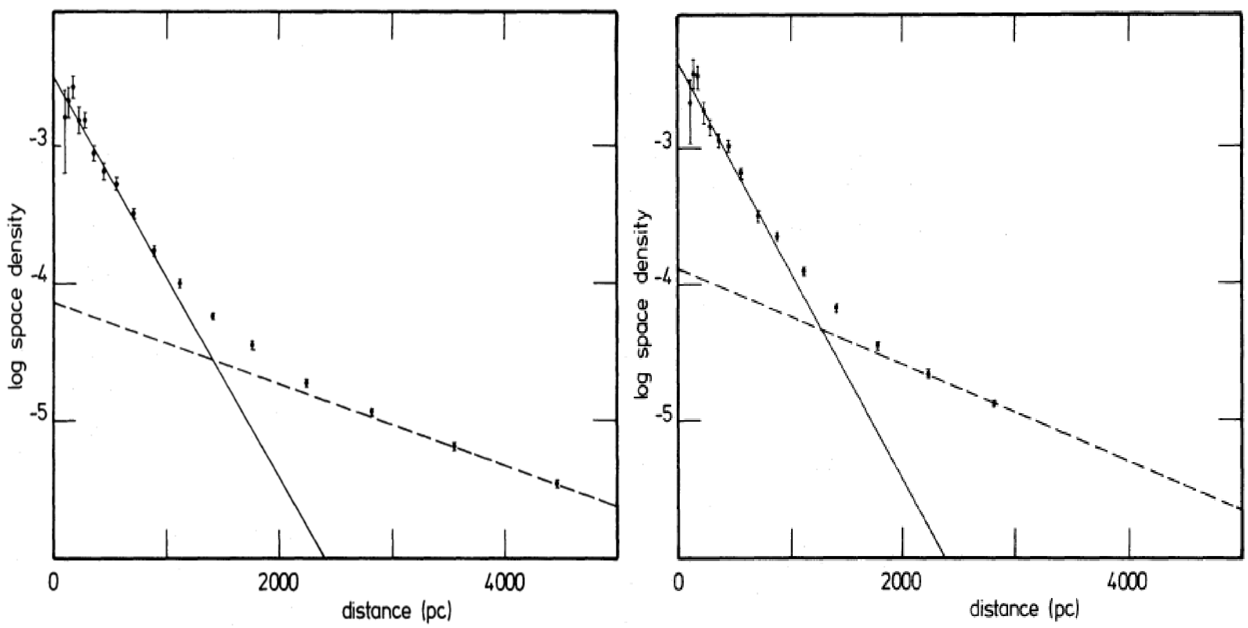


Figure 1.3: Left: The spatial density of stars as a function of distance away from the plane for a subsample of stars with $4 \leq M_V \leq 5$ (late F- to early G-type stars). The straight lines represent exponential fits to the data. A single exponential no longer fits at distances greater than about 1.5 kpc introducing the need for a second disk component. Right: Same as left, but for a subsample of stars with $5 < M_V \leq 6$ (late G- to early K-type stars). (Gilmore & Reid, 1983)

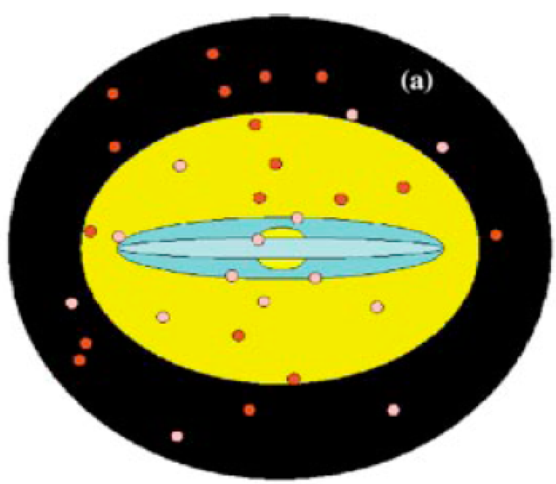


Figure 1.4: A cartoon depicting the major components of the Milky Way. The bulge is shown by the central circle in yellow. The thin disk is in light blue and the thick disk around it is shown in darker blue. Surrounding the bulge and disks is the stellar halo in yellow. Finally, the dark halo is shown in black and the globular clusters by filled circles. (Freeman & Bland-Hawthorn, 2002)

## 1.2 Current View of Galactic Structure

### 1.2.1 Bulge and Supermassive Black Hole

Although a bar in the central region of the Milky Way was first introduced in the 1960's (Rougoor & Oort, 1960; de Vaucouleurs, 1964) with the discovery of non-circular motions in the center of the Galaxy, it wasn't until the early 1990's that it became generally established that the Milky Way is a barred spiral. The existence of a central bar has been confirmed by kinematic, photometric, and star count techniques (López-Corredoira et al., 2007; Morris & Serabyn, 1996). Its mass is $\sim 10^{10} M\odot$, extends roughly $\sim 5$ kpc from the center, rotates at about 200 km/s, and is misaligned with our line-of-sight to the Galactic center at an angle of $\sim 45°$ (López-Corredoira et al., 2007; Morris & Serabyn, 1996; Rougoor & Oort, 1960).

Recently, new constraints have been made on the properties of the supermassive black hole at the center of the Galaxy. This is largely due to new precision radial velocity measurements of the high velocity stars very near the black hole (Ghez et al., 2008). Ghez et al. (2008) determined the distance to the black hole is $8.0 \pm 0.6$ kpc, the mass is $4.1 \pm 0.6 \times 10^6 M\odot$, and a radial velocity consistent with zero.

The central parsec around the supermassive black hole is an important region of interest. In particular, the central density profile may serve as a simple test for the existence of a central black hole (Do et al., 2009). Theory states that as the orbits of stars bring them close to a central black hole, the star is destroyed and its energy is balanced by increasing the density of the central region surrounding the black hole. This results in a "cuspy" density profile, $\sim r^{-7/4}$, although in the absence of a black hole a flat or "cored" density profile is expected, $\sim r^{-1/2}$ (Bahcall & Wolf, 1976; Schödel et al., 2007; Do et al., 2009). However, studies are finding a significant lack of old, low mass, stars near the center of the Galaxy, resulting in a flat, maybe declining, density profile of $\sim r^{-0.3}$ (Do et al., 2009; Bartko et al., 2010; Schödel et al., 2007).

### 1.2.2 Thin & Thick Disks

The existence and current observations of the thick disk can be explained by a number of formation theories. Understanding how the thick disk formed will help to constrain theories of Galactic formation and interaction history.

One possible formation mechanism for the thick disk is through accretion of satellite galaxies. The simulations of Abadi et al. (2003), shown in Figure 1.5, imply that the majority of stars in the thick disk, $\sim 75\%$, are the debris of tidally stripped satellites. This theory suggests that the thick disk formed completely independent from a pre-existing thin disk.

The thick disk may have alternatively formed by the kinematic heating of the thin disk through minor mergers. Villalobos & Helmi (2008) consider this thick disk formation mechanism in their simulations of galaxy mergers. They merge satellites with $\sim 10\%$ of the mass of a host galaxy which already contains a disk, seen in Figure 1.6. From these mergers they find that thick disks form with similar kinematics to what is observed in the Milky Way (Villalobos & Helmi, 2008).

Another possible formation mechanism of the thick disk comes in the form of scattering, or radial migration, of stars due to asymmetric structures in the Galaxy such as the bulge or spiral arms. One study that investigates this theory was performed by Schönrich

& Binney (2009). They used the chemical abundances of solar neighborhood stars and their space motions to evolve their orbits and recover the signatures of both thin and thick disks in the absence of any interactions with external objects (Schönrich & Binney, 2009). A similar study by Bird et al. (2011) simulates the effects of a bar and spiral structure compared to the effects of satellites on radial migration in disk galaxies. Figure 1.7 shows the stellar distribution in the initial disks (top with scale height, $z_d$ = 200 pc, bottom with $z_d$ = 400 pc) on the left, and the stellar distributions after 2.5 Gyr in isolation and in the presence of satellites, center and right panels respectively. Although a bar and noticeable spiral structure forms in the thinner disk, satellite interactions have a much more pronounced effect on the migration of the disk stars (Bird et al., 2011).

A competing theory is that the disks formed *in situ* from a 'clumpy' distribution of material as the result of a major gas rich merger (Bournaud et al., 2007). The simulations of Bournaud et al. (2007) show, in Figure 1.8, in addition to a clumpy primordial galaxy being required to form an exponential disk, the time it takes to form the disk from clumpy material is much shorter than the time it takes spiral arms to disrupt a thin disk into an exponential disk.

Carollo et al. (2010), in addition to providing support for the two-component stellar halo, see Section 1.2.3, proposed an additional metal-weak thick-disk is needed to accurately describe the thick disk stellar population. In this study, they employ the distribution of rotational velocity, $V_\phi$, and fit a minimum number of gaussian curves to sufficiently describe the data. As a result, they claim a metal-weak thick-disk is required with $V_\phi$ of about 100-150 km/s and a peak metallicity $[Fe/H] = -1.3$, compared with the 'regular' thick disk which has $V_\phi$ ~182 km/s and a peak metallicity $[Fe/H] = -0.8$

(Carollo et al., 2010). This result is depicted in Figure 1.9, where the histograms represent the number of stars with a particular rotational velocity, the red curves represent each of the components used in the model, and the blue lines are the sum of all components. The left panel shows the distribution for a subsample of stars 1-2 kpc above the plane in varying metallicity bins. Similarly, the right panel shows stars in a distance slice between 2 kpc and 4 kpc. As shown by this figure, a single component is not sufficient to recover the distribution of observed rotational velocities (Carollo et al., 2010).

In 2011, a new study has challenged the determination of the thick disk scale length, believed to be roughly the same as that of the thin disk, $\sim$ 3 kpc. Bensby et al. (2011) add the metallicity distribution of a sample of 20 outer disk giants, further from the center than the Sun, to a sample of $\sim$ 40 inner disk giants, between the bulge and the Sun. They then compare this to the sample of solar neighborhood stars of Alves-Brito et al. (2010) where they were able to distinguish thin disk from thick disk populations based on their metallicity determinations. What they found is a significant lack of stars with thick disk chemistry at large distances. This can be seen clearly in Figure 1.10, where the left panel shows the 40 inner disk giants, the center shows the solar neighborhood, and the right panel shows the 20 outer disk giants (Bensby et al., 2011). In each of these panels the red and blue lines show the metallicity distributions of the thick and thin disks, respectively, as they were determined from the solar neighborhood sample (Bensby et al., 2011).

A mono-abundance study of the SEGUE G dwarf sample revealed that each sub-population can be described by a single exponential function (Bovy et al., 2012a). This is shown in Figure 1.11, where stellar density is plotted against vertical scale height for sub-populations in bins of metallicity and alpha-abundance; the black line shows the total stellar density. Hence, Bovy et al. (2012a) suggest that "thick disk" stars do not comprise a distinctly separate component from the thin disk. Similarly, Bird et al. (2013) considered mono-age sub-populations in hydrodynamic simulations of Milky Way-like disk galaxies. Figure 1.12 shows the vertical mass density profiles for the mono-age populations in the inner disk, Solar neighborhood, and outer disk, respectively. Each sub-population can be described by a single exponential function. However, the composite of all sub-populations to form the total vertical mass density profile requires a fit by two exponential profiles (Bird et al., 2013)– apparently explaining the origin of the thin disk/thick disk dichotomy.

In summary, there is still much that is undetermined about the Galactic disk despite that it is the dominant stellar component in the solar neighborhood. The idea that there is a "thick disk" in the Milky Way is generally accepted. However, the nature, formation, and even the exact definition of what constitutes the thick disk is the subject of much debate.

### 1.2.3 Stellar Halo

In the previous section, the halo component of the Galaxy refers to a smooth stellar halo hosting low metallicity globular clusters (Eggen et al., 1962). This component only contains ∼1% of the stellar mass, $\sim 10^9 M_\odot$, in the Milky Way and has close to zero angular momentum compared to the disk and bulge components (Morrison, 1993; Freeman, 1987; Freeman & Bland-Hawthorn, 2002). Now, we know this metal poor stellar halo component is riddled with substructure, and it is believed that it formed, in part, from the accretion of small, somewhat evolved, metal poor satellite galaxies (Searle & Zinn, 1978; Freeman & Bland-Hawthorn, 2002).

Carollo et al. (2007, 2010) added to the substructure of the halo by providing strong evidence for a two-component stellar halo– an inner halo and an outer halo shown in Figure 1.13. These two halos differ kinematically, chemically, and in spatial density suggesting that they formed from entirely different mechanisms. (Carollo et al., 2007, 2010).

The inner halo exhibits a small net prograde rotation of 0 to 50 km/s, large orbital eccentricities, a metallicity peak at $[Fe/H] = -1.6$, and dominates up to distances of about 15 kpc. The outer halo, on the other hand, shows a net retrograde motion of $-40$ to $-70$ km/s, low eccentricities, a peak metallicity around $[Fe/H] = -2.2$, and dominates beyond 15 kpc (Carollo et al., 2007, 2010).

It is proposed that the inner halo formed from dissipational mergers (containing gas) of low-mass clumps into higher-mass clumps. Then the nearly radial merger of the resulting massive clumps resulted in highly eccentric orbits and star formation in the recently merged gas created the higher metallicity stars. Whereas, the outer halo formed through random dissipationless (gasless) mergers of low mass, low metallicity satellites (Carollo et al., 2007). It is the random orientation of the mergers that help to explain the slight retrograde motion observed in this region.

### 1.2.4 Dark Halo

In addition to the stellar halo component of the Galaxy as previously discussed, we know now that a massive dark matter halo surrounds the Milky Way. Navarro et al. (1997) have theorized that all dark matter halos follow the same density profile regardless of halo mass. The profile follows $r^{-1}$ at small radii, and $r^{-3}$ at large radii (Navarro et al., 1997).

Dark matter cosmological simulations predict that there should be many more dark matter satellites surrounding the Milky Way than the number of dwarf galaxies that had been discovered in the early 1990's (e.g., Simon & Geha, 2007; Kauffmann et al., 1993). This discrepancy has become known as the "missing satellite" problem. With the advent of the Sloan Digital Sky Survey (SDSS, see Section 1.3) the number of satellite galaxies around the Milky Way, and in the Local Group, has increased to about 50 (York et al., 2000a; Simon & Geha, 2007). Although this does not solve the "missing satellite" problem, it does dramatically alter our understanding of the Milky Way's local environment. Membership determinations of satellite galaxies require reliable distances and radial velocities (Freeman & Bland-Hawthorn, 2002). Given the intrinsic low luminosity of the objects and the current limitations of our surveys (SDSS has only imaged $\sim$1/5 of the sky), it isn't unreasonable that many more dwarf galaxies within the Local Group simply haven't been discovered yet (Simon & Geha, 2007).

From this follows the idea that some of the satellites may be "missing" because they have been disrupted by interactions with the Galaxy. This question was addressed by Morrison et al. (2000) and the "Spaghetti" Survey. This survey was designed to map the substructure of the halo from the velocities of distant giants[8], and ultimately to determine the fraction of mass in the halo that was accreted from satellites (Harding et al., 2001).

With this survey, in combination with modeling the orbits of the halo giant stars, they were able to recover the stripped remains of accreted satellites in the form of long streams surrounding the Galaxy (Harding et al., 2001). An example of this is shown in Figure

[8]Giant here refers to the stellar evolutionary stage that occurs after a star has fused all of its core Hydrogen into Helium. In this stage the accelerated fusion rate in the shells surrounding the core cause the star to expand and cool dramatically.

1.14, which shows the X-Y and Z-Y projections of three satellites after 1 Gyr, larger points, and 10 Gyr, smaller points, through its orbit around the Milky Way (Harding et al., 2001). Similarly, shown in Figure 1.15, images from the SDSS have uncovered a "field of streams" throughout the halo (Belokurov et al., 2006a). Typically, the mass of one of these streams will be in the range $10^7 - 10^9 M_\odot$ (e.g., Law & Majewski, 2010; Harding et al., 2001)

Since the gravitational potential of the Galaxy is dominated by dark matter at large radii, observations of the large tidal features in the halo can be used to constrain the shape, mass, and orientation of the dark matter in the Milky Way (Law & Majewski, 2010). Law & Majewski (2010) model the Sagittarius stream in different Milky Way dark matter halos, varying the overall shape of the potential. Axisymmetric halos are not able to reproduce the observed positions and distances of the stream. However, they suggest a triaxial halo with minor/major axis ratio, $c/a = 0.72$, and intermediate/major axis ratio, $b/a = 0.99$, to explain the observed structure.

The current picture of the Milky Way consists of a central supermassive black hole, surrounded by a somewhat box-shaped bulge. The majority of the stellar material is concentrated in a thin disk, which also contains spiral arms and a thin layer of gas that warps at the very edges. Encasing the thin disk is a diffuse thick disk population. These components all exist within an inner, prograde, stellar halo, an outer, retrograde, stellar halo, and a massive dark matter halo housing the extremely metal poor globular clusters, streams, and satellite galaxies. An image of the Milky Way from the Cosmic Background Explorer (COBE) satellite can be seen in Figure 1.16. The figure clearly shows the boxy shape of the bulge and the thin disk. More difficult to discern are the diffuse thick disk, thin Hydrogen layer, and halo material.

This picture, although significantly more elaborate that what was described in Section 1.1.3, is still evolving. The desire to understand the center, disk(s), halo, formation, and evolutionary history of the Milky Way is the driving factor for much of on-going research today. This is especially exciting with more and more data becoming available. The Sloan Digital Sky Survey (SDSS; York et al., 2000a) is only one example of a large survey dedicated to such topics. Its contributions are described in Section 1.3.

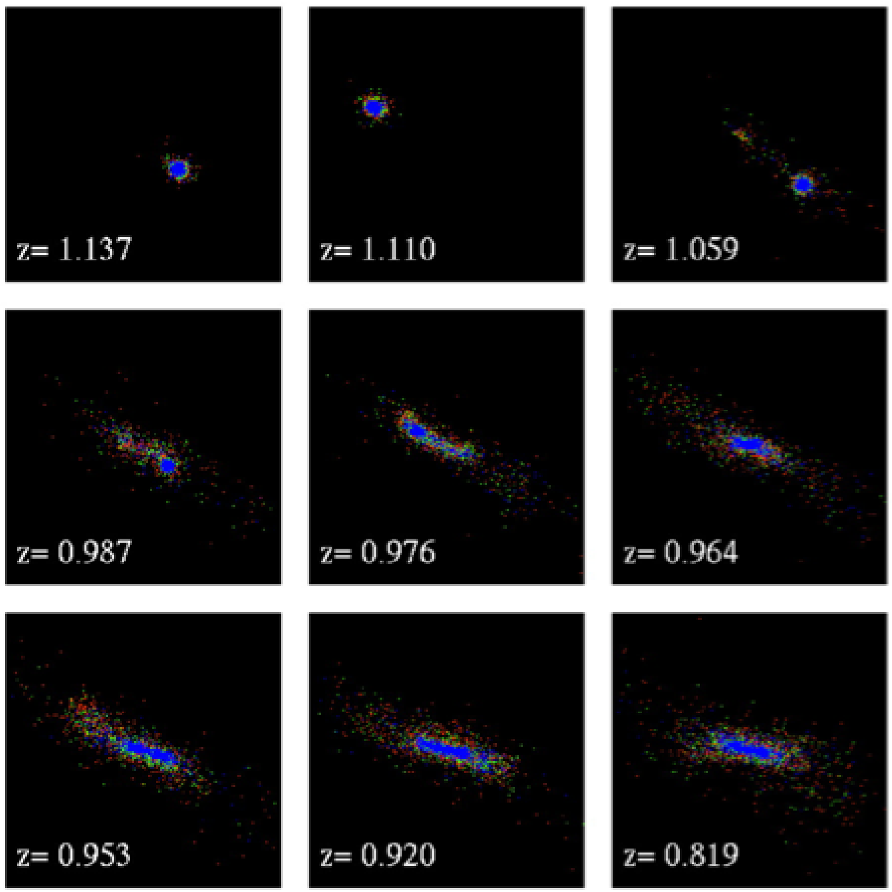


Figure 1.5: The disruption of a satellite over time seen edge-on with respect to the main galaxy (not shown). A significant fraction of the stars in the satellite contribute to a thick disk population. (Abadi et al., 2003)

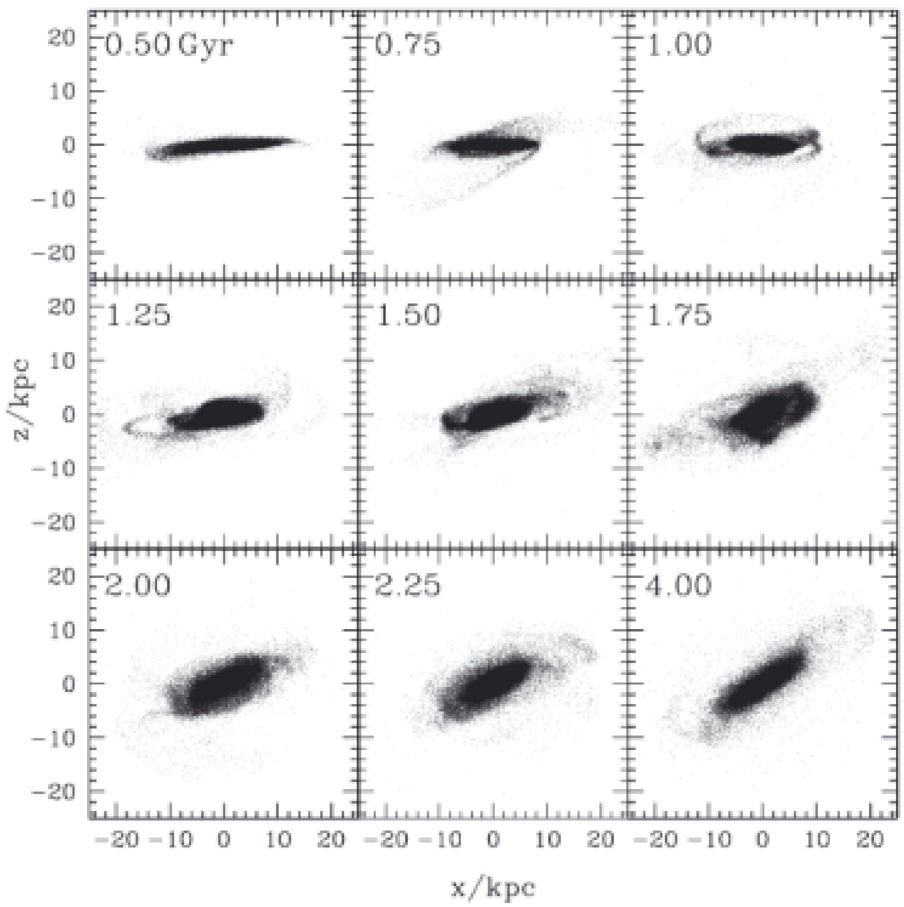


Figure 1.6: The disk of a host galaxy during a merger with a satellite (not shown). Over time the merger causes the existing disk to thicken. (Villalobos & Helmi, 2008)

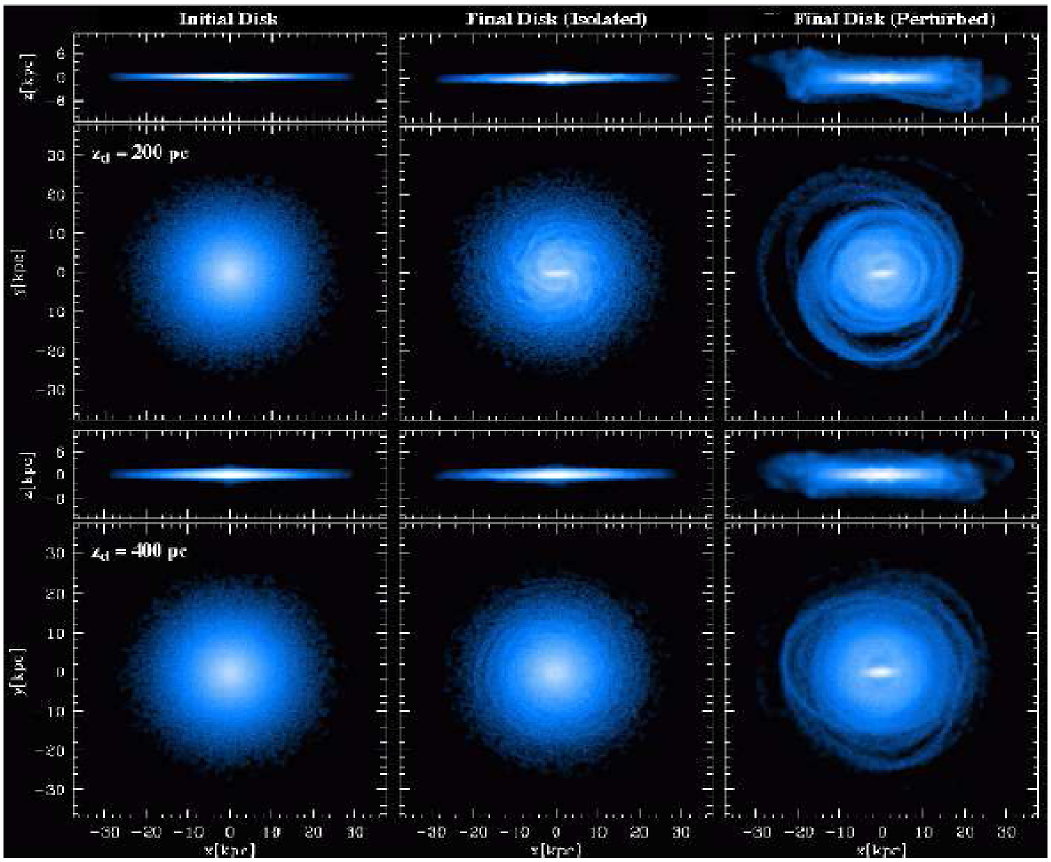


Figure 1.7: Left: Stellar distribution of galactic disks with different scale heights ($z_d = 200$ pc in the top panels and $z_d = 400$ pc in the bottom panels). The disk in the bottom panels more closely resembles the Milky Way disk. Middle: The disks after evolving in isolation for 2.5 Gyr. A bar and slight spiral structure form in the $z_d = 200$ pc disk. Right: The disks after evolving under satellite perturbations for 2.5 Gyr. Bars, spiral structure, and disk thickening occur in both cases. (Bird et al., 2011)

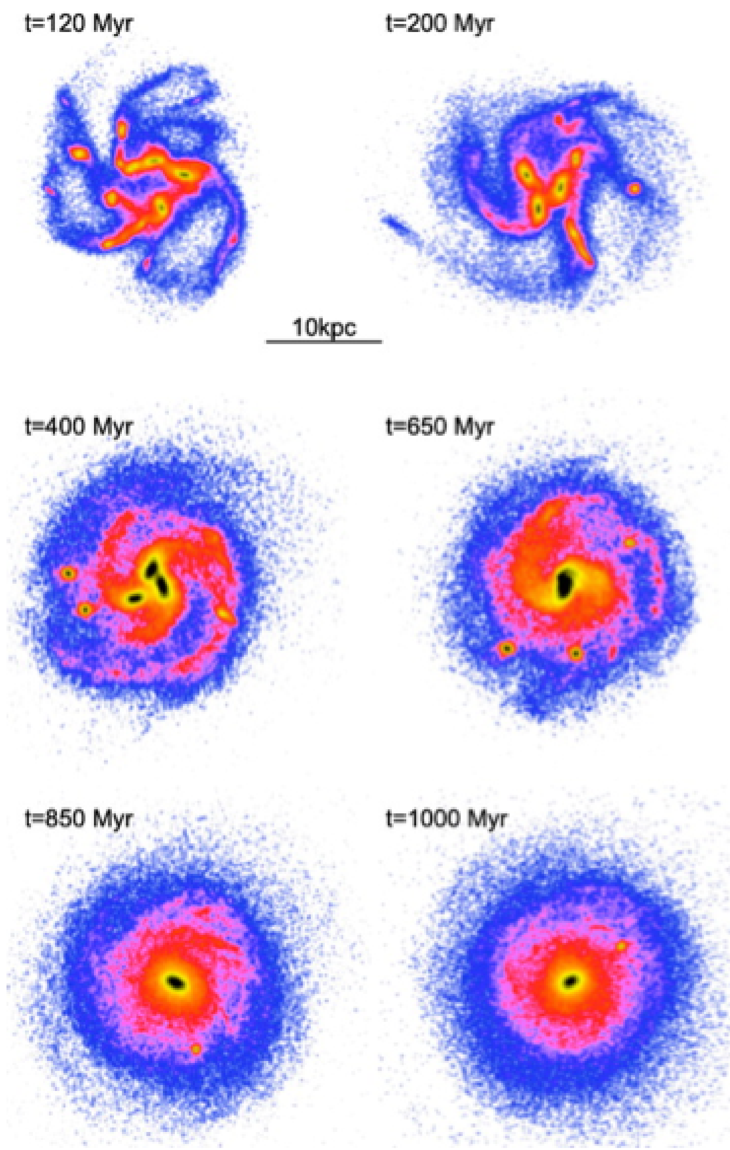


Figure 1.8: Face-on views of the evolution of a clumpy galaxy. The result is a spiral disk galaxy with central bulge and 2-component disk (not shown in this projection). (Bournaud et al., 2007)

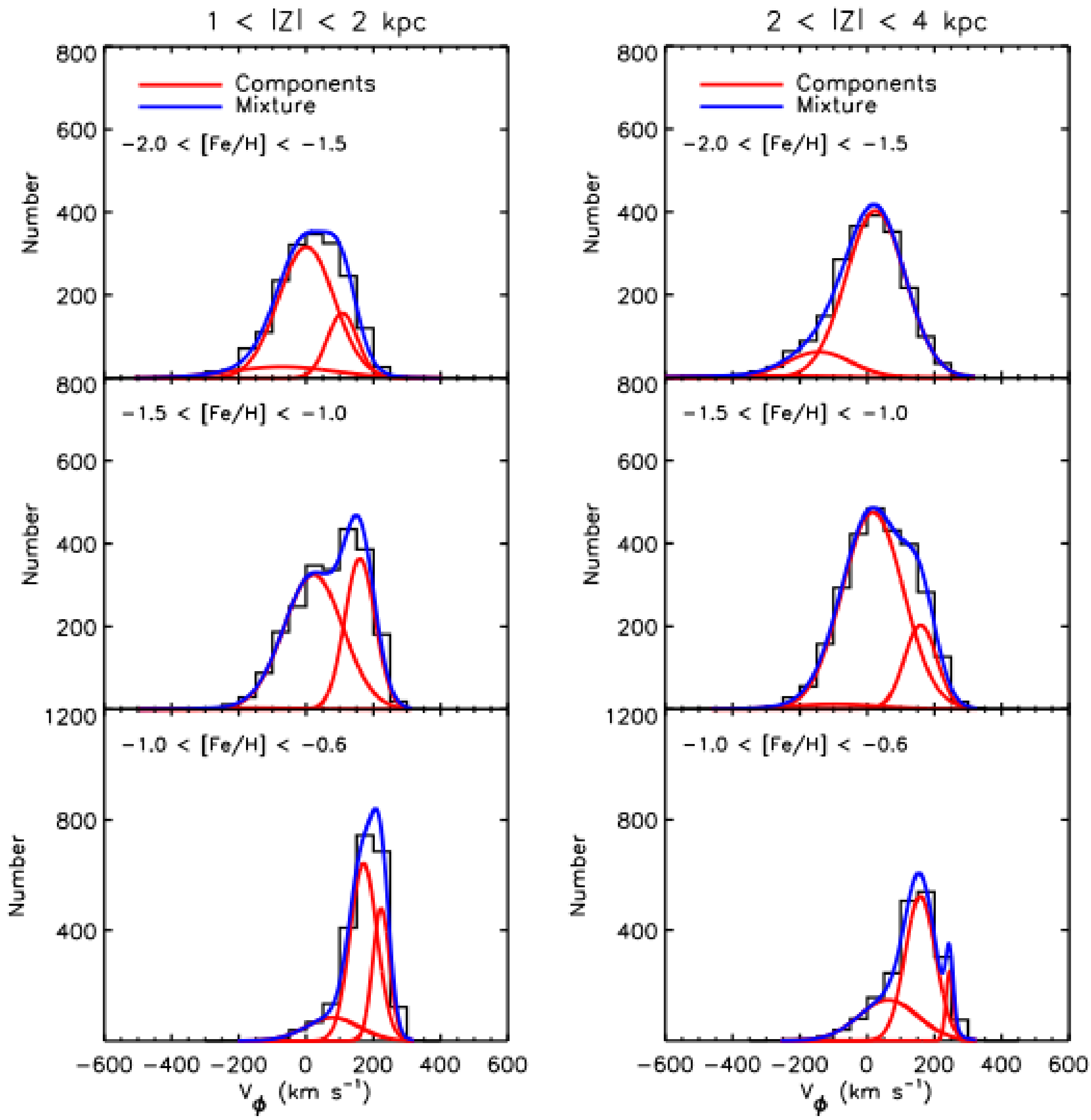


Figure 1.9: Left: The number of stars as a function of rotational velocity in varying metallicity bins for stars between 1-2 kpc from the plane, with the combined model for the distribution of velocities depicted by the blue line. The red lines are the Gaussian distributions for each component in the model. Right: Similarly, for stars between 2-4 kpc from the plane. (Carollo et al., 2010)

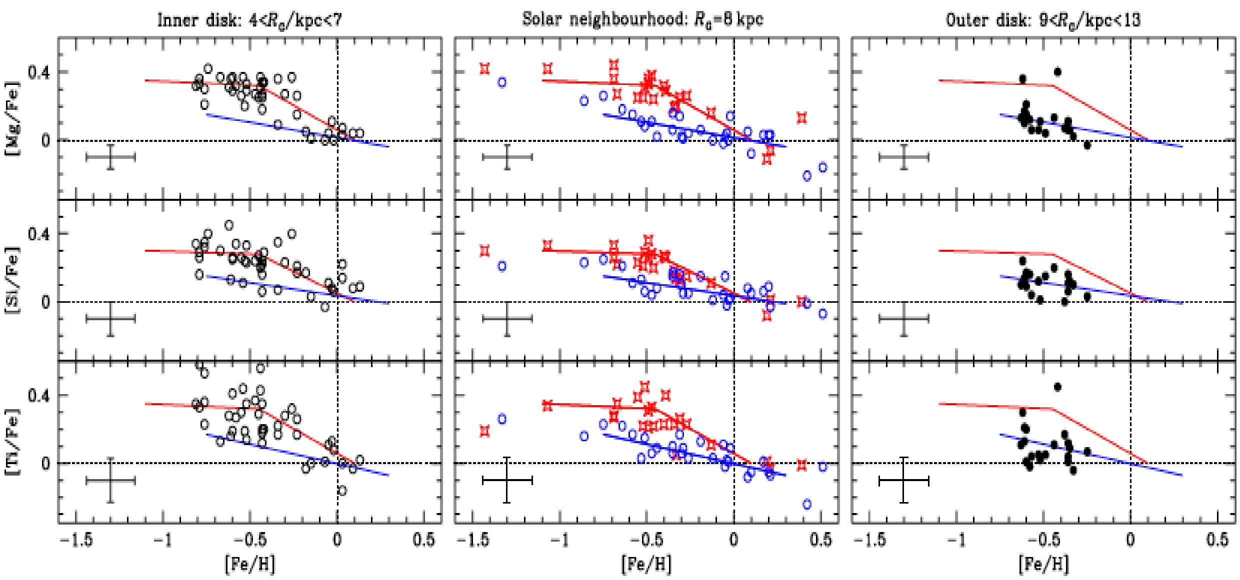


Figure 1.10: The center panel shows the metallicity of solar neighborhood disk stars. Red points are thick disk stars, fit by the red line, and blue points are thin disk stars, fit by the blue line. The left and right panels show the inner disk (open circles) and outer disk (filled circles) samples, respectively. Each is compared to the trends determined by the solar neighborhood sample. There is a distinct lack of stars following the thick disk metallicity trend at distances greater than 9 kpc. (Bensby et al., 2011)

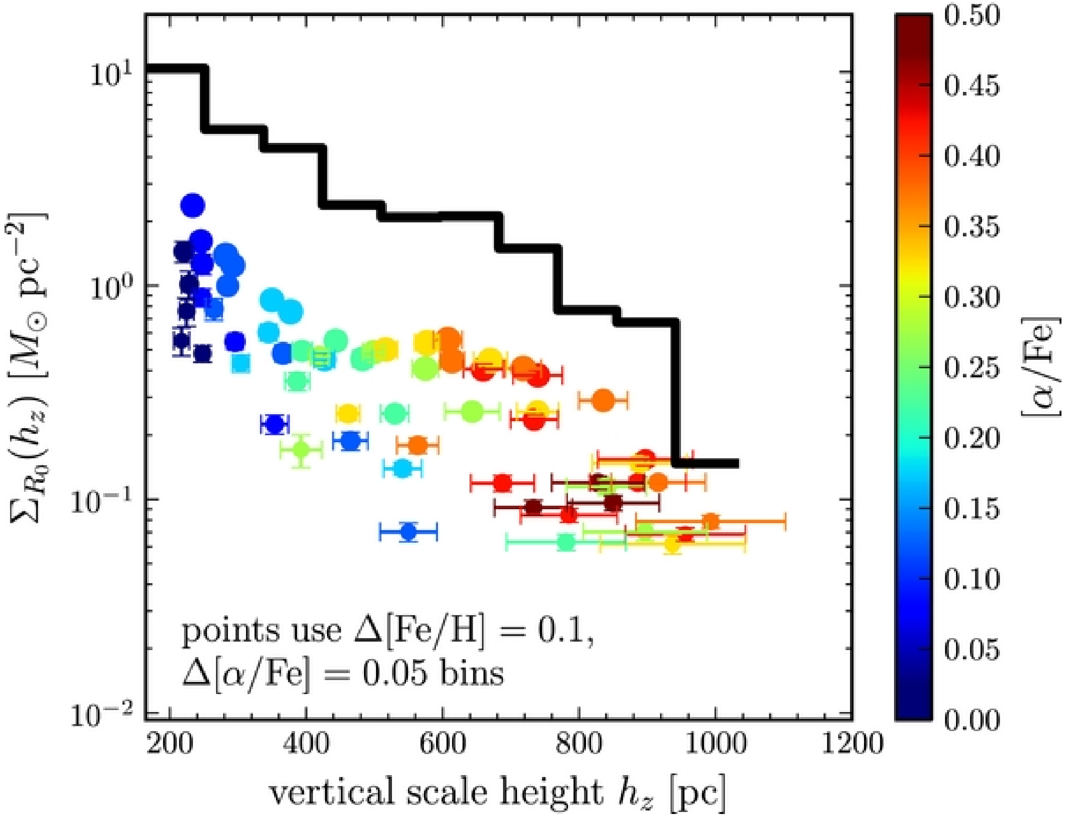


Figure 1.11: Stellar density versus scale height for mono-abundance sub-populations of SEGUE G dwarfs. Each population can be described by a single exponential function. The total stellar density is represented by the solid black line.

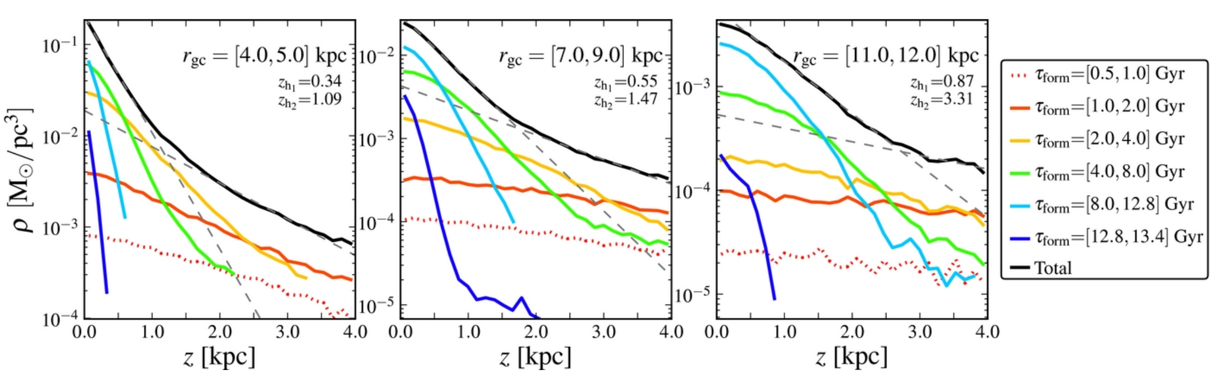


Figure 1.12: Each colored line represents the vertical mass density of a mono-age population in the inner disk (left), Solar neighborhood (center), and outer disk (right). Each mono-age population can be described by a single exponential function. However, the composite of all populations (black curve) requires two exponential profiles (grey dashed lines) (Bird et al., 2013).

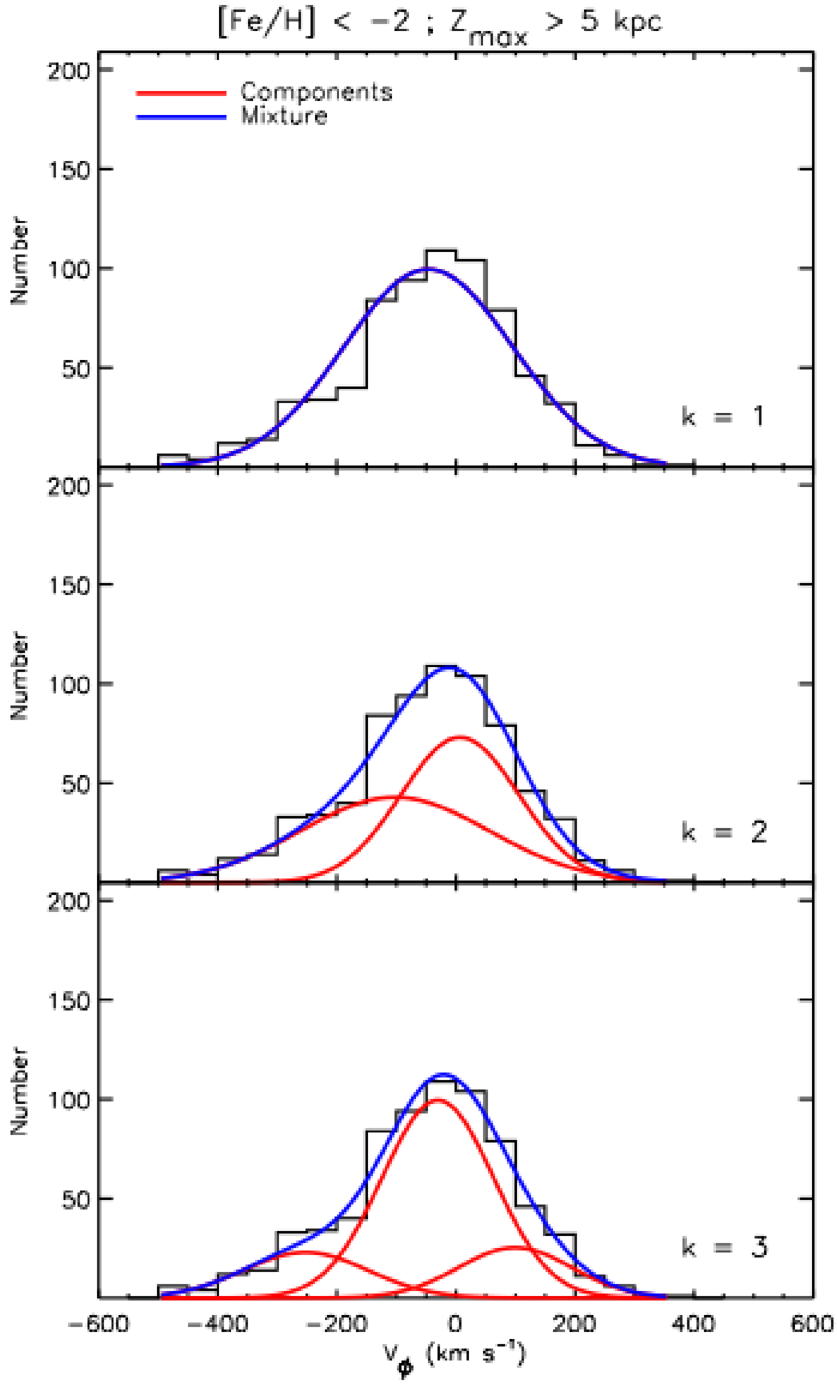


Figure 1.13: The number of stars with $[Fe/H] < -2$ and $Z_{max} > 5$ as a function of rotational velocity, with the combined model for the distribution of velocities depicted by the blue line. The red lines are the Gaussian distributions for each component in the model. The parameter k is the number of components used in the model. When k=1 the fit is not descriptive of the data. However, k=2 does much better at fitting the data with only slight improvement at k=3, signifying that the 2-component model is accurate. (Carollo et al., 2010)

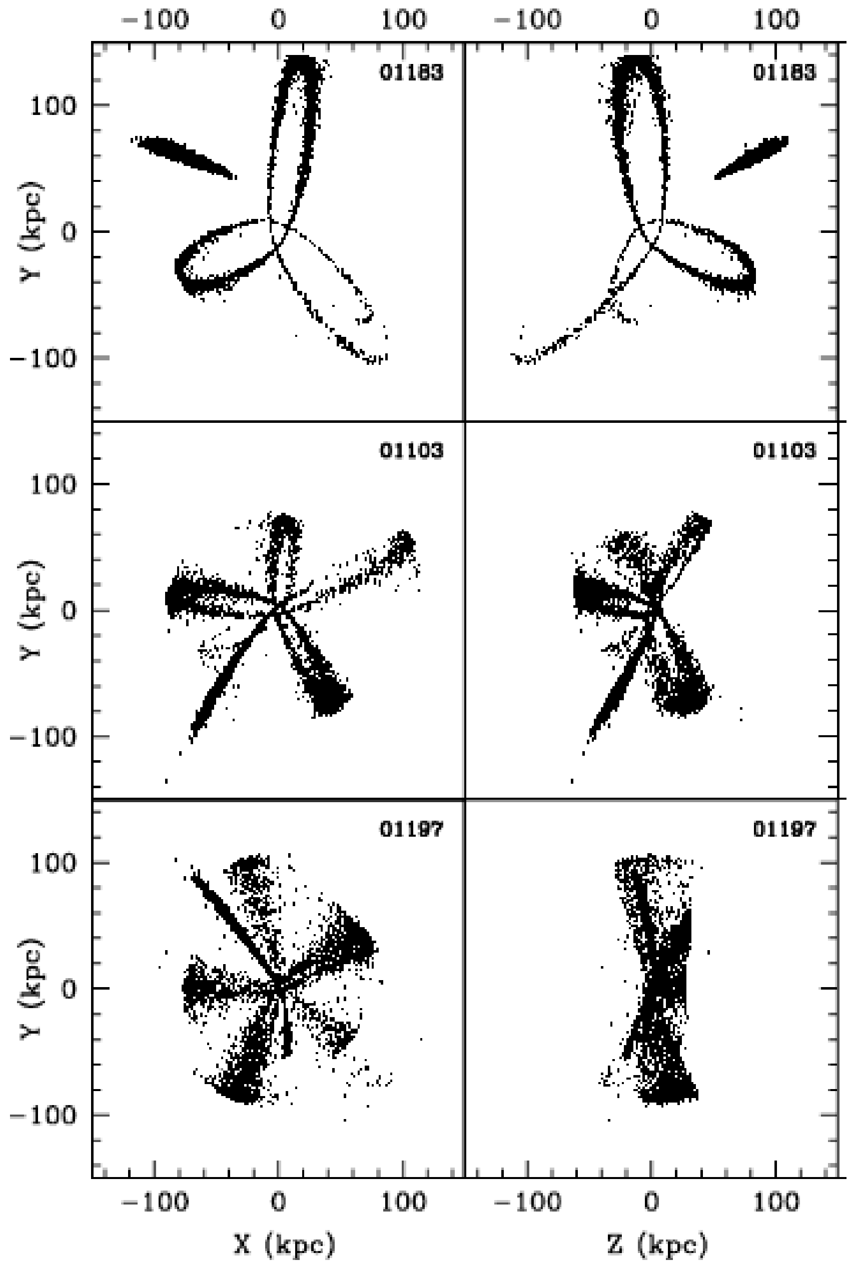


Figure 1.14: The X-Y and Z-Y projections of three separate satellites, identified numerically in the upper-right of each panel, at 1 Gyr and 10 Gyr (larger and smaller points, respectively–although, difficult to distinguish) throughout their orbit. This figure shows the disruption of satellites over time into large streams surrounding the Galaxy. (Harding et al., 2001)

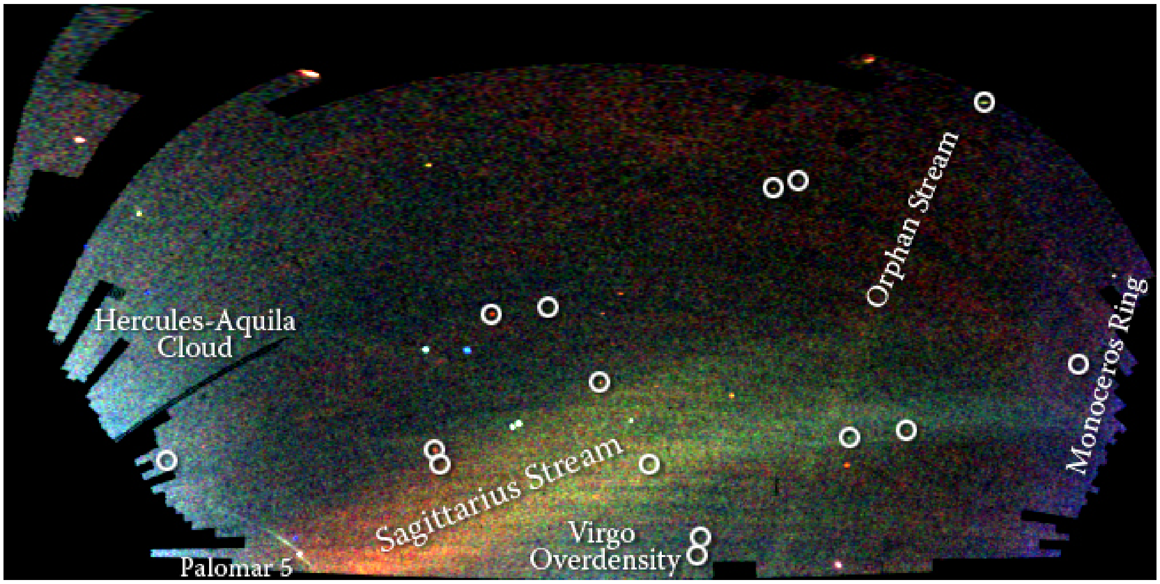


Figure 1.15: A map of the sky as seen by SDSS images showing the structure of the halo. Circles denote the location of globular clusters and satellite galaxies discovered by the SDSS. Other structures in this image include the Sagittarius, Orphan, and Monoceros streams. (Image courtesy of `http://www.sdss.org` (????).)

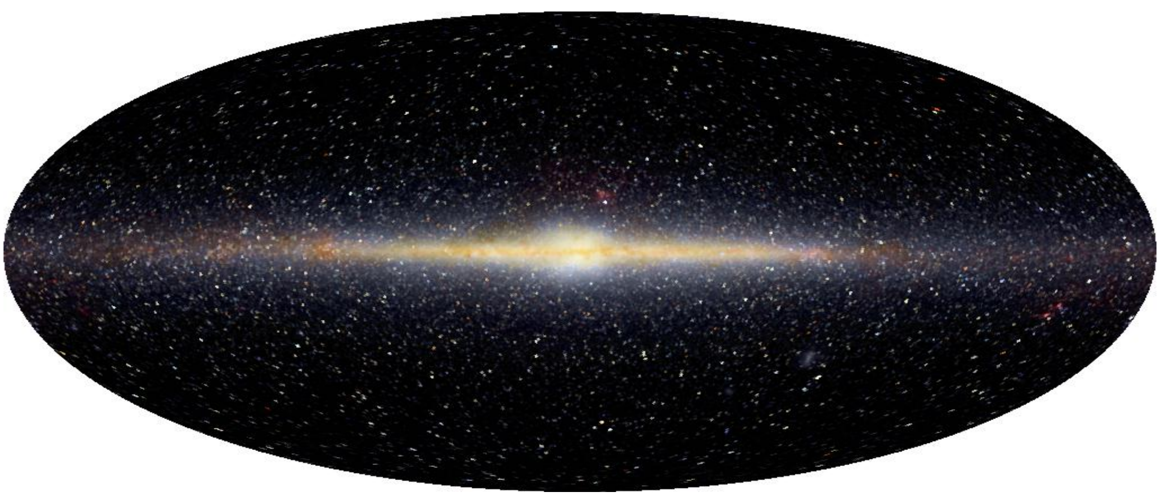

Figure 1.16: This image of the Milky Way was taken with the COBE-DIRBE (Cosmic Background Explorer- Diffuse Infrared Background Experiment) satellite. The image shows the boxy shape of the bulge and the dust throughout the disk has a slight reddish color. Also shown are the diffuse thick disk and the spattering of globular clusters and satellites throughout the halo. (Image courtesy of Ned Wright and gsfc.nasa.gov.)

## 1.3 The Sloan Digital Sky Survey

Large spectroscopic surveys help to map the structure of the Milky Way both spatially and kinematically (Rockosi et al., 2009). Furthermore, measuring chemical abundances in today's stellar populations helps explore the star formation history of the Galaxy (Rockosi et al., 2009). The Sloan Digital Sky Survey (SDSS; York et al., 2000a) is one such survey that has proved itself pivotal in understanding galaxy structure and formation.

The third generation, SDSS-III, is a six year program that includes four surveys- BOSS, MARVELS, SEGUE-2, and APOGEE. The SDSS-III surveys focus on the following three themes: 1) dark energy and cosmology, 2) the structure, dynamics, and chemical evolution of the Galaxy, and 3) the construction of planetary systems (Rockosi et al., 2009). See Sections 1.3.1 below for a more detailed discussion of the SEGUE surveys.

Some of the Sloan Digital Sky Survey's many contributions to date include (SDSS-III, 2008; Rockosi et al., 2009):

- Discovery of distant quasars beyond redshift of 6, revealing supermassive black holes in the early Universe;
- Using weak gravitational lensing to map extended mass distributions around galaxies, demonstrating that dark matter halos extend to 200 kpc or more;
- Demonstration of substructure around the Milky Way, revealing new tidal streams;
- Large samples of white dwarfs, used to obtain an accurate luminosity function to study the cooling of white dwarfs and estimate the age of the Galactic disk;
- Discovery of many new satellites around the Milky Way and M31, nearly doubling

the known number of Milky Way satellites;

- Discovery of stars escaping the Galaxy, revealing encounters with the black hole at the Milky Way's center.

### 1.3.1 Sloan Extension for Galactic Understanding and Exploration

The Sloan Extension for Galactic Understanding and Exploration (SEGUE and SEGUE-2) surveys provide stellar parameters, kinematics, and metallicities of stellar populations from the disk and inner halo to the large distances of the outer halo (Rockosi et al., 2009). SEGUE-2 added an additional 140,000 stars to the sample size of SEGUE, totaling 380,000 stars, and doubled the number of halo stars observed in SEGUE (Rockosi et al., 2009).

The stars targeted by SEGUE were selected to be largely thick disk stars within 10 kpc of the plane, while SEGUE-2 stars were selected to consist of halo stars with distances greater than 10 kpc (Rockosi et al., 2009). The target selection for SEGUE-2 was predominantly inspired by the desire to study the transition between the inner and outer halos occurring at roughly 15 kpc (Rockosi et al., 2009).

A sample of the science goals of the SEGUE/SEGUE-2 surveys includes: detection and analysis of stellar streams in the inner and outer halos, improved estimates of the mass of the Milky Way, determination of velocities of thick disk, metal weak thick disk, inner halo, and outer halo components, and to provide constraints on models of galaxy formation (Rockosi et al., 2009).

## 1.4 The Unbound Stellar Population in the Milky Way

Stars can become unbound through a variety of mechanisms. We see this, for example, in galaxy cluster environments where violent interactions are common. Galaxy harassment– minor perturbations over extended timescales (Moore et al., 1996), and tidal stripping from in-falling galaxies (Mihos, 2004; Byrd & Valtonen, 1990) can wrestle stars from the underlying potential and result in a population of unbound stellar outcasts. We see these diffuse collections of stars, called intracluster light (ICL), abandoned to the space between galaxies in large clusters, such as Virgo shown in Figure 1.17 (Mihos et al., 2005). Anywhere from $10\% - 70\%$ of the total cluster luminosity may be comprised of ICL (Mihos, 2003; Murante et al., 2004). Determining the fraction of cluster luminosity contributed by the ICL provides insights into the assembly history and evolution of galaxy clusters (e.g.; Napolitano et al., 2003; Feldmeier et al., 2004b).

In the Local Group, home to our Milky Way, which is devoid of major galaxy interactions, the unbound stellar population is more likely generated by three-body interactions (Holley-Bockelmann et al., 2005). The preferred method of ejecting stars, called the Hills mechanism (Hills, 1988), involves a binary star system and a supermassive black hole (SMBH). One of the stars is captured by the SMBH, angular momentum is transferred to the companion and it is flung from the galaxy with velocities approaching 1,000 km/s. Figure 1.18 follows the orbital trajectories of a pair of stars as they become disrupted via the Hills mechanism. The ejected companions are called hypervelocity stars (HVS). Semi-analytic models predict $O(100)$ HVS as a result this mechanism (Yu & Tremaine, 2003). Alternatively, this same effect can be achieved with a single star and binary black holes.

A recent simulation study showed that it is possible to boost stars to hyper-velocities via binary disruption scenarios in the disk (Tauris, 2015), Figure 1.19. These disruption scenarios involve a binary star system, located within the Galactic disk, in which the more massive star undergoes a supernova explosion and its companion is flung from the disk. Contrarily, previous works showed that the ejection velocity resulting from a binary disruption mechanism is a relatively modest $300 - 500$ km/s generating, instead, high velocity runaway stars (e.g.; Blaauw, 1961; Leonard & Dewey, 1993; Napiwotzki & Silva, 2012). The frequency of bona fide HVS ejected from disk binaries with velocities ∼1,000 km/s is yet undetermined[9].

The following chapters present initial steps towards probing the existence and origin of the unbound stellar population in the Milky Way and how it fits in the larger framework of Galactic structure, formation, and evolution.

[9]We perform a rough estimation of the expected number of low-mass HVS generated from the supernova binary disruption mechanism in Appendix A.

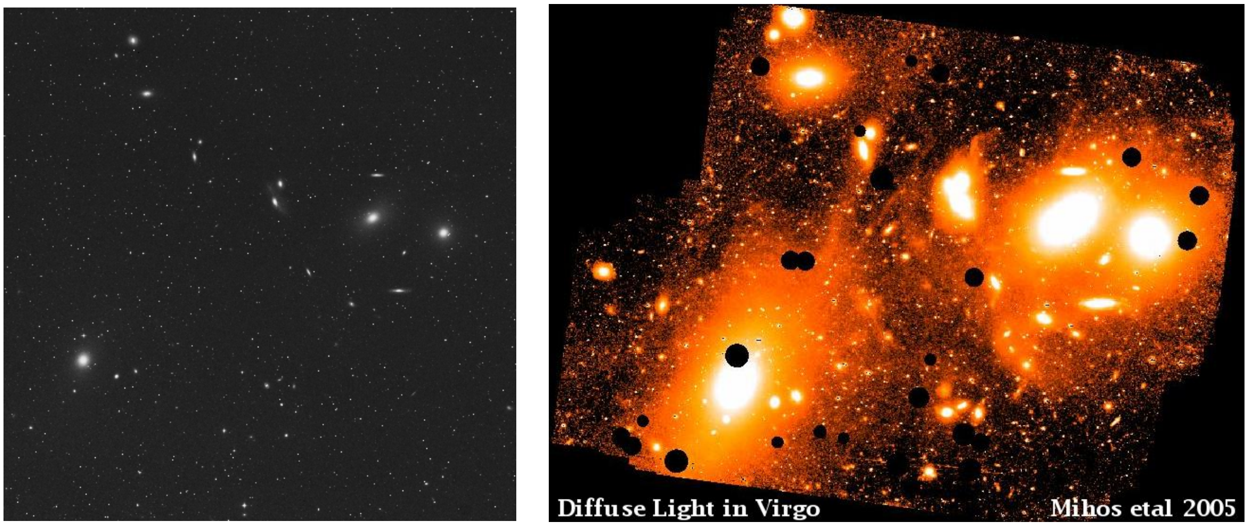


Figure 1.17: Left: Image of the Virgo Cluster captured by the Digital Sky Survey. Right: Long exposure image of the Virgo Cluster from Mihos et al. (2005) revealing the faint intracluster light between the galaxies.

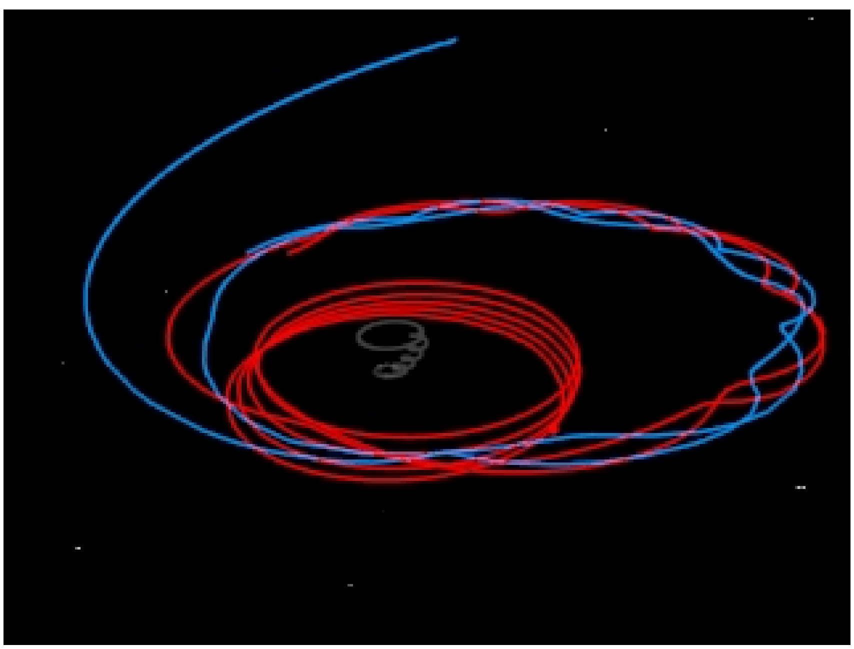

Figure 1.18: Still of an animation depicting the Hills mechanism (Image/animation credit: Andreas Irrgang). Red and blue lines trace the orbits of a binary star system around a SMBH (grey). The red star is captured into a tight orbit around the SMBH and the blue star is ejected from the system.

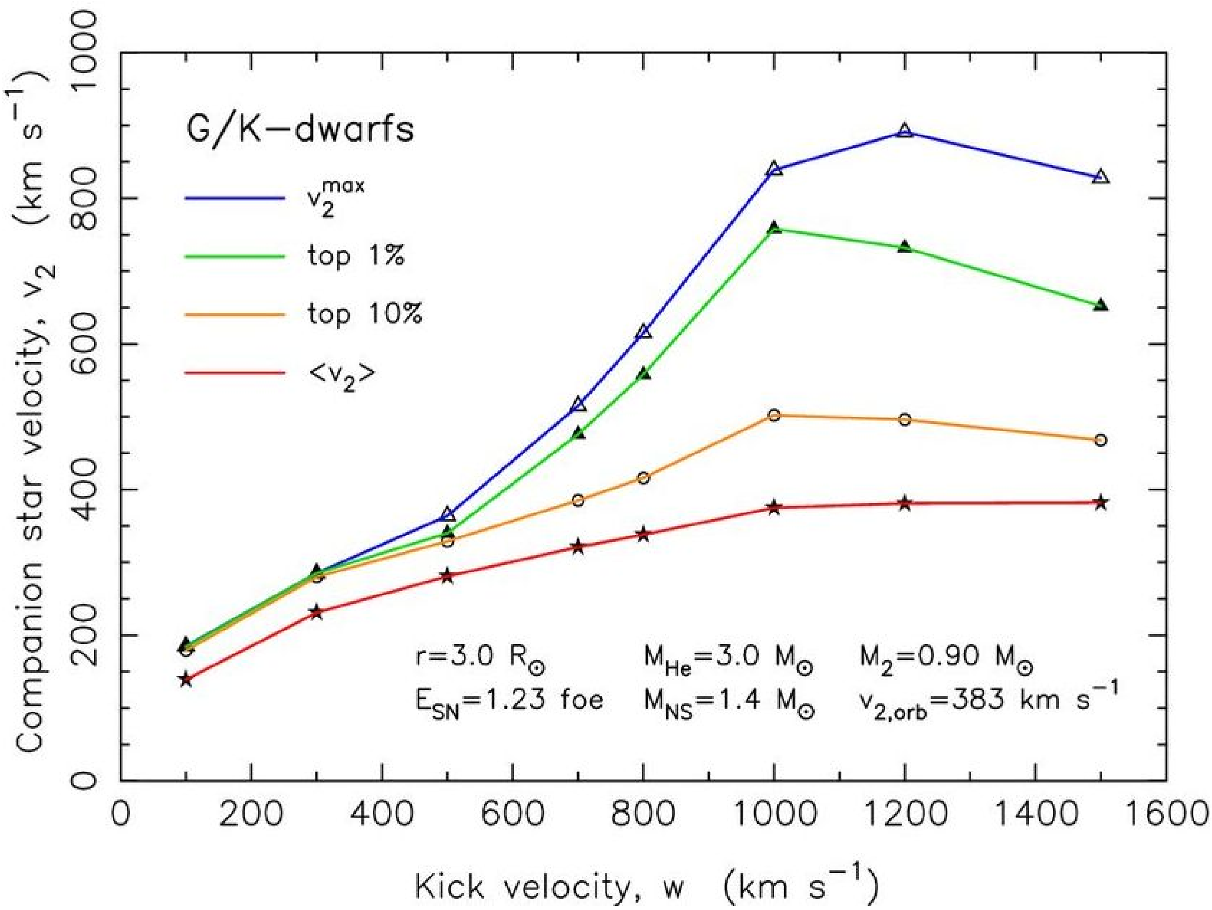


Figure 1.19: Companion star ejection velocity as a function of supernova-induced kick velocity. Colored lines indicate results of the disk disruption simulations of Tauris (2015). The blue line represents the maximum ejection velocity of $\sim 1,200$ km/s, showing it is possible to eject G/K-dwarf HVSs from the disk with velocities comparable to the G/K-dwarf HVs candidates of Palladino et al. (2014).

# Chapter II

## IDENTIFYING HIGH METALLICITY M GIANTS AT INTRAGROUP DISTANCES WITH SDSS

Here we reprint, in its entirety, work published in the Astronomical Journal, 2012, Vol. 143, Article ID 128.

### 2.1 Abstract

Tidal stripping and three-body interactions with the central supermassive black hole may eject stars from the Milky Way. These stars would comprise a set of 'intragroup' stars that trace the past history of interactions in our galactic neighborhood. Using the Sloan Digital Sky Survey DR7, we identify candidate solar metallicity red giant intragroup stars using color cuts that are designed to exclude nearby M and L dwarfs. We present 677 intragroup candidates that are selected between 300 kpc and 2 Mpc, and are either the reddest intragroup candidates (M7-M10) or are L dwarfs at larger distances than previously detected.

### 2.2 Introduction

A significant fraction of the stellar component of a galaxy cluster is not confined to any galaxy. These stars between galaxies form luminous halos, called intracluster light (ICL), with very low surface brightness that can extend out to several hundred kiloparsecs around individual galaxies (eg., Abadi et al., 2006; Krick & Bernstein, 2007). The brightest ICL is less than 1% of the brightness of the night sky (Mihos, 2003; Feldmeier et al., 2004b), thus making a complete census of ICL very difficult to obtain. High resolution N-body simulations estimate that ICL could comprise 10%-70% of the total cluster luminosity (Mihos, 2003; Murante et al., 2004).

It is commonly thought that intracluster stars are caused by one of three main channels: 1) stripping from galaxies as the cluster assembles either via high speed galaxy encounters, tidal shocking, or a rapidly changing galaxy cluster potential (Byrd & Valtonen, 1990; Merritt, 1984), 2) long-lived, low level cluster perturbations in the form of "galaxy harassment" (Moore et al., 1996), or 3) tidal stripping within in-falling galaxy groups (Mihos, 2004; Rudick et al., 2009). These processes will generate a stellar 'debris field' that is highly inhomogeneous, with distinctly non-Gaussian velocities that reflect an unrelaxed intracluster population (Napolitano et al., 2003). Thus far, ICL has been identified via planetary nebulae (PNe) (Feldmeier et al., 2004b; Aguerri et al., 2005), Red Giant Branch stars (Durrell et al., 2002; Williams et al., 2007), intracluster globular clusters (Lee et al., 2010; Peng et al., 2011), and ultra-deep surface photometry (Feldmeier et al., 2002, 2004a; Mihos et al., 2005).

The properties of ICL may provide insights into the accretion history and evolution of galaxy clusters (Mihos, 2003, 2004; Napolitano et al., 2003; Feldmeier et al., 2004b; Conroy et al., 2007). Although there is some debate about the role that tidal stripping plays in ICL production, it is expected that ICL substructure is correlated with the dynamical state of the cluster (Murante et al., 2007; Mihos, 2004). Since the vast majority of galaxies reside in poor groups, rather than in large clusters, it is of great interest to determine the fraction of unbound stars that reside in these environments.

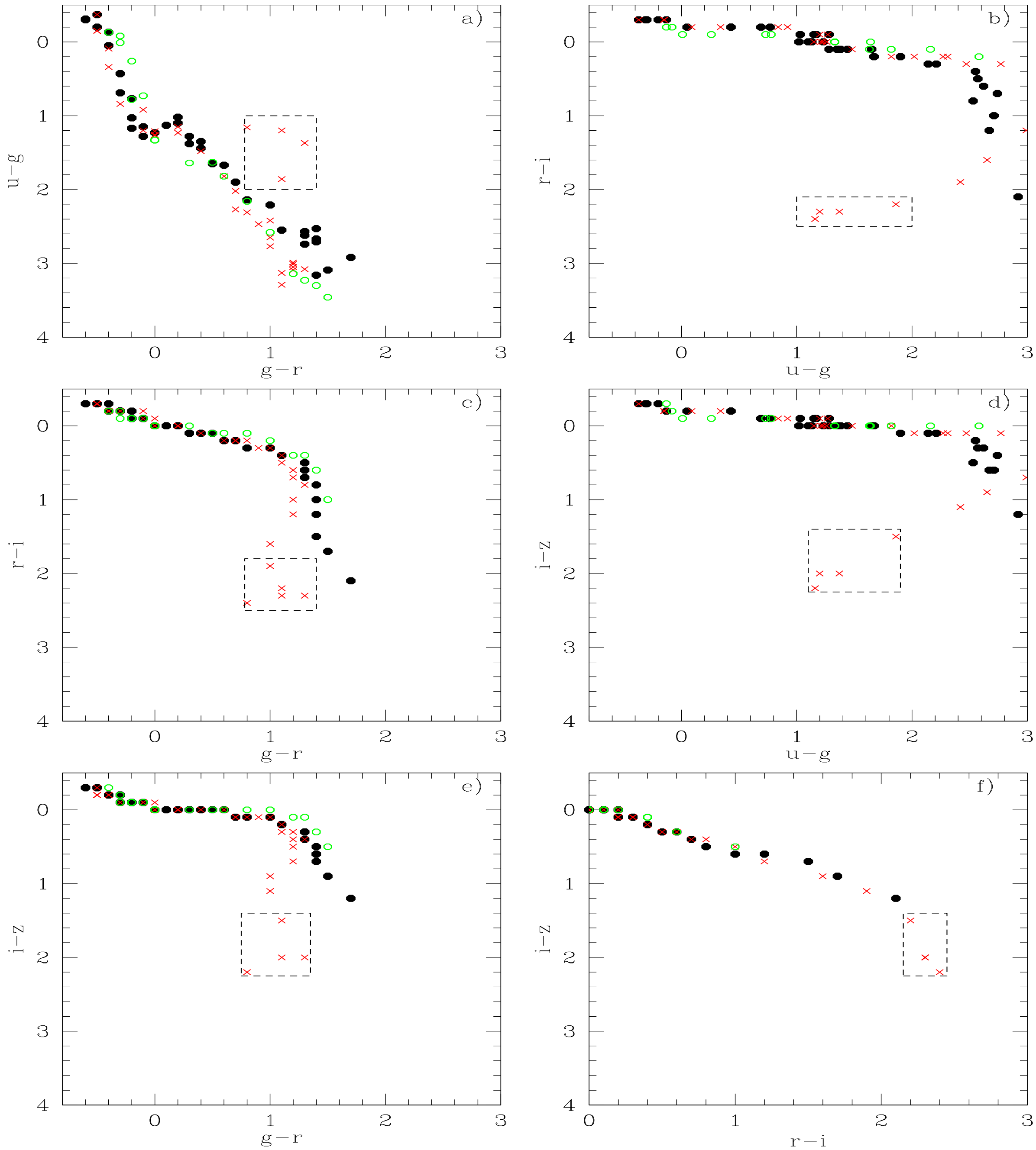


Figure 2.1: Color-color diagrams of the Covey et al. (2007) sample data. Main sequence stars are marked with black dots, giants with red crosses, and supergiants with green circles. Note that the reddest giants (M7-M10), identified by the black dashed regions, are isolated from the stellar locus. This figure is a theoretical demonstration that very late M giants have the potential to be isolated in color space in the *ugriz* bands, and these dashed regions are meant only to highlight the spectral types of interest and do not represent our color selection criteria (given explicitly in equations 1 and 2). In particular, we drop the $u-g$ and $g-r$ cuts because objects at these distances are likely too faint in the $u$ and $g$ bands. The locus of sub-solar metallicity giants is generally indistinguishable from the dwarf locus, and thus not plotted here.

In the Local Group, ICL has not been observed, though deep observations and star counts have revealed a "field of streams" (e.g., Belokurov et al., 2006b). These streams have been detected out to 100 kpc and are bound to the Milky Way (e.g., Yanny et al., 2000; Ibata et al., 2001). Similarly, faint streams have been detected in the outskirts of M31 (McConnachie et al., 2009; Ibata et al., 2007). Given that the Milky Way and M31 are not yet interacting and may not even be part of the same dark matter halo, it is more likely that Local Group ICL, if it exists, would be a product of a different process altogether.

One of the more recent suggestions for ICL production is via three-body interactions (Holley-Bockelmann et al., 2005). For example, stars can be thrown out from the galaxy through tidal disruption of a binary star system by a supermassive black hole (Hills, 1988; Yu & Tremaine, 2003); this is the most common explanation for 'hypervelocity' stars such as SDSS J090745.0+0204507, with a galactic rest frame velocity of $\sim 700$ km/sec (Brown et al., 2005). During this process, energy and angular momentum are transferred from the black hole to one of the stars in the binary. The second star loses energy and becomes bound to the black hole while the first is ejected from the galaxy. This is expected to occur at a rate of $10^{-5}(\eta/0.1)\,\mathrm{yr}^{-1}$, where $\eta$ is the stellar binary fraction (Magorrian & Tremaine, 1999).

Another three-body interaction that is likely to expel stars is a close encounter of a single star with a binary black hole (Yu & Tremaine, 2003). This is expected to occur at a rate of $10^{-4}(\eta/0.1)\,\mathrm{yr}^{-1}$ (Magorrian & Tremaine, 1999). In this case, the star gains energy from the binary black hole and is flung out of the galaxy while the black hole orbit shrinks (e.g., Quinlan, 1996; Sesana et al., 2006).

To become gravitationally unbound, stars must exceed the escape velocity of the Galaxy, now estimated to be 500-600 km/sec (e.g., Smith et al., 2007). Semi-analytic models predict that there may be approximately 100 hypervelocity stars within 8 kpc of the galactic center if the binary stars have equal masses (Yu & Tremaine, 2003). However, intragroup stars (IGS) may not be solely comprised of hypervelocity stars; they may still be bound but on very large, highly eccentric orbits– this can increase the potential number of IGS. One way to get stars on such eccentric orbits is through three-body galaxy ejections of satellites like Leo I (Sales et al., 2007; Mateo et al., 2008).

As a first attempt to probe for a population of intragroup stars, we develop a technique to search for M giant stars in between the Local Group galaxies. In this paper we present our technique for identifying candidate IGS from the Sloan Digital Sky Survey (SDSS) by applying color, distance, and proper motion cuts. Section 2.2 describes our technique. We present our results in Section 2.3, and we discuss possible sources of contamination in Section 2.4. Section 2.5 concludes and discusses methods to confirm the candidates.

## 2.3 Methods

During its eight years of operation, the Sloan Digital Sky Survey (SDSS; York et al., 2000a) obtained deep, multi-colored images covering more than a quarter of the sky. The SDSS uses 5 optical bandpasses ($u, g, r, i$, and $z$; Fukugita et al., 1996a; Gunn et al., 1998; Hogg et al., 2001; Gunn et al., 2006) with magnitude limits 22.0, 22.2, 22.2, 21.3, and 20.5, respectively. The DR7 data set contains 12,000 square degrees of images and a catalog of over 350 million objects with spectra of 460,000 stars.

As individual red giant stars in M31 have been observed down to the SDSS magnitude

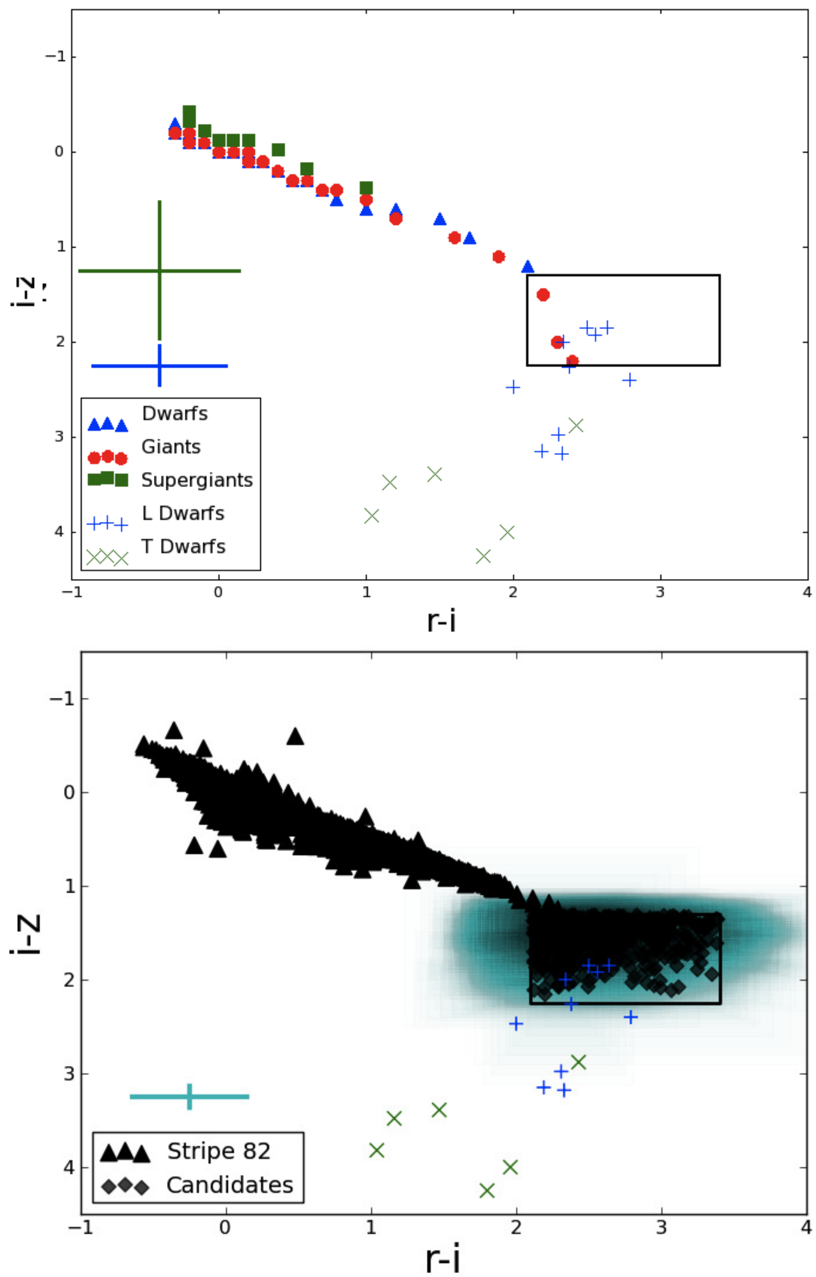


Figure 2.2: Left: Color-color diagram similar to Figure 2.1, including L and T dwarfs from Hawley et al. (2002). The region of color space containing our IGS candidates is marked by the black rectangle. Blue triangles represent dwarfs, green squares represent supergiants, red dots represent giants, blue crosses and green stars represent L and T dwarfs. The blue and green error bars in the bottom left corner are representative of the typical 1-$\sigma$ error bars for L and T dwarfs, respectively. Note that late M (M7-M9) and L dwarfs also contaminate the space. Right: Same as figure on the left, using SDSS Stripe 82 stars (filled triangles) to represent the spread in the stellar locus (the errors are contained within the size of the point) (Ivezić et al., 2007) and 677 extinction-corrected IGS candidates (filled diamonds). The cyan cloud results from the sum of gaussian-distributed errors on each candidate, i.e. the darkest cyan region represents the most probable location of the data. Similarly as in the left panel, the cyan error bar in the bottom left corner is representative of the typical 1-$\sigma$ error bars for each candidate.

limits (e.g., Zucker et al., 2007), intragroup red giant stars will be observable. Indeed, at a distance of 300 kpc, all supergiants and roughly half of any giants would be detectable in the $r, i$, and $z$ bands.

We developed our technique using the synthetic SDSS and 2 Micron All Sky Survey (2MASS) photometry (Covey et al., 2007) of flux calibrated spectra of *solar metallicity* main sequence, giant, and supergiant standard stars (Pickles, 1998). With simulated SDSS and 2MASS colors (Schlegel et al., 1998), we obtained a stellar locus to search for giants or supergiants that are isolated in a 'clean' region of color space. These color-color diagrams are shown in Figure 2.1. We choose solar metallicity standards to probe for IGS generated by three-body interactions within the central regions of the Galaxy, as discussed in Section 2.1.

Unfortunately, most supergiants and giants lie along the main sequence locus, and would therefore be indistinguishable by SDSS colors. However, there is a small area in each of the color-color diagrams, shown with dashed boxes in Figure 2.1, where the rarest M giants (M7-M10) are isolated from dwarfs and supergiants of the same spectral types. Considering the distances we are probing and the very red colors of these spectral types, we restrict our color selection to the $r, i$, and $z$ bands as follows:

$$2.1 < r - i < 3.4, \tag{2.1}$$

$$1.3 < i - z < 2.2 \tag{2.2}$$

Again, we drop the $u - g$ and $g - r$ cuts because objects at these distances are likely too faint in these bands.

Since these objects are so red, they may be confused with other nonstellar objects[1]. However, we find that even quasars with $z > 4.6$ are too blue in $i - z$ to fall in our color space (Richards et al., 2002; Fan et al., 2001).

A more worrisome source of contamination comes from L and T dwarfs. To investigate this, we compared our color selection region to the colors of L and T dwarfs (Hawley et al., 2002) and find that they also are contained in the color region, albeit with large uncertainties, as shown in Figure 2.2. From current observational studies, we estimate that there may be $O(1000)$ early L dwarfs in the SDSS footprint within the magnitude limits of SDSS (Burgasser et al., 2010). Since we expect more dwarfs than giants at these faint magnitudes, it is likely that a greater number of dwarfs are scattered into the selection area through large errors than the number of giants scattered out. Objects in our selection box that are not IGS are, nevertheless, likely interesting astrophysical objects yielding more distant L dwarfs than currently known. We discuss ways to differentiate between IGS and contaminants in section 2.5.

From the DR7 Star Table, we identified all stars that satisfy our color criteria and are positioned at $|b| > 20$ to exclude potential disk contamination (including disk L and T dwarfs). To ensure that each candidate has a stellar point spread function, we confirmed that the object type flag in all 5 bandpasses were stellar[2]. We then removed all objects

[1] Background red galaxies have colors roughly $0.35 < r - i < 0.45$ and $0.15 < i - z < 0.3$ at z=0.1 (Blanton et al., 2003). These colors will become redder with increasing redshift. For example, the brightest and reddest galaxies in SDSS, LRGs at z=0.5, have $r - i = 0.7$ and $i - z = 0.4$ (Blanton et al., 2003). Since these colors do not approach our color selection region and since we have ensured stellar point spread functions for our candidates, we do not consider background galaxies as a significant source of contamination.

[2] Although we restrict our color criteria to the $r, i$, and $z$ bands, in order to be conservative, we still require the objects to have stellar point spread functions in the $u$ and $g$ bands as well.

that would be nearer than 300 kpc and further than 2 Mpc in the redder bandpasses, assuming an M giant average absolute magnitude in each bandpass ($M_r = 0.8, M_i = -1.5, M_z = -3.5$) yielding the following magnitude cuts: $23.2 < r, 20.9 < i, 18.9 < z$ — since the r band is effectively below the magnitude limits of SDSS, we searched for null detections in this band as well. We also eliminated objects that triggered any of the following flags: BADSKY, BLENDED, CHILD, COSMIC_RAY, EDGE, MAYBE_CR, MAYBE_EGHOST, MOVED, NODEBLEND, and PSF_FLUX_INTERP.

We cross-checked our candidates with the 2MASS J-H color cut of Majewski et al. (2003) since dwarfs and giants have distinctive J-H colors: $J - K_s > 0.85$, $J - H < 0.561(J - K_s) + 0.36$, $J - H > 0.561(J - K_s) + 0.22$ (top panel of Figure 2.3). Although, note that the Majewski et al. (2003) color cut selects sub-solar metallicity M giants with [Fe/H]$= -0.4 \pm 1.1$ dex (Chou et al., 2007). This will make the giants selected by the Majewski et al. (2003) cut bluer than the solar-metallicity giants selected in our sample.

The middle panel of Figure 2.3 shows a clear separation of the synthetic spectral standard giants and dwarfs from Pickles (1998) at a J-H color around 0.8 (Bessell & Brett, 1988). In general, J, H, and $K_s$ magnitudes for our IGS candidates (16.86, 15.78, and 15.56, respectively, for an M7III according to Covey et al. (2007)) are too faint to appear in the 2MASS catalog. Since appearing in 2MASS would indicate that the source is too bright or too close to be an IGS M giant we removed any candidate that did appear in the 2MASS catalog, and to verify that they are nearby dwarfs, we plotted their J-H colors shown in the bottom panel of Figure 2.3.

The completeness limits of J, H, and K filters in the UKIDSS (Lawrence et al., 2007) survey are appropriate for our targets, however our search through the publicly-released database (DR4) did not result in any matches to our candidates since we expect our candidates lie in parts of the sky not yet covered by this release. Moreover, once the UKIDDS survey is complete it will only cover about half of the area in the SDSS footprint.

After removing known dwarfs in 2MASS, we cross-referenced the IGS candidates with the USNO-B catalog, an all-sky catalog that contains positions, proper motions, and magnitudes in various optical passbands. Here, we removed those candidates with discernible proper motions, ranging from 3 to 1412 mas/year, since the distances determined by the proper motions indicate that they are likely objects closer than 353 pc. This eliminated 782 candidates.

### 2.3.1 Testing the color selection region with real data

Since our current technique for finding very late M giant IGS is based on idealized solar metallicity spectra and synthetic colors, it is important to determine how robust these colors are for known M7 III-M10 III stars. Unfortunately, there are no confirmed very late M giant stars in the SDSS DR7 (or DR8) database with both spectra and colors. While it is true that these stars are rare, the real difficulty is that spectral classification of M giants is notoriously difficult, and the latest M giants can be spectral type variables, as well. Since the SDSS database did not explicitly include the latest M giants, we decided to take a three-pronged approach in checking M giant colors.

First, we searched through Simbad for spectroscopically-confirmed M7-M10 giants, finding 53, 28, 4, and 0, respectively; many of these were listed in the Catalogue of Stellar Spectral Classifications (Skiff, 2010). For each object, we cross-checked the spectral type through all other publically-available catalogs on VizieR to determine if the star was a known significant spectral variable, and if so, we discarded it. We then searched DR7 for any star within 2 arcseconds of the target and obtained the photometry. Many of these objects were nearby and saturated, and therefore appeared as several non-stellar sources in the DR7 database – these were also discarded if the composite, corrected photometry was not available. Only one of the remaining stars returned a result in the CAS and appears as the blue star in Figure 2.4, which lies within our color cut.

Second, we acquired spectra of late-type giants observed as part of a study to quantify the effects of gravity on the spectra of cool objects. These spectra were obtained with the Low Resolution Imaging Spectrometer (LRIS, Oke et al., 1995) on the 10-m W. M. Keck Observatory as part of a campaign to construct a systematic surface gravity "grid" to further constrain spectral classifications of brown dwarfs (Kirkpatrick, in prep.). We estimated the spectral type and log g parameters by eye and separated the latest M giant subset for analysis, totaling 13 spectra. Examples of these spectra are shown in Figure 2.5. Using the SDSS transmission curves, we calculated the colors in the Sloan bands, and as can be seen by the red stars in Figure 2.4, most of these stars do indeed lie in the predicted color space.

Finally, as a further check of our M giant colors we used the Bruzual-Persson-Gunn-Stryker (BPGS, hereafter; Laidler, V. et al, Synphot User's Guide, Version 5.0 (Baltimore STScI), 2005) stellar atlas of standard stars to obtain synthetic colors using the IRAF Synphot task *calcphot* [3]; the green points in Figure 2.4 represent these standard stars– there were no available M9III-M10III standards in the atlas, which is expected because

[3]The i-z colors returned by *calcphot* for the M dwarfs are unreliable due to negative flux values in the BPGS stellar atlas.

these objects are all spectrum variables.

Figure 2.4 shows that the color cut we defined from synthetic SDSS colors is consistent with the colors of known M giants from all three techniques.

If the reader is interested in seeing the colors of the stars we used from the BPGS stellar atlas in the Johnson-Cousins filter set, a figure will be available online [4]. The UBV colors of these stars are consistent with the colors reported by Worthey & Lee (2006), as well.

## 2.4 Results

We found a small region of color space, shown in Figure 2.2, in which the reddest solar-metallicity M giants are isolated from the rest of the stellar locus. This region hosts M7III-M10III stars, along with L dwarfs (Hawley et al., 2002).

Using our color selection criteria, we found 159,108 extinction-corrected objects in SDSS DR7. After applying the distance cut and checking the data flags, we narrowed the sample to 4181 objects. We then cross-correlated our sample with the 2MASS and USNO-B surveys, removing any stars with dwarf-like J-H colors and any stars with non-zero proper motions. Our final sample contains 677 IGS candidates. Table II.1 lists positions, asinh magnitudes, $r - i$, and $i - z$ colors for all 677 candidates. The right panel of Figure 2.2 shows the location of the final set of IGS candidates with errors in $r - i/i - z$ color space.

[4] http://astro.phy.vanderbilt.edu/~palladl2/

## 2.5 Discussion

As discussed in Section 2.1, IGS could be formed from several different methods. Considering the Local Group's current level of interactions, this population may likely be comprised of high metallicity hypervelocity stars (HVS) ejected through the three body mechanism. However, not enough is known about HVS and Local Group formation to say this definitively, so probing the IGS sample may help us to constrain either or both of these.

If every candidate were a solar metallicity IGS giant, they would be rare tracers of a large underlying IGS population. Assuming a single burst of star formation 10 Gyrs ago and a Salpeter initial mass function (IMF), these candidates represent $O(10^{-4})$ of the total number of IGS and $O(10^{-3})$ of the total mass in IGS, and varies only slightly for differing choices of IMF.

It is useful to compare this to theoretical predictions of stellar ejections from the Milky Way (Kollmeier et al., 2009). Stars ejected from the galaxy center through three-body interactions with a SMBH will typically have much higher metallicity than stars that were stripped from satellite galaxies originating in the outskirts of a galaxy halo (e.g., Jacoby & Ciardullo, 1999a; Kirby et al., 2008). For example, if we assume that all of the IGS are solar metallicity hypervelocity stars ejected by three-body interactions with a binary black hole consisting of a SMBH and an intermediate mass black hole (IMBH), then the total mass in stellar ejecta will be roughly equal to the mass of the IMBH (Yu & Tremaine, 2003; Quinlan, 1996). Given the Milky Way SMBH mass of $4 \times 10^6 M_\odot$ (Ghez et al., 2008), we would require an IMBH with mass roughly $10^5$ $M_\odot$ as the companion, independent of initial mass function. This IMBH mass is similar to the mass of the IMBH proposed to be responsible for ejecting stars in the central region of the Galaxy (Lang et al., 2011). This yields several IGS per square degree of sky and roughly tens of red giant hypervelocity IGS in the SDSS footprint[5].

Similar back of the envelope calculations suggest that there are $O(1000)$ L dwarfs located in the SDSS footprint, and realizing that late-type dwarfs are more common in general, we anticipate that the majority of our IGS candidates are likely L dwarfs. If these IGS candidates do turn out to be L dwarfs, then we have identified L-type dwarfs at distances of 100-200 pc, which is up to 4 times farther than currently known (Schmidt et al., 2010).

In an attempt to determine if the IGS sample has a distinct spatial distribution, we conducted a set of 2-dimensional K-S tests that compared our candidates with template samples drawn from 3 characteristic distributions: 1) an exponential disk with a scale height of 300 pc to mimic an old stellar population, and a distance cut off of 200 parsec to resemble an L dwarf distribution; 2) a random distribution; 3) and a set of observed hypervelocity stars (Brown et al., 2009). We convolved each template data set with the SDSS footprint and employed the same galactic latitude cut as in our IGS sample. Assuming that these are very cool dwarfs, the IGS sample should exhibit the same distribution on the sky as the exponential disk, but the 2-d K-S test revealed otherwise: the probability that these two samples come from the same underlying distribution is only $10^{-4}$. This is ultimately not surprising since we removed any objects with a measurable proper motion, strongly selecting against L dwarfs within the disk. The second test with a random

[5]We expand on the expected number of total IGS and red giant IGS in Appendix A.

distribution resulted in an even smaller probability of $10^{-5}$, while the third test with the hypervelocity sample yielded a somewhat higher probability of $10^{-2}$. Figure 2.6 shows the position of our IGS candidates on the sky compared to the hypervelocity sample used here.

## 2.6 Summary and Conclusions

We identified 677 intragroup stellar candidates from the SDSS DR7 using color cuts based on solar metallicity spectral standards. These are extremely red stars with $1.3 < i - z < 2.2$, though the color would shift bluer with lower metallicity. As shown in Figure 2.2, the M giants in the region are not completely isolated. The latest M dwarfs and early L dwarfs are possible sources of contamination.

Followup photometric observations of our candidates in the near to mid-infrared wavelengths may differentiate between late dwarfs and M giants. Future followup photometric observations with a 4m class telescope may be promising, albeit impractical. For example, the FLAMINGOS instrument on the NOAO 4m telescope could image all of our candidates with a 113 hour total exposure time in each of the J and H bands, and over 600 hours of total exposure time in the K band for a 10-sigma detection, while this likely would not be sufficient to distinguish M giants from dwarfs. Similarly, the J, H, and K magnitude limits of NIRI on Gemini are appropriate for our targets, although would require a prohibitively long total exposure time of 2031 hours to achieve a S/N of about 12.

Also, it is possible with long-term photometric followup observations on a 1m class telescope to differentiate between dwarfs and giants based on variability, as late-type M

Table II.1. IGS candidates remaining after all criteria cuts [Complete version provided in Appendix C].

| Object ID | RA | DEC | u | u err | g | g err | r | r err | i | i err | z | z err | r-i | i-z |
|---|---|---|---|---|---|---|---|---|---|---|---|---|---|---|
| 758882136836343139 | 60.5013 | 80.8760 | 24.4 | 1.3 | 24.7 | 0.6 | 24.3 | 0.7 | 22.0 | 0.2 | 20.3 | 0.2 | 2.3 | 1.7 |
| 758882137910740030 | 62.9212 | 82.5298 | 25.2 | 1.2 | 25.0 | 0.6 | 23.2 | 0.4 | 21.0 | 0.1 | 19.6 | 0.1 | 2.2 | 1.4 |
| 758882626993718584 | 63.3170 | 81.6950 | 26.5 | 0.6 | 24.8 | 0.6 | 25.3 | 0.7 | 22.0 | 0.2 | 20.3 | 0.2 | 3.3 | 1.6 |
| 758877527803168329 | 94.6323 | 63.7038 | 25.1 | 0.9 | 24.1 | 0.3 | 24.5 | 0.5 | 21.2 | 0.1 | 19.8 | 0.1 | 3.3 | 1.4 |
| 758877527266231607 | 94.8017 | 63.2633 | 24.6 | 0.7 | 24.4 | 0.5 | 24.5 | 0.6 | 21.8 | 0.1 | 20.4 | 0.1 | 2.7 | 1.4 |
| 758877527266493955 | 95.9369 | 63.5501 | 25.2 | 0.7 | 24.8 | 0.6 | 25.6 | 0.5 | 22.7 | 0.3 | 20.7 | 0.2 | 2.9 | 2.0 |
| 758878272976455144 | 105.3459 | 66.8553 | 25.3 | 0.9 | 24.4 | 0.4 | 24.1 | 0.4 | 21.8 | 0.1 | 20.2 | 0.1 | 2.3 | 1.6 |
| 758878271902778853 | 105.8427 | 66.0785 | 23.8 | 0.7 | 24.7 | 0.4 | 24.6 | 0.5 | 22.3 | 0.2 | 20.8 | 0.2 | 2.3 | 1.5 |
| 758884768580109918 | 107.9936 | 38.3022 | 24.8 | 1.1 | 25.1 | 0.7 | 24.4 | 0.6 | 21.9 | 0.1 | 20.4 | 0.2 | 2.6 | 1.4 |
| 587738067260998978 | 109.5721 | 39.4395 | 25.3 | 0.9 | 25.7 | 0.6 | 24.6 | 0.7 | 22.1 | 0.2 | 20.0 | 0.1 | 2.5 | 2.1 |

giants tend to be highly variable.

Naturally, low resolution spectroscopic follow-up observations of these IGS candidates would be ideal to confirm their luminosity class. The Calcium II Triplet (CaT) feature at 8498Å, 8542Å, and 8662Å is particularly useful for distinguishing late M dwarfs from giants, being much more prominent in the spectra of late-type dwarfs (Reid & Hawley, 2005). In addition, the strength of the Calcium Hydride (CaH) feature between 6800Å and 7000Å is a good indicator of luminosity class (Cohen, 1978).

Once the confirmation is complete, we can test the efficiency of our color selection technique, which will be useful for large data surveys like LSST. In fact, two surveys set to launch in the coming year will be particularly well-tuned to find IGS M giants. The DECam survey on the CTIO 4-meter telescope will observe over 1000 square degrees, with magnitude limits of r=23.4, i=24.0, and z=22.9 – over two magnitudes deeper than SDSS in z. An even deeper survey will launch on the Subaru telescope; the HyperSuprimeCam plans to observe 2000 square degrees down to z=24.9 and y=23.7. Eventually, deeper observations of IGS can reveal the metallicity of these stars – an important clue to their original birthplace within the group or in situ in the intergalactic medium.

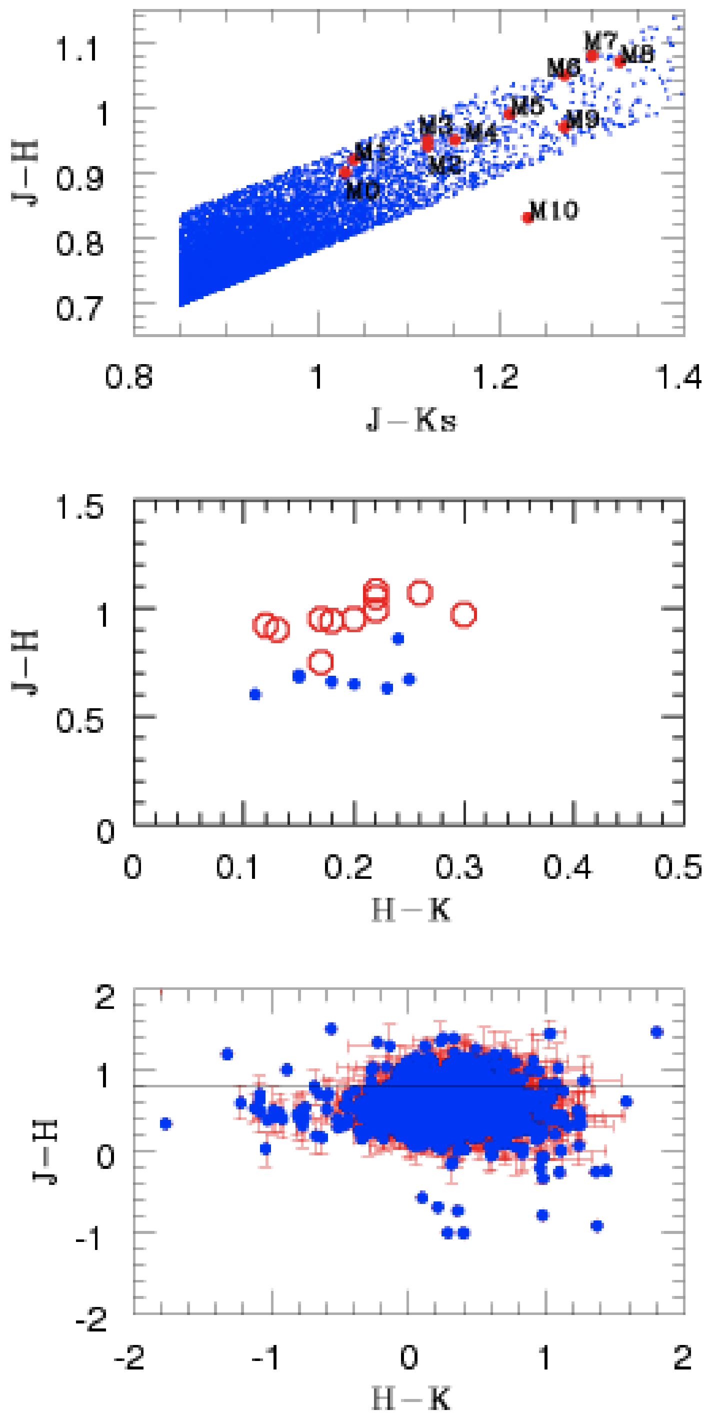


Figure 2.3: Top: Blue dots are SDSS Stripe 82 stars (Ivezić et al., 2007) that satisfy the Majewski et al. (2003) M giant color cuts. Larger red dots are M giants from Covey et al. (2007). The point located outside the color cut corresponds to an M10 spectral type. Also note that the late M giants (M7-M10) are located in the part of this color region that is least populated, so they will be least likely to be identified by this cut. Middle: Red open circles are M giants from Covey et al. (2007). Blue dots are M dwarfs from Covey et al. (2007). Bottom: IGS candidates with 2MASS JHK colors. The solid line represents the J-H = 0.8 separation between dwarfs and giants.

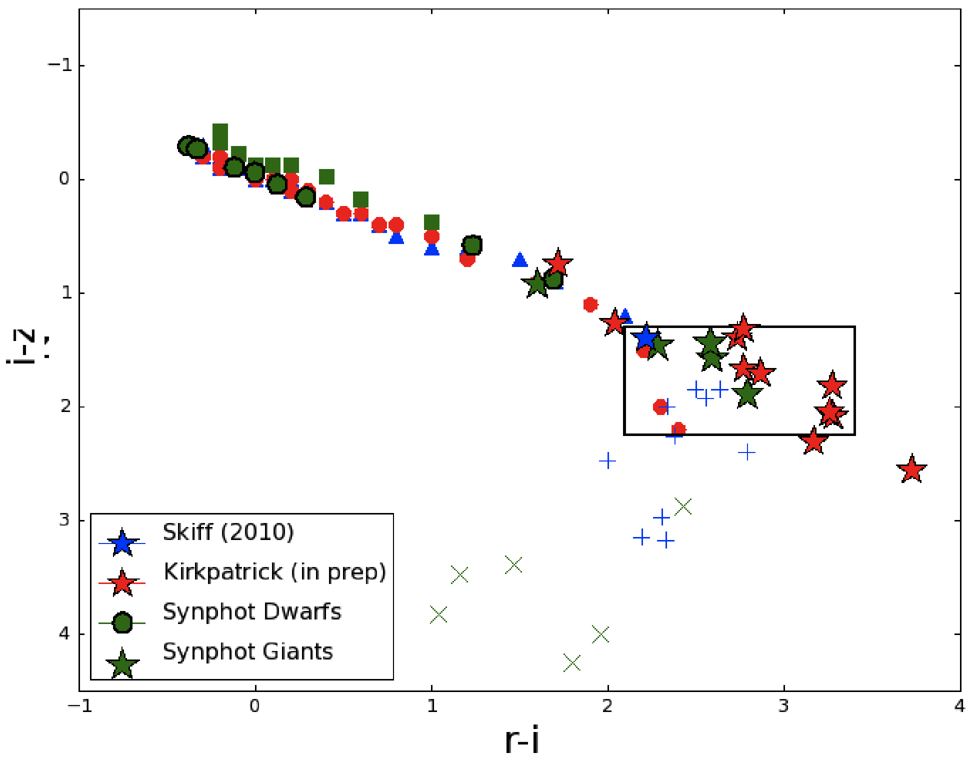


Figure 2.4: Same as the left panel of Figure 2.2. The green stars overplotted here represent M-giant standards, with spectral types between M6III and M8III, from the BPGS stellar atlas. The larger green dots are dwarfs with spectral types O through M, from the same atlas. The photometry for these stars was obtained by implementing IRAF *synphot* tasks. The blue star represents the M giant identified from the Catalogue of Stellar Spectral Classifications (Skiff, 2010) with confirmed SDSS photometry. The red stars are the M giant contaminants in the Kirkpatrick (in prep.) data for which we received spectra.

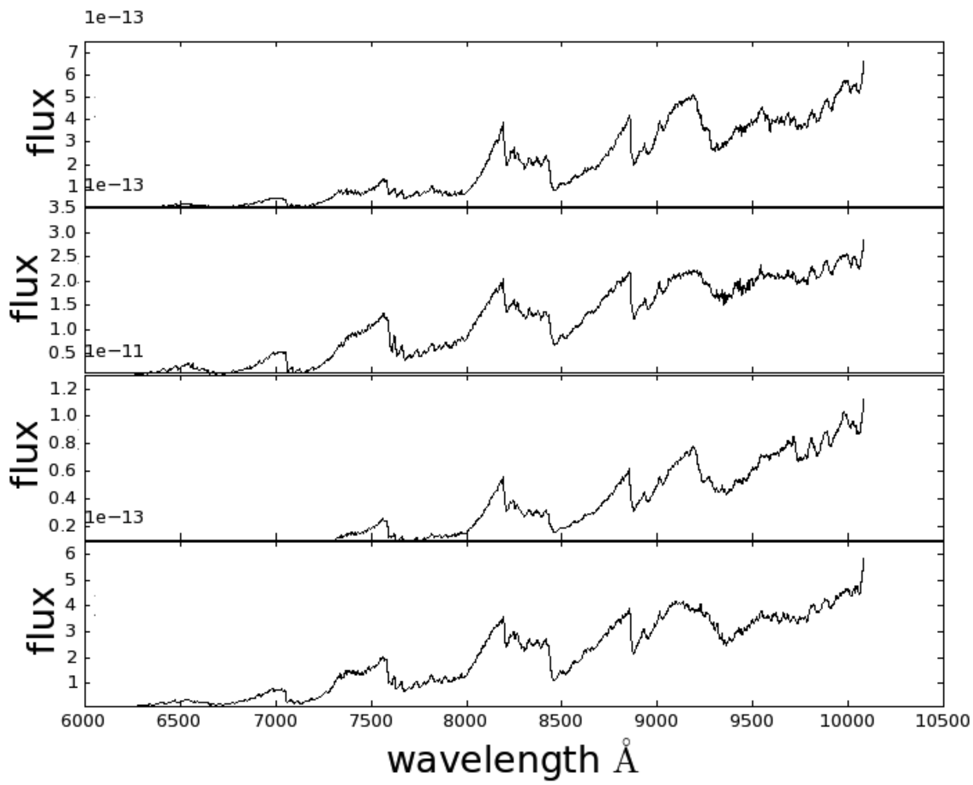


Figure 2.5: Four of the spectra used to compare colors to our IGS candidates. The resulting colors are shown in Figure 2.4.

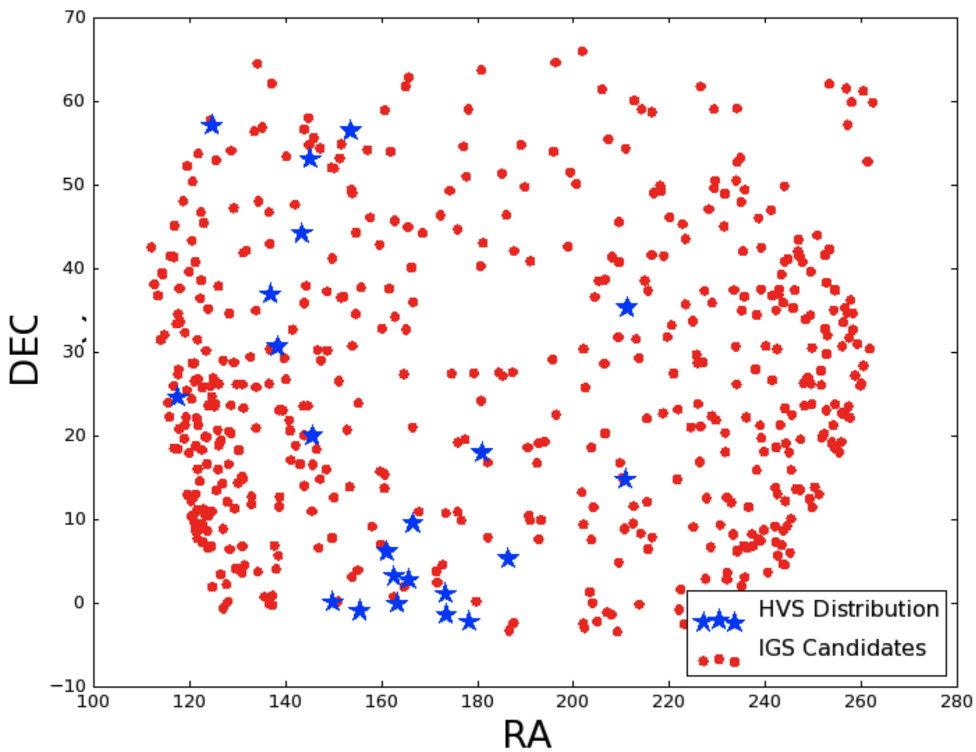


Figure 2.6: The relative positions of our IGS candidates and the hypervelocity stars of Brown et al. (2009) that were compared with the 2-d K-S test. The comparison was made between 522 IGS candidates, red dots, and 22 HVS, blue stars. Notice the higher density of IGS candidates at the edges of the footprint signifying larger numbers of these stars at lower Galactic latitudes.

# Chapter III

## HYPERVELOCITY STAR CANDIDATES IN THE SEGUE G & K DWARF SAMPLE

Here we reprint, in its entirety, work published in the Astrophysical Journal, 2014, Vol. 780, Article ID 7.

### 3.1 Abstract

We present 20 candidate hypervelocity stars from the Sloan Extension for Galactic Understanding and Exploration (SEGUE) G and K dwarf samples. Previous searches for hypervelocity stars have only focused on large radial velocities; in this study we also use proper motions to select the candidates. We determine the hypervelocity likelihood of each candidate via Monte Carlo simulations, considering the significant errors often associated with high proper motion stars. We find that nearly half of the candidates exceed their escape velocities with at least 98% probability. Every candidate also has less than a 25% chance of being a high velocity fluke within the SEGUE sample. Based on orbits calculated using the observed 6-d positions and velocities, few, if any, of these candidates originate from the Galactic center. If these candidates are truly hypervelocity stars, they were not ejected by interactions with the Milky Way's supermassive black hole. This calls for a more serious examination of alternative hypervelocity star ejection scenarios.

## 3.2 Introduction

Hypervelocity stars (HVSs) are believed to be ejected by three-body interactions with the supermassive black hole (SMBH) at the Galactic center (e.g., Hills, 1988; Yu & Tremaine, 2003; Brown et al., 2005). During this process, energy and angular momentum are transferred from the black hole to one of the stars in a binary system. The second star loses energy and becomes bound to the black hole while the first is ejected from the Galaxy. In this scenario HVSs can probe conditions in the Galactic center such as the binary fraction, and even place limits on the existence of a second, tightly bound SMBH. Semianalytical models predict that there may be approximately 100 HVSs within 8 kpc of the Galactic center due to the break up of equal-mass binaries (Gould & Quillen, 2003; Yu & Tremaine, 2003).

While the SMBH at the Galactic center remains the most promising culprit in generating HVSs, other hypervelocity ejection scenarios are possible, such as a close encounter of a single star with a binary black hole (Yu & Tremaine, 2003). In this case, the star gains energy from the binary black hole and is flung out of the Galaxy while the orbit of the black hole binary shrinks (e.g., Quinlan, 1996; Sesana et al., 2006). Another alternative hypervelocity ejection model involves the disruption of a stellar binary in the Galactic disk; here a supernova explosion in the more massive component can accelerate the companion to hypervelocities (e.g., Blaauw, 1961; Leonard & Dewey, 1993; Napiwotzki & Silva, 2012).

At least 18 HVSs have been discovered in the Milky Way within the past decade with velocities as high as 700 km $s^{-1}$ (e.g., Brown et al., 2005; Edelmann et al., 2005; Hirsch et al., 2005; Brown et al., 2009, 2012). So far, all confirmed HVSs are massive B-type stars such as those observed around the central SMBH (e.g., Brown et al., 2009, 2012). However, since the ejection mechanisms described above apply to any stellar mass, it is important to search for HVSs among the larger set of longer-lived, lower mass stars (e.g., Quinlan, 1996). If a SMBH ejection mechanism is at play, then metal-rich stars originating from the Galactic center ought to pollute the metal-poor halo. Previous attempts to mine Sloan Extension for Galactic Understanding and Exploration (SEGUE) and SEGUE-2 stellar halo data found no metal-rich, old ejected stars (Kollmeier et al., 2009, 2010). The lack of a significant population of old, metal-rich HVSs suggests that the initial mass function at the Galactic center is mildly top-heavy. Alternatively, hypervelocity ejection mechanisms may be more complex than previously thought.

In this paper we identify the first set of G- and K-type candidate HVSs from SEGUE. We discuss candidate selection in Section 3.2, including a description of the G and K dwarf sample, and we address the significant proper-motion errors in Section 3.3. Section 3.4 contains orbital parameters for the HVS candidates, and Section 3.5 discusses possible alternative origin scenarios. Finally, we summarize and conclude in Section 3.6.

## 3.3 Identifying HVS Candidates

Our candidates are drawn from the G and K dwarf stars in SEGUE (Yanny et al., 2009) from the Sloan Digital Sky Survey (SDSS) Data Release 9 (DR9; SDSS-III Collaboration et al., 2012). As part of SDSS (York et al., 2000b), SEGUE provides medium-resolution ($R \approx 1800$) spectroscopy over a broad spectral range (3800–9200 Å). Probing more than 150 lines of sight, SEGUE covers $\approx$3500 deg$^2$ of the sky, with spectroscopy of $\approx$240,000

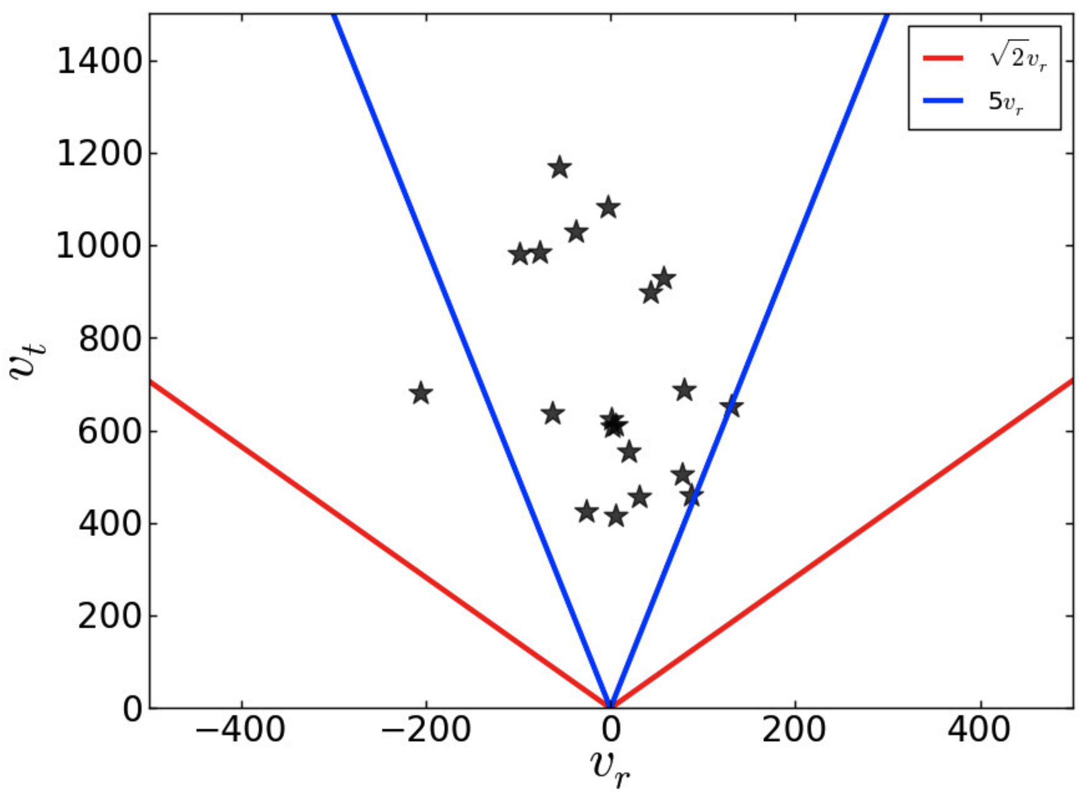


Figure 3.1: Transverse versus radial velocities of our HVS candidates, in kilometers per second. Red lines indicate a transverse velocity $\sqrt{2}$ times higher than the radial velocity, as expected for an isotropic stellar distribution. Blue lines represent a transverse velocity 5 times higher than the radial velocity. The majority of our candidates show large transverse-to-radial velocity ratios, characteristic of a sample strongly affected by large proper-motion errors. We caution that some of our HVS candidates may be high-velocity flukes, and we calculate the likelihood of this in Section 3.3.2.

stars over a range of spectral types. Technical information about SDSS has been published on the survey design (York et al., 2000b; Eisenstein et al., 2011), telescope and camera (Gunn et al., 1998, 2006), and spectrographs (Smee et al., 2013), as well as the photometric system (Fukugita et al., 1996b) and astrometric (Pier et al., 2003) and photometric (Ivezić et al., 2004) accuracy.

G and K dwarfs are selected from the SDSS photometric data using simple color and magnitude selection criteria. The 42,901 SEGUE G dwarfs are defined as having $14.0 < r_0 < 20.2$ and $0.48 < (g-r)_0 < 0.55$, while the 28,332 K dwarfs have $14.5 < r_0 < 19.0$ with $0.55 < (g-r)_0 < 0.75$ (Yanny et al., 2009). The subscript zero indicates that the color and magnitude have been corrected for dust extinction, using estimates derived from Schlegel et al. (1998). Each spectrum is analyzed with the DR9 SEGUE Stellar Parameter Pipeline (SSPP), which provides estimates of effective temperature, surface gravity ($\log g$), [Fe/H], and [$\alpha$/Fe] (Lee et al., 2008a,b; Allende Prieto et al., 2008; Smolinski et al., 2011; Lee et al., 2011). We follow the quality protocol of Schlesinger et al. (2012) to remove targets with poor signal-to-noise ratio (S/N <10), incalculable atmospheric parameters, excessive reddening (greater than 0.5 mag in $r$), saturated photometry ($r_0 < 15$), or flags indicating temperature or noise issues. We also use the SSPP $\log g$ estimates to ensure the stars are dwarfs, using a cut on $\log g$ as a function of [Fe/H] to isolate dwarf stars (K. J. Schlesinger et al. 2014, in preparation).

For each star that satisfies these criteria, we determine its distance using the isochrone-matching technique described by Schlesinger et al. (2012). Briefly, each star is matched in [Fe/H] and $(g-r)_0$ to 10 Gyr isochrones from the empirically corrected Yale Rotating Stellar Evolution Code set (An et al., 2009). There are systematic distance uncertainties introduced by using 10 Gyr isochrones, as well as the possibility of undetected binarity; this leads to a systematic shift in distance of $-3\%$ for the most metal-rich stars, while metal-poor stars are largely unaffected; this is factored into our distance estimates. There are also random distance errors from uncertainties in photometry, [Fe/H], [$\alpha$/Fe], and, finally, isochrone choice. The total random distance uncertainty is dominated by uncertainties in [Fe/H] and ranges from around 18% for stars with [Fe/H] $> -0.5\%$ to 8% for more metal-poor stars.

To identify HVSs, we convert the radial and tangential velocities to Galactic Cartesian coordinates, as described below in Section 3.4.1, and choose a simple but conservative initial total velocity threshold of 600 km s$^{-1}$ to identify stars that exceed the Galaxy's escape velocity (e.g.; Smith et al., 2007). We then verify that each candidate exceeds the escape velocity at its current location within the Galaxy. This procedure yields 42 preliminary HVS candidates of varying quality, which we further glean as described in Section 3.3.1 below.

## 3.4 Estimating the Fidelity of Our Candidates

### 3.4.1 Proper-Motion Quality Cuts

The proper-motion distribution in SDSS is skewed toward large proper-motion errors. We must ensure that the extreme velocities of our candidates are real rather than the product of large errors. We describe our technique to ensure the robustness of our candidates in this section. The first step in defining a clean hypervelocity sample is to assess the quality of the proper-motion measurement. To determine the proper motions for SDSS targets, Munn et al. (2004, 2008) matched each SDSS point source to the USNO-B catalog. The resulting SDSS+USNO-B catalog is 90% complete to $g$ <19.7 and has statistical errors of approximately 3−3.5 mas yr$^{-1}$ and systematic errors of ≈0.1 mas yr$^{-1}$ for each component.

Munn et al. (2004) defined a number of criteria to ensure that the SDSS+USNO-B proper motions are reliable; these conditions resulted in a version of the USNO-B catalog with a contamination of less than 0.5%. The criteria were later revised by Kilic et al. (2006) and are as follows[1]:

- The number of objects in USNO-B within a 1" radius of the SDSS target should be 1 (`match=1`).

- The rms residual for the proper-motion fit in right ascension and declination must be less than 525 mas (`sigRA < 525 and sigDEC < 525`).

- There must be at least six detections (including the SDSS observations) used to determine the proper motion (`nFit = 6`).

- The distance to the nearest neighbor with $g < 22$ must be greater than 7" (`dist22 > 7`).

Only three of our 42 preliminary candidates met all of the proper-motion quality criteria, and we categorize these as "Clean." We performed an in-depth analysis for the remaining 39 stars, assigning each a likelihood of proper-motion contamination based on the same criteria adopted by Kilic et al. (2006) for their white dwarf sample. They found

[1]The parameters listed in parentheses are available in the DR9 proper motions catalog in the SDSS Catalog Archive Server (CAS).

that the chance of contamination for a target with

- Six detections and a neighbor within 7" is less than1.5%;
- Five detections and no near neighbors is 1.5%;
- Five detections and a neighbor within 7" is 35%;
- Four detections and no neighbor within 7" is 51%; and
- Three detections and no neighbor within 7" is 89%.

We further checked for any potential blending issues by visually inspecting each candidate.

We categorize 17 stars as having "Reliable" proper motions, with 1.5% or less chance of contamination and no visual blending. We categorize 10 stars as "Possible," meaning they have between 35% and 51% chance of contamination. Twelve stars were removed because of visual blending.

We choose to consider only those candidates with "Clean" and "Reliable" designations. Thus, our final sample contains 20 HVS candidates, all with greater than 98.5% probability of robust proper-motion estimates.

We do expect that this final sample contains false-positive HVS detections. One way to illustrate this is with Figure 3.1, which compares the transverse and radial velocities of our HVS sample. For a random isotropic stellar distribution, the transverse velocity should be roughly $\sqrt{2}$ times higher than the radial velocity, and the fact that this sample is predominantly composed of stars with much larger transverse-to-radial velocity ratios is a classic signature of contamination by large proper-motion errors. While this does not prove that all of the candidates are spurious, it does indicate that many of them may be. Of course, a true hypervelocity sample would not be well represented by a random, isotropic distribution, but we caution that it is premature to say that we have identified 20 HVSs. We conducted further statistical tests, described below, to evaluate the likelihood that each HVS candidate is real.

### 3.4.2 Monte Carlo Sampling

Although the typical error in proper motion in the SEGUE database is $\sim$ 10 mas $\mathrm{yr}^{-1}$, proper-motion errors can, for some stars, be much larger than expected for a normal distribution, especially at the high-velocity end (Gould, 2003; Gould & Salim, 2003; Gould & Kollmeier, 2004; Munn et al., 2004, 2008; Bond et al., 2010). With this in mind, we consider the possibility that these HVS candidates may have true velocities much lower than can be explained by the reported errors and that they are in fact bound to the Galaxy.

In order to determine the true range of velocities for our HVS candidates, as well as the probability that these candidates are bound given a more realistic error distribution, we built a Monte Carlo simulation to sample possible orbital parameters for each HVS candidate. Dong et al. (2011) obtained a proper-motion error distribution for the SDSS+USNO-B catalog by compiling proper motions for a sample of SDSS quasars that met the Kilic et al. (2006) criteria. We randomly resampled a million realizations of each HVS candidate's kinematics from the Dong et al. (2011) non-Gaussian proper-motion error distribution and Gaussian radial velocity errors. We also resampled each candidate's position, assuming Gaussian errors in the distance determinations as well. We find that 13 of the 20 candidates remain hypervelocity with greater than 90% probability.

Figure 3.2 shows the distribution of velocities drawn randomly from the errors for the three least and most bound candidates. In most cases, the drawn velocity well exceeds the escape velocity, represented by the vertical dashed lines.

We performed a second Monte Carlo test to quantify the chance that these high velocities are simply the extreme tail end of the velocity error distribution within the entire SEGUE G and K dwarf sample. Here we construct a new mega-SEGUE sample built from 1000 realizations of each SEGUE star, in which each realization is drawn from the error distribution in proper motion, radial velocity, and distance as described above. We then calculate the "interloper likelihood" for each candidate with respect to the mega-SEGUE sample; this is the probability that a slow, noncandidate star within our sample could have had the observed velocity of a particular candidate, given the errors:

$$P(\text{interloper}, \mathrm{i}) = 1 - \frac{\mathrm{n_{HVS}}(\mathrm{v} \geq \mathrm{v_{cand,i}})}{\mathrm{n_{tot}}(\mathrm{v} \geq \mathrm{v_{cand,i}})}, \tag{3.1}$$

where $\mathrm{n}_{HVS}(v \geq v_{\mathrm{cand,i}})$ is the number of stars in the mega-SEGUE sample with velocity greater than or equal to the observed velocity of candidate $i$ that were originally tagged as hypervelocity in the data and $\mathrm{n}_{tot}(v \geq v_{\mathrm{cand,i}})$ is the total number of stars in the Monte Carlo sample with velocity greater than or equal to the candidate's velocity. All candidates have less than a 25% "interloper likelihood," and more than half have less than 10%. Together, these two tests indicate that some of our candidates may in fact be the result of a statistical fluke. However, we expect the bulk of the candidates to remain hypervelocity.

Table III.1 lists the velocity of each candidate determined from the proper motions reported in DR9, the minimum velocity calculated from a million realizations of the proper motion, radial velocity, and distance errors, the escape velocity for each candidate in a spherically symmetric Galaxy, the probability that the candidate may be bound given the escape velocity at its position, and the interloper likelihood as described above.

## 3.5 Orbits of HVS Candidates

### 3.5.1 Galaxy Model

We construct an analytical, multicomponent model of the Milky Way gravitational potential to predict the orbits of stars in the Galaxy based on the initial six-dimensional observed position and velocity. The model is easily modifiable and can be tuned to reflect the observed Galactic structural parameters.

Our model includes the following components: a central SMBH with $M_{\rm SMBH} = 4 \times 10^6 M_\odot$; a spherical Hernquist bulge (Hernquist, 1990) with $M_{\rm bul} = 4.5 \times 10^9 M_\odot$ and $r_{\rm bul} = 2.5$ kpc; Miyamoto–Nagai thin and thick disks (Miyamoto & Nagai, 1975) with $M_{\rm thin} = 6 \times 10^{10} M_\odot$, $M_{\rm thick} = 6 \times 10^9 M_\odot$, 0.3 kpc thin-disk scale height, 1 kpc thick-disk scale height, and 3 kpc scale lengths for both; and a Navarro–Frenk–White (NFW) dark matter halo (Navarro et al., 1997) following the formalism of Łokas & Mamon (2001); we chose $M_{\rm NFW} = 10^{12} M_\odot$, $R_{\rm vir} = 200$ kpc, and $c = 10$ for the Milky Way. Recent studies have argued for a shorter thick-disk scale length (e.g.; Cheng et al., 2012; Bovy et al., 2012b; Bensby et al., 2011); however, this change would have a negligible effect on our results because of the comparatively low mass of the thick disk component.

The model can also be tuned for varying degrees of axisymmetry or triaxiality in the halo. For this study we use both spherical and triaxial models. For the triaxial model, we adopt the axis ratios $b/a = 0.99$ and $c/a = 0.72$ (Law & Majewski, 2010).

The Galactic Cartesian coordinate system used here is centered on the Galactic center; the $x$-axis points from the center toward the Sun (located at $x = 8.2$ kpc (Schönrich, 2012)), the $y$-axis points along the direction of Galactic rotation, and the $z$-axis points toward the North Galactic Pole. To calculate velocity in this coordinate system, we convert radial velocity, distance, and proper motions to $U$, $V$, and $W$ in the Galactic coordinate system. Note that issues with astrometry in DR8, as explained in Section 3.3.5 of Aihara et al. (2011b) and the associated erratum (Aihara et al., 2011a), have been resolved for the DR9 astrometry used here. We choose the velocity of the local standard of rest to be 238 km s$^{-1}$, and the motion of the Sun with respect to that is $U = -13.8$ km s$^{-1}$, $V = 12.24$ km s$^{-1}$, and $W = 7.25$ km s$^{-1}$ (Schönrich, 2012; Schönrich et al., 2010). This Galactic model is consistent with the measured proper motion of SgrA*, $6.379 \pm 0.026$ mas yr$^{-1}$ (Reid & Brunthaler, 2004). Then, $U$, $V$, and $W$ are transformed into the Galactic Cartesian coordinate system, and we calculate the orbits backward in time for 1 Gyr using a fourth-order Runge−Kutta integrator. The choice of 1 Gyr is sufficient to discern the direction of origin while not being significantly influenced by a changing Galactic potential.

We examine the variation of each candidate's orbit given the errors described in Section 3.3.2. Figure 3.3 shows the $1\sigma$ and $2\sigma$ orbits for HVS 20, indicating that for some of the candidates the velocity errors are sufficiently large that the candidate itself may be bound. We find that the differences between orbits in the spherical versus the triaxial model are negligible for unbound orbits, since the stars have little time to respond to the halo potential. Therefore, for simplicity, when discussing unbound orbits we show only those in the spherical case. However, in instances when the orbit may be bound, as for HVS 20 in Figure 3.3, the halo shape definitely influences the candidate's trajectory, suggesting that marginally bound stars may help constrain halo triaxiality.

### 3.5.2 Origins

As shown in Figure 3.4, the trajectories of these HVS candidates do not originate from the Galactic center, which would be expected if the stars were ejected by three-body interactions with the SMBH. Instead, they appear to be coming from all directions, which suggests that other ejection processes may be at play.

We considered the SMBH at the center of M31 as a possible source (Sherwin et al., 2008), and given the velocities of the stars, we find the required flight time to reach the solar neighborhood would be approximately 1 Gyr. Figure 3.4 shows the orbits corresponding to the seven most unbound candidates, each with a $1\sigma$ "wedge" of possible orbits. It can be seen that the candidates could not have come from M31's SMBH position 1 Gyr ago (dashed lines). The orbits of the other 13 candidates are consistent with not arriving from M31. Therefore, the SMBH at the center of M31 is not responsible for ejecting these stars. However, this does not exclude other Galactic and extragalactic sources such as globular clusters, satellite galaxies, or the centers of distant galaxies within $\sim 10$ Mpc.

## 3.6 Discussion

### 3.6.1 Chemical Tracing

Since it is more difficult to trace the past orbits of globular clusters and known satellite galaxies because of tidal stripping, shocks, and other mass-loss effects, we cannot say with certainty whether these stars could have originated in the Galactic disk, the bulge, or globular clusters. Another approach to determine whether these candidates belong to a particular population is to examine their chemical compositions.

We compared the metallicities of our candidates with the metallicity distribution functions (MDFs) of known globular clusters (Harris, 1997), the SEGUE G and K dwarf samples representative of the Milky Way disk population (Schlesinger et al., 2012), the Galactic bulge (Sadler et al., 1996), and by extension the bulge of M31, assuming a peak metallicity of +0.23 (Jacoby & Ciardullo, 1999b). We also compared the metallicity distribution of our candidates with the MDF of the Galactic halo, although with a peak at [Fe/H] $< -1$ (An et al., 2013) it is clearly inconsistent with our candidates.

The MDFs for each population are shown in Figure 3.5. As perhaps expected, the metallicity of the HVS candidates is consistent with the G and K dwarf samples in the disk. Their metallicities are also largely consistent with the high-metallicity end of the globular cluster population and the low-metallicity end of the Galactic (and M31) bulge. Similarly, the stars' [$\alpha$/Fe]-values are broadly consistent with these stellar populations. Unfortunately, based on the information here, none of these populations can be decisively ruled out as a possible source, although it is clear that these HVSs do not originate from the metal-poor globular cluster system.

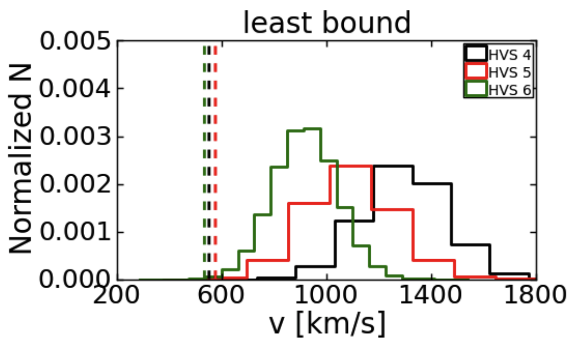


Figure 3.2: Velocity distribution for a million random samples of the velocity error distribution for the three least and most bound HVS candidates. Dashed lines show escape velocity of each candidate.

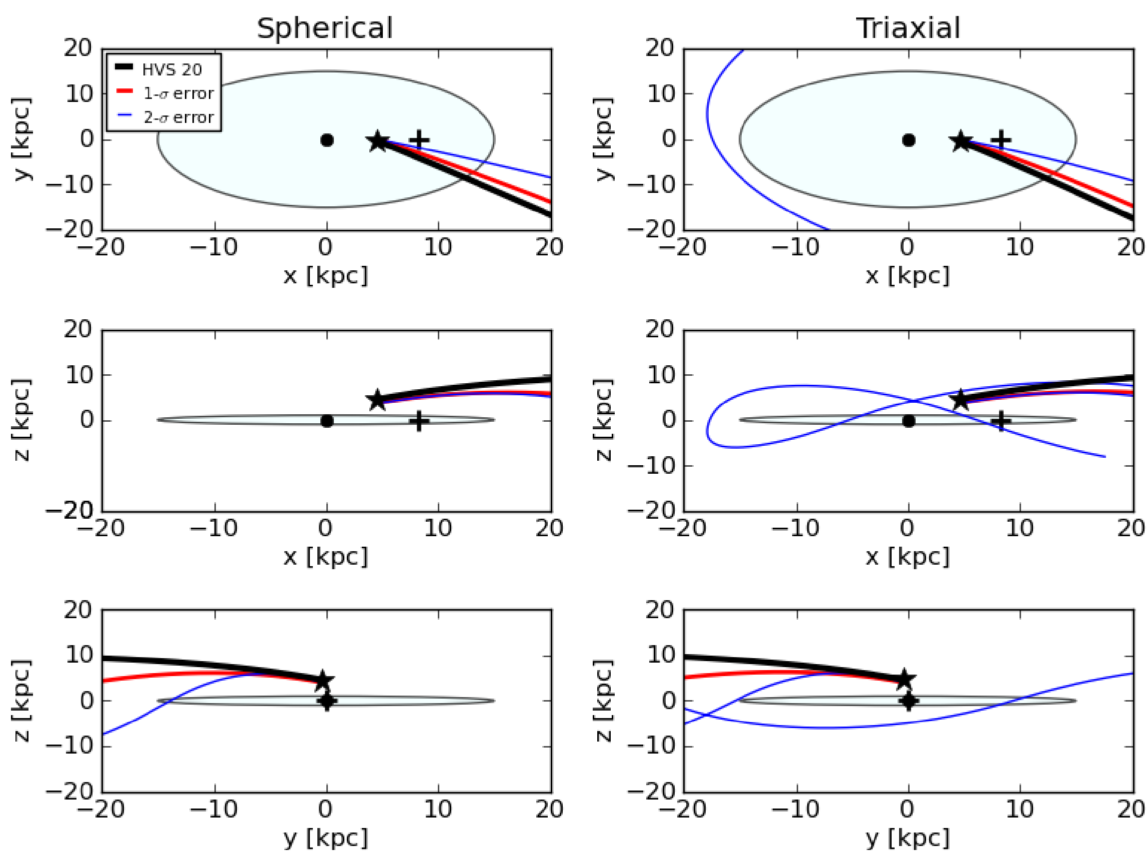


Figure 3.3: Orbit of HVS 20, a candidate with a "Reliable" proper-motion measurement but the largest probability of being bound, shown by the black lines. Also shown are the resulting orbits for the same candidate with $1\sigma$ (red lines) and $2\sigma$ (blue lines) velocity errors from the million Monte Carlo realizations. Left, two-dimensional projections in the spherical dark matter halo; right, the same for the triaxial model. The black dots and plus signs represent the locations of the Galactic center and the Sun, respectively, while the pale blue ellipses provide a rough scale for the extent of the disk. The five-pointed star in each panel marks the current position of HVS 20. The top row is a top-down view of the Galaxy while the middle and bottom rows are side views along the disk. Here we show that some candidates may in fact live on very bound orbits, and in such cases the shape of the orbit is strongly influenced by the triaxiality of the halo.

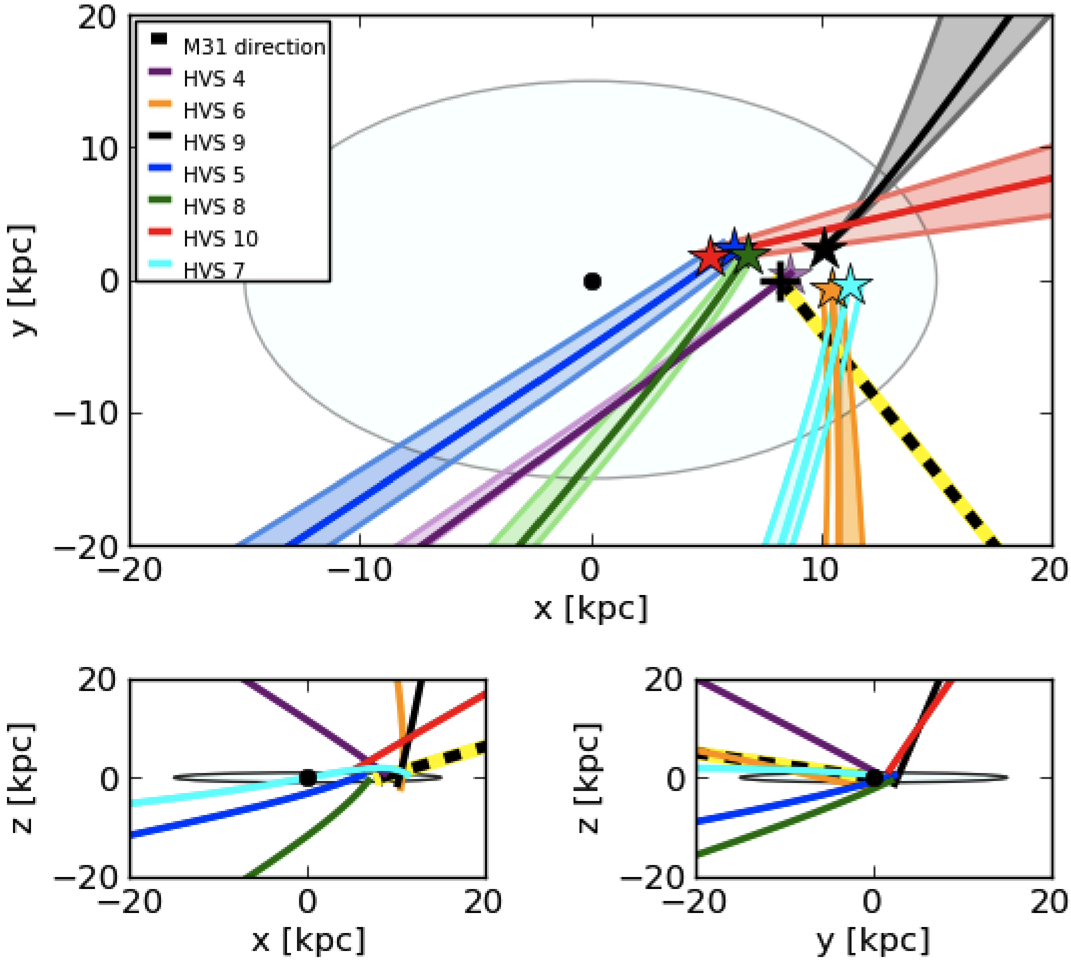


Figure 3.4: Orbits of the seven HVS candidates that are unbound with at least 98% proability, over the past 1 Gyr. As in Figure 3.3, the black dots and plus signs represent the locations of the Galactic center and the Sun, respectively, while the pale blue ellipses provide a rough scale for the extent of the disk. The shaded regions flanking the orbits of the same color represent the "wedges" of possible orbits given the $1\sigma$ velocity errors for the corresponding candidate. The like-colored stars mark the current positions of the candidates. None of the orbits plotted here intersect near the Galactic center, suggesting a different origin for these stars. In additional, if these stars had been traveling for 13 Gyr, they may have originated from as far as tens of megaparsecs away. The dashed lines, highlighted in yellow for visibility, point toward M31's location 1 Gyr ago, assuming M31 proper motion, radial velocity, and distance from Sohn et al. (2012). This interval was chosen to roughly coincide with the travel time of a hypervelocity star originating in M31. None of these HVS candidates seem to be coming from M31, which therefore is ruled out as a possible origin.

Table III.1. Stellar and kinematic parameters for the 20 HVS candidates.

| HVS | IAU Name | $r_0$ | [Fe/H] | [$\alpha$/Fe] [a] | d (kpc) | $v_r$ [b] | $v_t$ [c] | $v$ [d] | $v_{\rm min}$ [e] | $v_{\rm esc,Sph}$ [f] | % Bound | "Interloper Likelihood" | Rating |
|---|---|---|---|---|---|---|---|---|---|---|---|---|---|
| 1 | $J$060306.77 + 825829.1 | 18.07 | −0.06 | 0.10 | 3.70 | −76.0 | 56.1 | 802.2 | 92.2 | 533.6 | 6.35 | 0.02 | Clean |
| 2 | $J$023433.42 + 262327.5 | 19.01 | −0.15 | 0.09 | 5.68 | −25.6 | 15.7 | 628.6 | 290.0 | 517.3 | 7.43 | 0.18 | Clean |
| 3 | $J$160620.65 + 042451.5 | 19.01 | −0.91 | 0.40 | 4.06 | 31.7 | 23.7 | 641.8 | 195.1 | 588.9 | 34.88 | 0.15 | Clean |
| 4 | $J$113102.87 + 665751.1 | 16.15 | −0.83 | 0.46 | 1.04 | −54.9 | 237.7 | 1296.7 | 587.4 | 552.3 | 0.0 | 0.00 | Reliable |
| 5 | $J$185018.09 + 191236.1 | 18.16 | −0.34 | 0.19 | 3.19 | 58.0 | 61.5 | 1086.8 | 378.9 | 576.5 | 0.04 | 0.00 | Reliable |
| 6 | $J$035429.27 − 061354.1 | 18.07 | −0.55 | 0.26 | 3.13 | 80.2 | 46.2 | 916.3 | 286.6 | 534.5 | 0.07 | 0.01 | Reliable |
| 7 | $J$064337.13 + 291410.0 | 18.01 | −0.55 | 0.35 | 3.06 | 20.4 | 38.1 | 793.9 | 285.0 | 530.2 | 0.30 | 0.02 | Reliable |
| 8 | $J$202446.41 + 121813.4 | 17.74 | −0.65 | 0.26 | 2.48 | 6.26 | 51.8 | 769.1 | 376.3 | 570.3 | 1.01 | 0.03 | Reliable |
| 9 | $J$011933.45 + 384913.0 | 18.26 | −0.67 | 0.22 | 3.31 | −36.9 | 65.5 | 937.3 | 185.2 | 536.3 | 1.20 | 0.00 | Reliable |
| 10 | $J$172630.60 + 075544.0 | 18.46 | −0.67 | 0.39 | 3.82 | −2.2 | 59.7 | 992.9 | 233.5 | 591.0 | 1.34 | 0.00 | Reliable |
| 11 | $J$073542.35 + 164941.4 | 18.35 | −0.23 | 0.12 | 3.70 | 78.2 | 28.8 | 712.9 | 285.4 | 527.3 | 2.89 | 0.07 | Reliable |
| 12 | $J$025450.18 + 333158.4 | 18.25 | −0.70 | 0.16 | 3.14 | −62.4 | 42.8 | 731.4 | 265.1 | 532.9 | 3.77 | 0.05 | Reliable |
| 13 | $J$134427.80 + 282502.7 | 18.32 | −1.27 | 0.44 | 2.91 | 2.5 | 44.0 | 715.7 | 270.5 | 557.0 | 4.42 | 0.07 | Reliable |
| 14 | $J$225912.13 + 074356.5 | 18.76 | −0.56 | 0.37 | 4.60 | −97.8 | 44.9 | 840.7 | 121.8 | 550.0 | 5.86 | 0.01 | Reliable |
| 15 | $J$095816.39 + 005224.4 | 17.51 | −0.80 | 0.28 | 2.22 | 1.6 | 59.2 | 649.8 | 248.7 | 546.5 | 15.98 | 0.14 | Reliable |
| 16 | $J$074728.84 + 185520.4 | 17.81 | −0.24 | 0.13 | 3.26 | 43.9 | 58.1 | 672.8 | 55.3 | 530.7 | 19.70 | 0.11 | Reliable |
| 17 | $J$064257.02 + 371604.2 | 16.87 | −0.33 | 0.21 | 1.78 | 6.2 | 49.1 | 601.4 | 305.4 | 540.9 | 20.01 | 0.24 | Reliable |
| 18 | $J$165956.02 + 392414.9 | 19.22 | −1.14 | 0.48 | 4.35 | −205.1 | 33.0 | 649.1 | 170.0 | 562.3 | 21.30 | 0.14 | Reliable |
| 19 | $J$110815.19 − 155210.3 | 19.01 | −0.99 | 0.35 | 4.56 | 131.2 | 30.1 | 622.7 | 162.0 | 545.8 | 23.69 | 0.19 | Reliable |
| 20 | $J$145132.12 + 003258.0 | 19.47 | −0.59 | 0.12 | 5.88 | 88.0 | 16.5 | 606.7 | 193.1 | 579.8 | 43.24 | 0.23 | Reliable |

[a] Note there are large uncertainties in these measurements at the S/N of these candidates.

[b] Radial velocity, in km $s^{-1}$, is taken straight from the SSPP without any corrections.

[c] Total proper motion, in mas $yr^{-1}$, is calculated from the $\mu_{RA}$ and $\mu_{Dec}$ values listed in the CAS without any corrections.

[d] This is the total velocity of the candidate, in km $s^{-1}$, after conversion to the Galactic Cartesian coordinate system described in §4.1, before any error consideration.

[e] The value here is the minimum total velocity, in km $s^{-1}$, determined from a million realizations of proper motion, radial velocity, and distance errors drawn from their distributions described in Section 3.3.

[f] The escape velocity, in km $s^{-1}$, at the star's position in a spherical potential.

### 3.6.2 Alternative Origins

As shown in Figure 3.4, none of the HVS candidates are coming from the Galactic center or from the direction of M31. The popular ejection mechanisms described inSection 3.1 involve a central SMBH and cannot explain these stars. The question where these stars originated, and how they gained such high velocities, remains.

One of the best-known hypervelocity mechanisms involves a binary system in the disk, in which a supernova explosion ejects the companion star (e.g.; Blaauw, 1961). There are many lesser known hypervelocity ejection mechanisms as well. For example, multibody ejections from the dense central regions of globular clusters (e.g.; Poveda et al., 1967) including globular clusters that may have dissipated over the lifetime of the Galaxy (e.g.; Gnedin & Ostriker, 1997; Chernoff & Weinberg, 1990; McLaughlin & Fall, 2008) may boost a star to hypervelocities. In addition, there could be a three-body interaction involving an intermediate-mass black hole or otherwise very massive star (e.g.; Gvaramadze et al., 2009). A final hypervelocity ejection mechanism involving a stellar dynamical process could be the partial tidal disruption of a single star around a SMBH (Manukian et al., 2013).

Furthermore, three-body interactions between galaxies, such as M31 (e.g.; Caldwell et al., 2010) and the Large and Small Magellanic Clouds (e.g.; Chandar et al., 2010), have been suggested as possible hypervelocity ejection mechanisms, although we have already ruled out M31 specifically. HVSs may also receive an energy boost during the tidal stripping process as long streams are stripped from an accreted satellite (e.g.; Abadi et al., 2009; Caldwell et al., 2010; Piffl et al., 2011; Fouquet et al., 2012; King et al., 2012).

### 3.6.3 Follow-up Analysis

A significant fraction of the candidates failed the `dist22` > `7` requirement, meaning that photometric blending from a near neighbor may have affected the proper-motion determination. A larger number of the candidates suffer from too few detections in the SDSS+USNO-B catalog. Confirming these candidates as HVSs would require additional astrometric analysis in order to verify their proper motions; the *Hubble Space Telescope* Fine Guidance Sensor may be appropriate.

There is also the possibility that these candidates are unresolved spectroscopic binaries, which could imprint a large radial velocity signal. Future, higher resolution spectroscopic observations could easily decide this issue and would also allow a more detailed chemical analysis to shed light on their origins.

### 3.6.4 Constraints on the Initial Mass Function

The fact that we find no low-mass HVSs coming from the Galactic center continues to pose a problem for a universal initial mass function and an unbiased binary ejection mechanism. If we simply assume a Salpeter initial mass function and a mass-blind dynamical process, we would naively expect roughly 150 HVSs in the $0.6-1.2$ solar mass range in our sample, compared with the 14 known $3-4$ $M_\odot$ HVSs (Brown et al., 2009). Either the initial mass function near the Galactic center is top-heavy or the process acting at the Galactic center ejects over 10 times more high-mass stars than low-mass ones. There is tentative evidence from the Arches and other young star clusters at the Galactic center that the initial mass function is top-heavy, with a slope of about $-1.6$ (Figer et al., 1999), although this is a matter of debate. If we adopt this slope for our initial mass function, then we still should have observed roughly 40 HVSs with spectral types G and K, which would require an ejection mechanism that favors massive stars by more than factor of 3[2].

Our constraints on the initial mass function are consistent with the findings of Kollmeier et al. (2010), who searched for metal-rich F/G halo HVSs. This earlier study placed stricter limits on the ejection mechanism, however, because F/G stars would be expected to accumulate in the halo over their main-sequence lifetimes, while our sample probes only stars passing through the solar neighborhood; stars ejected from the Galactic center through stellar binary disruption, for example, would reach and pass through our sample in mere tens of millions of years. Our results are also consistent with the constraints from Zhang et al. (2013), who considered the S stars at the Galactic center to be the captured companions of binary star tidal disruption, a process that ejects the second star.

[2]We expand on the determinations of the expected number of HVSs in Appendix D.

## 3.7 Summary and Conclusions

We report a set of 20 hypervelocity candidates from the SEGUE G and K dwarf sample. These candidates have velocities greatly exceeding the escape velocity at their respective positions in the Galaxy, albeit with large proper-motion errors. Monte Carlo estimates of the position and kinematics of these stars show that seven of the 20 exceed the escape velocity at their respective locations within the Galaxy with at least 98% probability and that each candidate's interloper likelihood is less than 25%.

Surprisingly, an orbit analysis indicates that none were ejected from the Galactic center. The confirmation of these candidates as HVSs argues for a more careful exploration of alternative ejection mechanisms such as interactions within globular clusters, dwarf galaxies, or tidal tails, as well as ejections from supernovae in the Galactic disk.

If these stars are truly hypervelocity, their spectra could already contain clues to their origin. For example, abundance patterns indicative of supernova contamination would confirm or rule out a candidate's having been ejected from a high-mass binary system (Przybilla et al., 2008).

One remaining question is why these stars were not identified in previous HVS campaigns. A possibility is that prior searches focused on extreme radial velocities (e.g.; Brown et al., 2005). While the radial velocities of our candidates are relatively modest, it is the addition of proper motions that boosts these stars into hypervelocity candidacy. Naturally, our sample also explored a cooler spectral type than previous work. Future surveys may be more successful in identifying HVSs with both radial velocity and proper-motion measurements.

We are expanding our search for HVS candidates to the entirety of the SDSS DR9 sample in order to include all spectral types. Analysis of any additional candidates identified in this search, as well as follow-up, is deferred to a future paper.

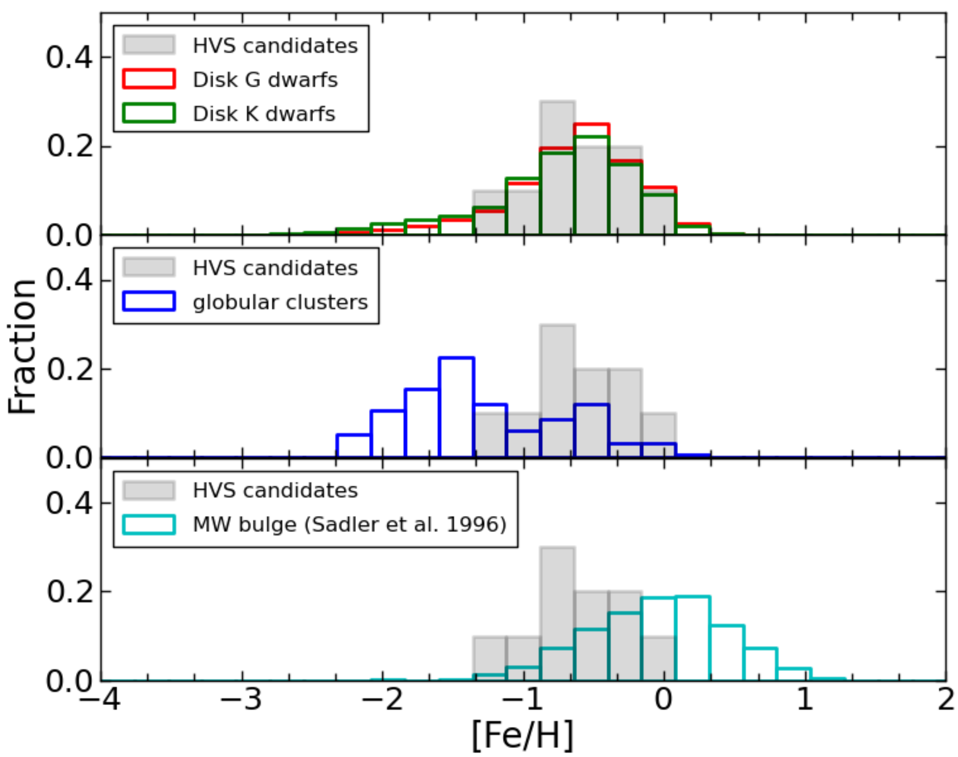


Figure 3.5: Normalized metallicity distribution functions of our candidates (shaded), compared with G dwarfs (red), K dwarfs (green), globular clusters (blue), and the Galactic bulge (cyan).

# Chapter IV

# WORK IN PROGRESS

## 4.1 A Global Search for G/K-type Hypervelocity Stars

### 4.1.1 Motivation

The G- & K-dwarf sample of Schlesinger et al. (2012), used in Palladino et al. (2014), was carefully selected to be representative of the disk around the Solar neighborhood. This sample, while statistically robust, introduces selection biases in a search for hypervelocity stars. Even if a HVS is ejected through interactions within the disk, the timescales on which HVSs traverse the Galaxy are such that we should not necessarily expect to find them lingering in the Solar neighborhood.

A true HVS found within the disk may be explained by a very recent, nearby, disk ejection (e.g.; Blaauw, 1961). Alternatively, the HVS could be 'just passing through' as a hypervelocity interloper originating from another region of the Galaxy, likely the bulge (e.g.; Hills, 1988; Brown et al., 2005, 2012). The area of the Solar neighborhood targeted by the Schlesinger et al. (2012) sample is such that either scenario would not contribute significantly to the total HVS population. Conversely, assuming an un-biased ejection geometry, regardless of origination site, it is more likely that HVSs are quickly flung out into the halo. So, while there are many advantages of using the G- and K-dwarf sample of Schlesinger et al. (2012), this section is dedicated to performing a global search for G/K-type HVSs within the SEGUE database by loosening the selection criteria to include stars outside the disk as well.

### 4.1.2 Candidate Selection

The global search for G/K-type hypervelocity stars was performed with a query of the twelfth and final data release of SDSS-III by selecting stars with extinction corrected $(g-r)_0$ colors and $r_0$ magnitudes indicative of G and K-type stars, as described in Section 3.3. The query returned 120,679 G-type stars and 173,790 K-type stars.

Subsequently, we remove any star for which effective temperature, surface gravity, spectral type, metallicity, or radial velocity were not determined (ie. values of -9999 or "unknown"). This cut results in 130,990 targets. We follow the additional quality assurances of Schlesinger et al. (2012) which also considered poor signal-to-noise, excessive reddening, saturation, and flags assigned by the SSPP. We do not, however, consider the magnitude limit and distance cuts of Schlesinger et al. (2012). Then, we apply the proper motion quality criteria of Kilic et al. (2006) and retain only those stars that satisfy the "clean" designation, described in section 3.4.1. This step results in a sample of 103,238 G/K-type stars.

An estimation of the distance to each star was determined by employing the distance modulus with average absolute magnitudes assigned by the following equation (Ivezić et al., 2008):

$$M_r = -2.85 + 6.29(g-i) - 2.30(g-i)^2 + \Delta M_r, \tag{4.1}$$

where

$$\Delta M_r = 4.50 - 1.11[\mathrm{Fe/H}] - 0.18[\mathrm{Fe/H}]^2. \tag{4.2}$$

Absolute magnitudes determined from this method are accurate to within 0.1 magnitude only for stars with $0.3 < (g-i) \leq 1.0$ (Ivezić et al., 2008). Finally, dwarfs were separated from giants with a simple log(g) cut at 3.5; dwarfs with log(g) > 3.5 and giants with log(g) < 3.5. There are 85,268 G- and K-dwarfs (17,970 giants).

To identify hypervelocity star candidates, we convert the radial and tangential velocities to Galactic Cartesian coordinates and choose the same initial total velocity threshold of 600 km/s as in Section 3.3, and a maximum velocity cut of 10,000 km/s. Again, as in Palladino et al. (2014), we require that each candidate exceed the escape velocity at its current location within the Galaxy. This procedure yields 28 HVS candidates.

### 4.1.3 Preliminary Results

As an initial comparison of the results of the global search to the sample of Schlesinger et al. (2012), we compare the positions of the samples on the sky in Figure 4.1. We note that both samples cover the SDSS footprint. The differences in the bottom panels of Figure 4.1 are due to the distance cuts placed by Schlesinger et al. (2012) to isolate a population of disk stars.

The HVS candidates presented in Palladino et al. (2014) have transverse velocities significantly greater than their radial velocities (cyan 5-pointed stars in Figure 4.2), an indication of a sample contaminated by large proper motion errors. We perform the same comparison of transverse and radial velocities for the HVS candidates identified from the global search for G/K-type stars (magenta 5-pointed stars in Figure 4.2). We find that this sample is not biased in velocity– if anything, there are more candidates with velocities dominated by the radial component, which is a reasonable expectation for a population of HVSs zipping out of the Galaxy.

Finally, at this stage of the investigation we look at the distributions of total velocity, Figure 4.3, and metallicity, Figure 4.4. We find the majority of the global-search HVS candidates have comparable velocities to the HVS candidates published in Palladino et al. (2014).

We also note that the metallicity distribution is bimodal (potentially trimodal) and does not strongly resemble any of the comparison populations– published HVS candidates, disk G/K-dwarfs, globular clusters, and bulge stars. The high-metallicity peak at [Fe/H] $> -0.5$ is especially interesting. Perhaps we are seeing a composite population of artificially velocity-boosted halo field stars and ejected bulge stars.

### 4.1.4 Discussion

The results presented in the previous section are preliminary and require further consideration. One critical question that needs to be addressed before publication is: If the Schlesinger et al. (2012) sample of G/K-dwarfs is only a subset of the global search for G/K-type stars, why did we not recover the HVS candidates of Palladino et al. (2014)?

Other, marginally less perplexing, questions include: Why did we need to enforce a maximum velocity cut of 10,000 km/s? and: Are the distances determined by equation 4.1 compared to the distances determined by Schlesinger et al. (2012), especially considering that we did not restrain the $g - i$ color of the sample to the range deemed valid for equation 4.1 (Ivezić et al., 2008)?

Once the initial candidate selection is refined, we can start to answer the more interesting science questions. To establish the probability that the candidates are HVSs requires errors on the distance determinations, which at present, we do not have (but can obtain by convolving the errors on the stellar parameters). Orbits for each candidate will need to be calculated to determine their place of origin, and whether a SMBH ejection can explain any or all of the new candidates. Furthermore, as an initial pass, we segregated the giants out for a fair dwarf-to-dwarf comparison. However, we ultimately want to consider the giants in the global sample as well and what they might contribute to the unbound stellar population in the Milky Way.

## 4.2 F-type Hypervelocity Star Candidates

### 4.2.1 Motivation

Since there are 18 confirmed O/B-type HVS, consistent with SMBH ejection (Brown et al., 2012) we know that the Hills mechanism operates at the center of the Galaxy. If we add that Palladino et al. (2014) found zero low-mass HVS candidates originating from the Galactic Center, we have compelling evidence that the ejection mechanism may preferentially boost only the most massive stars to hypervelocities and/or that the initial mass function at the Galactic center is extremely top-heavy. Now, we search for HVS candidates within a sample of SDSS F-type stars as an attempt to populate the intermediate mass range to constrain the mass-dependence of the ejection mechanism.

The sample we use for this search is adapted from the sample of Allende Prieto et al. (2014), originally selected to study abundances in the Sloan survey. I combine the distances determined by Fernandez-Alvar et al. (in prep) with proper motions, radial velocities, and stellar parameters from the SDSS Catalog Archive Server (CAS). The sample contains 12,673 F-type stars.

### 4.2.2 Candidate Selection

From the initial sample of 12,673 F-type stars, we perform a similar cleaning procedure as described in the sections above. First, we remove stars with undetermined effective temperature, metallicity, or surface gravity. Then, we apply the proper motion quality criteria of Kilic et al. (2006) and retain only those stars that satisfy the "clean" designation, described in section 3.4.1. This step results in a sample of 11,779 F-type stars.

Similarly, we separate dwarfs from giants with a cut on surface gravity at 3.5. This cut returns 10,590 F-dwarfs and 1,189 F-giants. For this sample, we rely on the distances determined by Fernandez-Alvar et al. (in prep).

F-dwarf hypervelocity star candidates are identified via the same procedure outlined in section 4.1.2. We find 98 preliminary HVS candidates with $v > 600$ km/s and 95 candidates with $v > V_{esc}$. With both distance and distance errors provided by Fernandez-Alvar et al. (in prep) we are able to initiate the statistical analysis stages of the investigation. Via Monte Carlo simulations, described in detail in section 3.4.2, we find that 34 of the preliminary F-dwarf HVS candidates are unbound at least 90 % of the time and 8 are unbound at least 95% of the time.

### 4.2.3 Preliminary Results

We identified 95 F-dwarf HVS candidates with total velocities exceeding the escape velocity at their respective locations. We performed the first statistical test to determine each candidate's probability of being bound to the Galaxy, described in Palladino et al. (2014) and section 3.4.2. We identified 34 F-dwarf HVS candidates that are unbound with at least 90% probability and 8 F-dwarf HVS candidates with at least 95% probability.

Figure 4.5 shows the velocity distribution of the 8 highly unbound candidates compared to the sample of 95 F-dwarf candidates. The F sample yields an overall similar distribution to that of the global G- and K-dwarf sample in section 4.1– the majority of the candidates with $v_{tot} < 2000$ km/s and a tail extending to much higher velocities at $\sim 6000$ km/s.

Figure 4.6 shows the metallicity distribution of the 95 F-dwarf HVS candidates and the 8 candidates that comprise the highly unbound subgroup. The F-dwarf HVS candidates are much more metal poor than even the F sample from which they were selected. However, the 8 highly unbound candidates, with a peak at [Fe/H] $\sim -1.7$, roughly align with the metal-poor peaks of both the F sample and globular cluster distributions.

#### 4.2.4 Discussion

The results presented in the previous section are preliminary and require further consideration. We are currently awaiting updated distance determinations for the F-star sample. Once in hand, we will be able to fully characterize any HVS candidates within the sample as was done in Palladino et al. (2014), including orbits and all statistical tests. We would also like to compare the distances determined by the methods of Allende Prieto et al. (2006, 2014) and Fernandez-Alvar et al. (in prep) to the distances determined by equation 4.1.

Again, we plan to ultimately consider F-giants as well, but for reasons outlined in Section 4.1.2 we postpone their analysis to a later date.

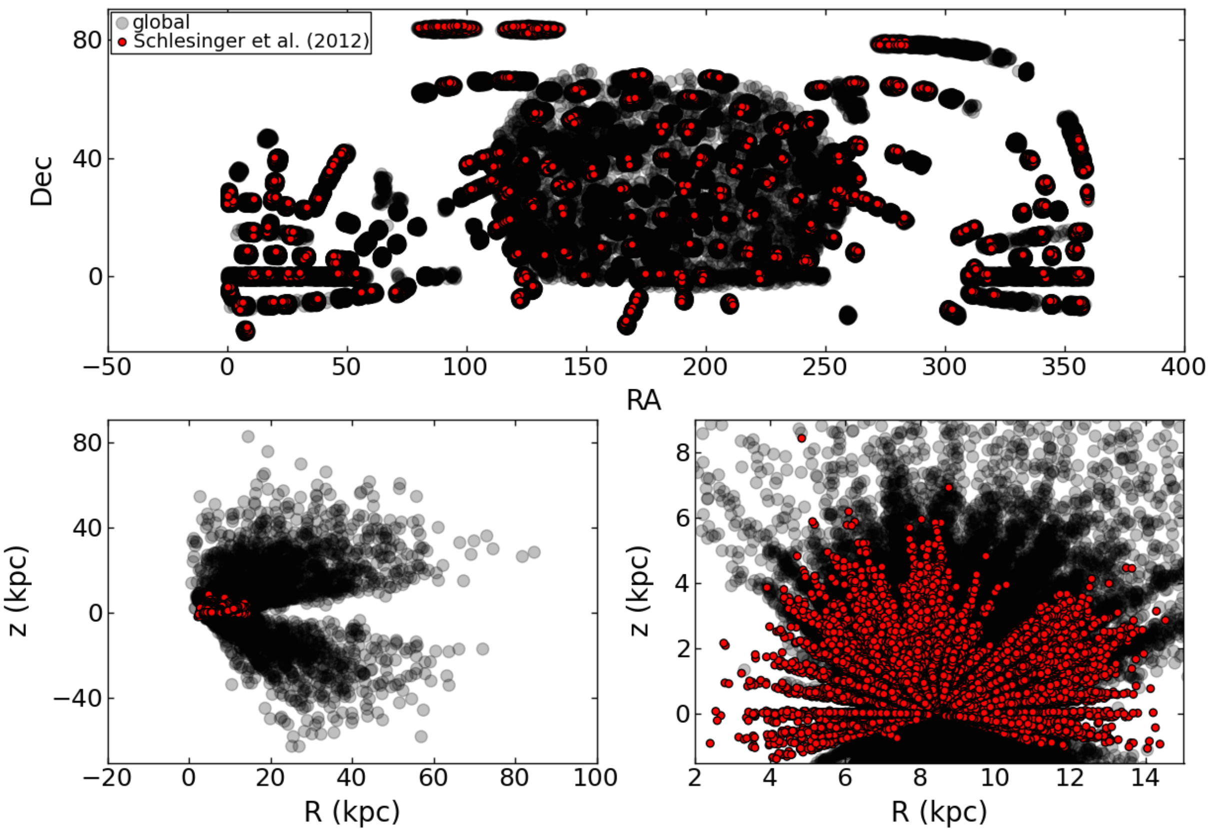


Figure 4.1: Top: Equatorial, RA and Dec, positions of the G/K-type stars returned by the global search (black) and the G/K-dwarfs of Schlesinger et al. (2012) (red). Both samples probe all areas of the SDSS footprint. Bottom left: Cartesian, R and z, positions of the two samples. Bottom right: Same as bottom left, zoomed in to see the extent of the Schlesinger et al. (2012) sample. The differences in the bottom two panels are due to the distance cuts applied by Schlesinger et al. (2012).

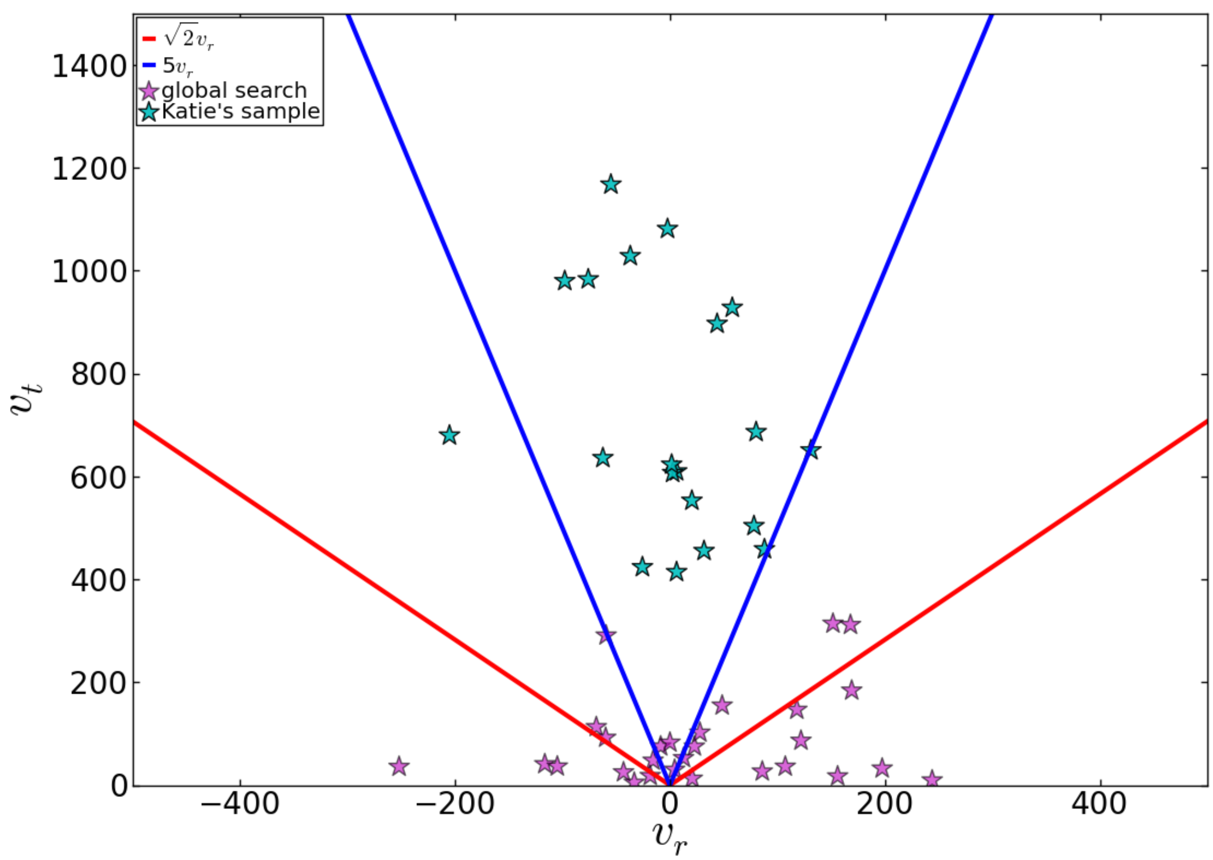


Figure 4.2: The transverse velocity, $v_t$, compared to the radial velocity, $v_r$, for the HVS candidates of Palladino et al. (2014) (cyan stars) and the global-search HVS candidates (magenta stars). The red lines indicate $v_t$ $\sqrt{2}$ times larger than $v_r$, expected for an isotropic stellar population. The blue lines represent $v_t$ 5 times larger than $v_r$, indicative of a sample dominated by the transverse velocity. The vast majority of the cyan points fall between the blue lines, suggesting that those candidates may suffer from large proper motion errors. Conversely, the magenta points are generally distributed throughout, suggestive of an unbiased sample. Upon close inspection, roughly half of the global-search HVS candidates fall below the red lines– a strong indication that they follow radial orbits, not unexpected for HVSs.

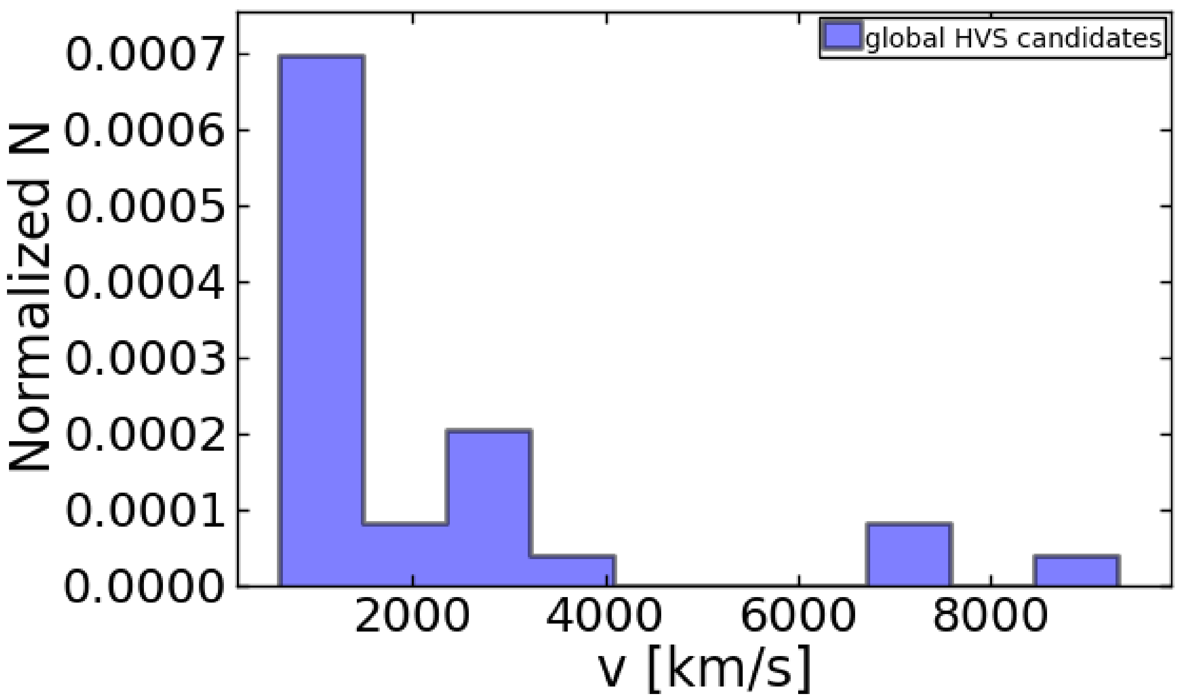


Figure 4.3: The velocity distribution of the global-search HVS candidates. All of the Palladino et al. (2014) HVS candidates fall within the first bin, with $v < 1500$ km/s. The majority of the HVS candidates represented here have similar velocities to the published candidates.

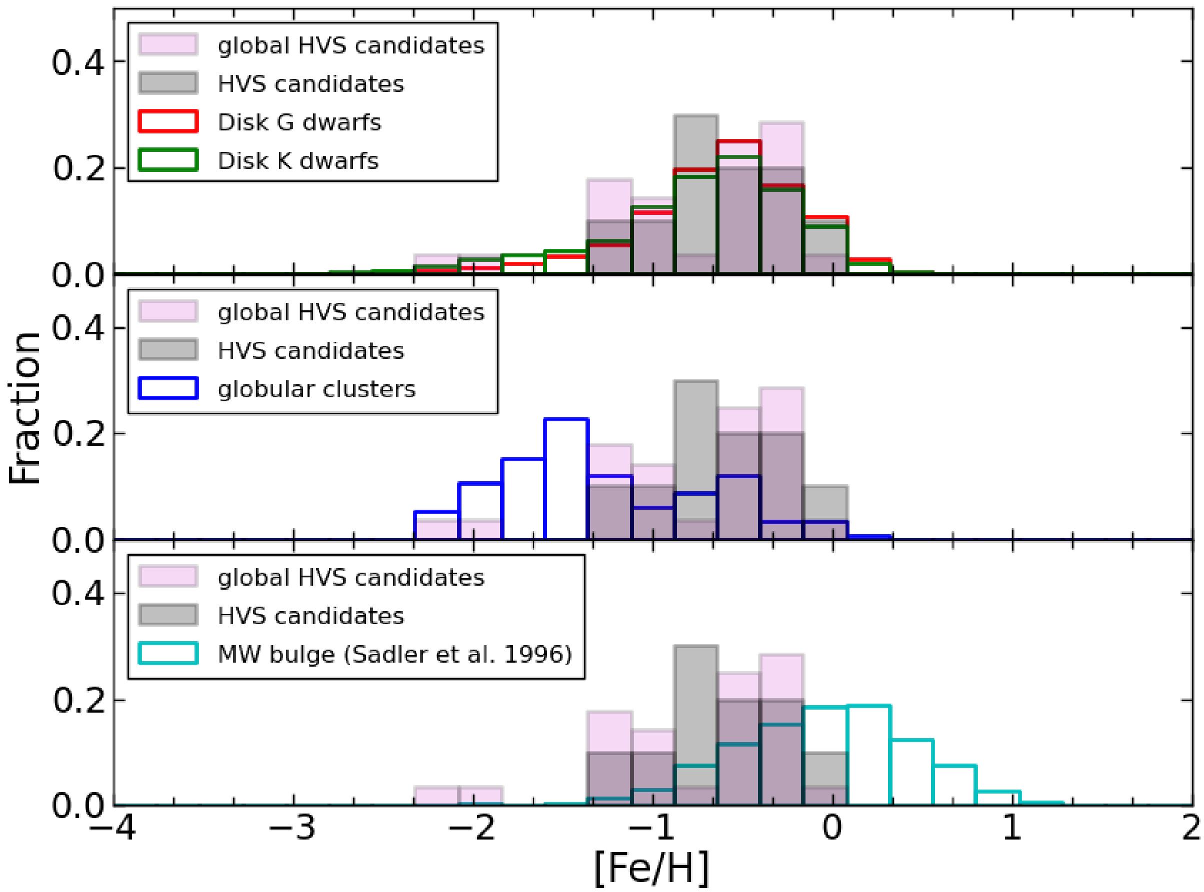


Figure 4.4: The metallicity distribution of the global-search HVS candidates (magenta) and the published HVS candidates (grey) compared to disk G/K-dwarfs (top), globular clusters (middle), and bulge stars (bottom). While the published HVS largely follow the distribution of the disk sample, the global-search candidates do not closely resemble any of the populations shown here.

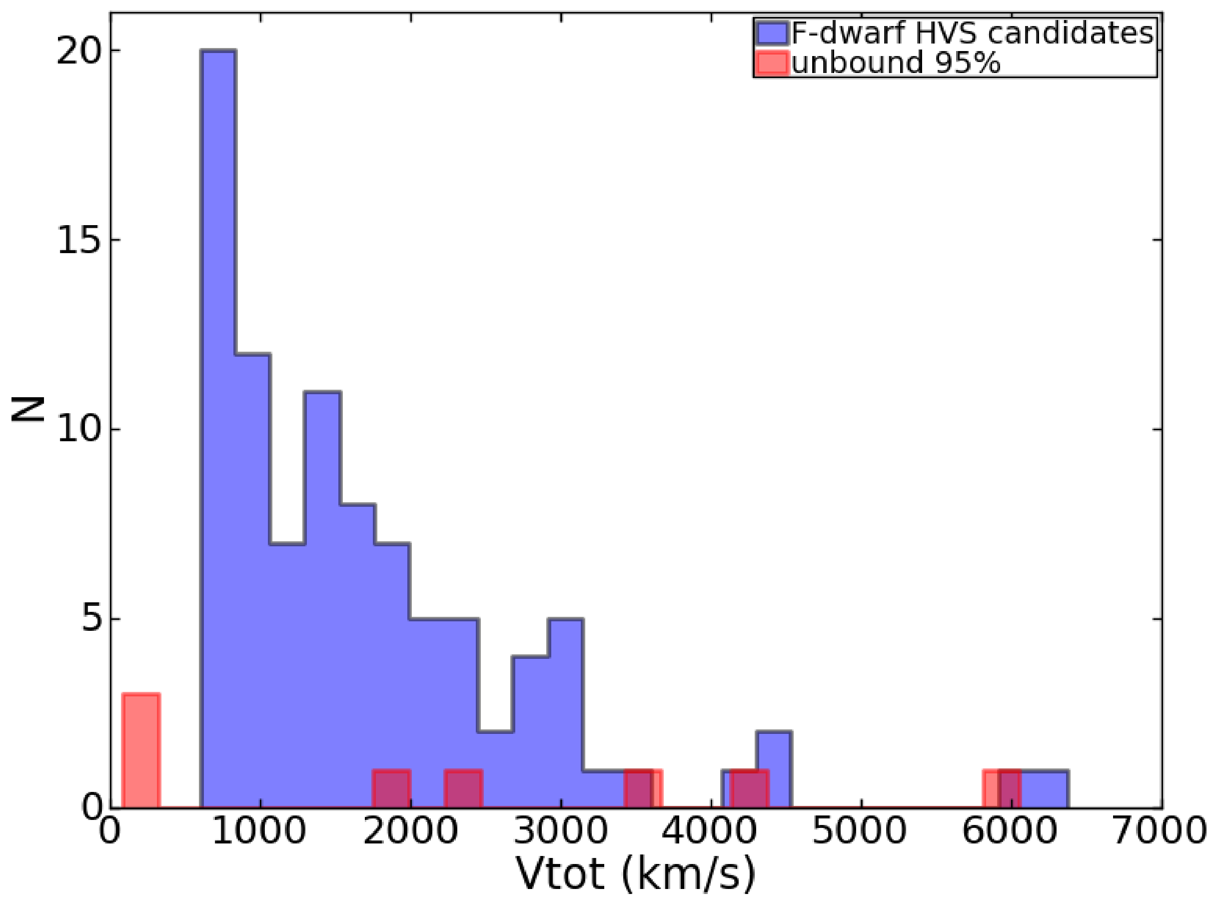


Figure 4.5: The velocity distribution of the 95 F-dwarf HVS candidates (blue) and the 8 candidates with at least 95% probability of being unbound.

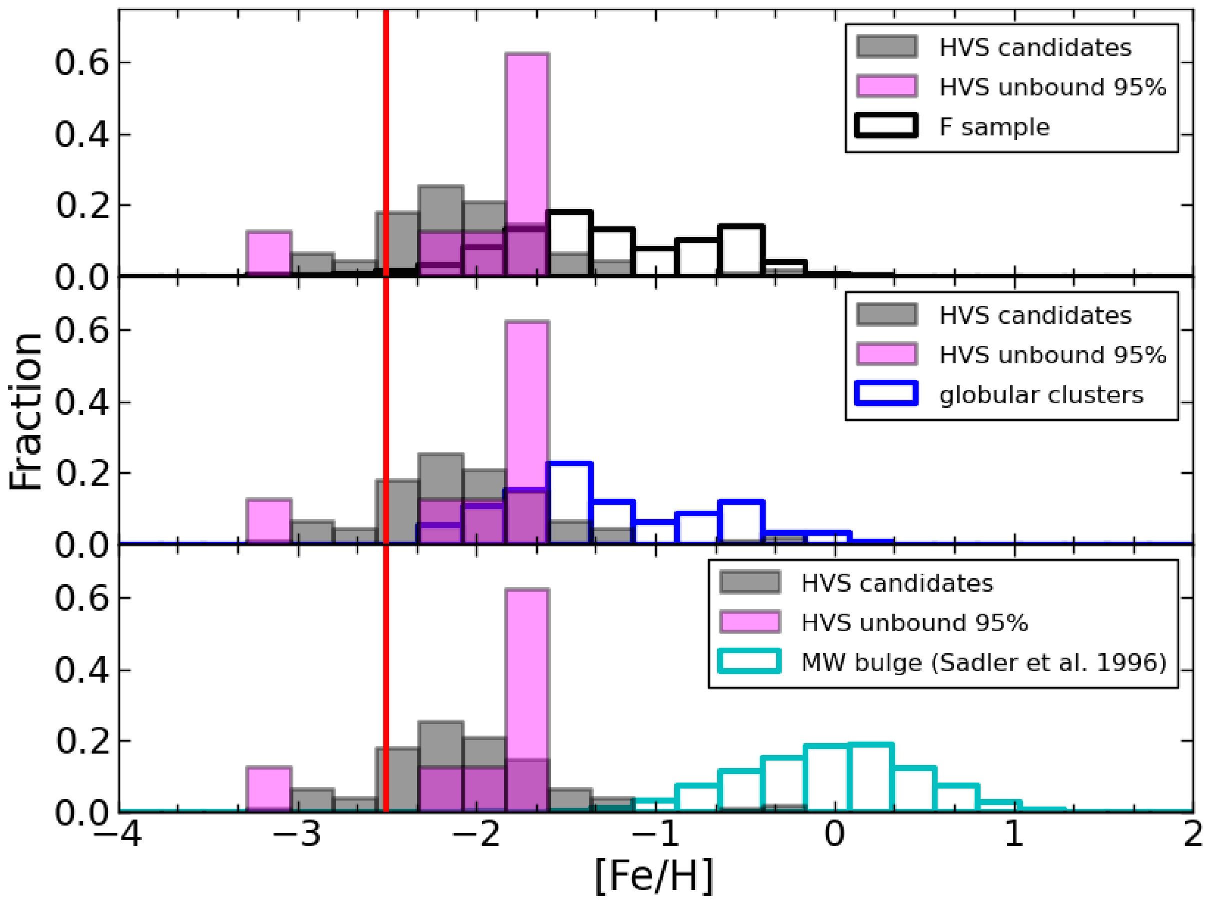


Figure 4.6: The metallicity distribution of the 95 F-dwarf HVS candidates (grey) and the 8 candidates that are unbound with at least 95% probability (magenta) compared to the entire F-star sample (black, top), globular clusters (blue, middle), and bulge stars (cyan, bottom). We note that the majority of the F-dwarf HVS candidates are extremely metal poor with only a couple relatively metal rich at [Fe/H] $\sim -0.5$. We caution, however, that the grid edge of the model atmospheres is at [Fe/H] $= -2.5$; any candidate more negative than the vertical red line is to be ignored (Allende Prieto et al., 2014, private communication).

# Chapter V

# CONCLUSION

In this thesis I described two complementary techniques to mine the Sloan Digital Sky Survey (SDSS) data to search for stars that are unbound to the Milky Way.

First, we developed a technique to identify distant M-giant intragroup stars (IGSs) within SDSS based solely on color. Using this technique, we identified 700 IGS candidates, between 300 kpc and 2 Mpc (Palladino et al., 2012). These IGS may constitute rare tracers of an underlying intracluster light (ICL) population surrounding the Milky Way. One possible explanation for the origin of these IGS is that they were ejected from the center of the Galaxy through interactions with our supermassive black hole as hypervelocity stars (HVSs).

Secondly, we identified candidate HVSs from a sample of SEGUE G- and K-dwarfs. We found that nearly half of the candidates exceed their escape velocities with at least 98% probability and no candidate's orbit is consistent with a Galactic Center origin (Palladino et al., 2014). The lack of HVS candidates originating from the Galactic Center is an indication that either the ejection mechanism is mass-dependent or the initial mass function at the center of the Galaxy is even more top-heavy than suggested in the literature (e.g.; Figer et al., 1999, Section 3.6.4).

We plan to continue the search for stars that comprise the unbound stellar population in the Milky Way. We are currently searching for HVS candidates in an extended G- and K-type sample that includes both dwarfs and giants and probes regions of the Galaxy beyond the disk. We are also searching for more HVS candidates within a sample of F-stars, containing dwarfs and giants, to constrain the mass-dependence of the supermassive black hole ejection mechanism operating at the center of the Milky Way.

## Appendix A

## ESTIMATION OF EXPECTED HVS VIA THE BINARY DISRUPTION MECHANISM.

Here we estimate on the number of G/K-type HVS we should expect to observe within SDSS resulting from the supernova binary disruption mechanism described in Section 1.4 and Tauris (2015).

In order to be consistent with the scenario described in Tauris (2015), we consider only type Ia supernovae for this estimation. We begin with the known supernova rate of 1 supernova per 100 years and the ratio of type II to type Ia supernova of $\sim 3.5$ (Sato et al., 2007), which gives us a rate of 1 type Ia supernovae per 350 years. Then, adopting an average velocity for our HVS candidates of 1,000 km/s, we determine it would take 5 million years for a star to travel from the disk to a distance of 5 kpc (consistent with our observations). Therefore, over a period of 5 million years, we would expect approximately 14,000 type Ia supernovae in the Milky Way.

From here, we consider the fraction of the sky observed by SDSS, and determine that there would be $\sim 3,000$ type Ia supernovae in the SDSS footprint from the past 5 million years.

Since, by definition, type Ia supernovae exist in binary systems, we must consider how many of these 3,000 binaries contain a low mass companion. Standard population synthesis models adopt a flat distribution for assigning the mass to the secondary stellar component of binaries (Abt, 1983)– if we group all spectral types (O/B, A/F, G/K, M/later), we will assume that roughly 1/4 of these binary systems contain G/K-type companions. This assumption determines that we should expect $\sim 750$ G/K-type companions to type Ia supernovae within the SDSS footprint from the past 5 million years.

According to Tauris (2015), only 1% of binary disruption scenarios with a low mass companion will result in an ejection speed of $v > 600km/s$. This velocity requirement yields that we should expect to observe $O(10)$ low mass HVS from a supernova binary disruption scenario within the SDSS footprint, which is consistent with our result of 20 candidates.

# Appendix B

## EXPANSION ON THE EXPECTED IGS CALCULATION.

Here we elaborate on the calculation outline in Section 2.5 determining the expected number of IGS in the SDSS footprint.

If we assume that the SMBH in our galaxy had a merger with an intermediate mass black hole (IMBH) with mass $3 \times 10^5 M_\odot$, it would 3-body scatter stars and eject them from the system isotropically. This means that the total mass of ejected stars will also be $3 \times 10^5 M_\odot$ (Yu & Tremaine, 2003). Assuming an average stellar mass of 1 $M_\odot$, then $3 \times 10^5$ stars will be ejected.

The total sky has 41,253 square degrees, which yields approximately 7 ejected IGS per square degree. Assuming the IGS formed 10 Gyr ago with a Salpeter IMF, then there would be 0.00124 red giant HVS per square degree. The area of sky observed by SDSS is 8000 square degrees, so this yields the expected tens of red giant IGS in the SDSS footprint resulting from SMBH ejection.

# Appendix C

## IGS CANDIDATES REMAINING AFTER ALL CRITERIA CUTS.

Table C.1. Complete and unabridged.

| Object ID | RA | DEC | u | u err | g | g err | r | r err | i | i err | z | z err | r-i | i-z |
|---|---|---|---|---|---|---|---|---|---|---|---|---|---|---|
| 758882136836343139 | 60.5013 | 80.8760 | 24.4 | 1.3 | 24.7 | 0.6 | 24.3 | 0.7 | 22.0 | 0.2 | 20.3 | 0.2 | 2.3 | 1.7 |
| 758882137910740030 | 62.9212 | 82.5298 | 25.2 | 1.2 | 25.0 | 0.6 | 23.2 | 0.4 | 21.0 | 0.1 | 19.6 | 0.1 | 2.2 | 1.4 |
| 758882626993718584 | 63.3170 | 81.6950 | 26.5 | 0.6 | 24.8 | 0.6 | 25.3 | 0.7 | 22.0 | 0.2 | 20.3 | 0.2 | 3.3 | 1.6 |
| 758877527803168329 | 94.6323 | 63.7038 | 25.1 | 0.9 | 24.1 | 0.3 | 24.5 | 0.5 | 21.2 | 0.1 | 19.8 | 0.1 | 3.3 | 1.4 |
| 758877527266231607 | 94.8017 | 63.2633 | 24.6 | 0.7 | 24.4 | 0.5 | 24.5 | 0.6 | 21.8 | 0.1 | 20.4 | 0.1 | 2.7 | 1.4 |
| 758877527266493955 | 95.9369 | 63.5501 | 25.2 | 0.7 | 24.8 | 0.6 | 25.6 | 0.5 | 22.7 | 0.3 | 20.7 | 0.2 | 2.9 | 2.0 |
| 758878272976455144 | 105.3459 | 66.8553 | 25.3 | 0.9 | 24.4 | 0.4 | 24.1 | 0.4 | 21.8 | 0.1 | 20.2 | 0.1 | 2.3 | 1.6 |
| 758878271902778853 | 105.8427 | 66.0785 | 23.8 | 0.7 | 24.7 | 0.4 | 24.6 | 0.5 | 22.3 | 0.2 | 20.8 | 0.2 | 2.3 | 1.5 |
| 758884768580109918 | 107.9936 | 38.3022 | 24.8 | 1.1 | 25.1 | 0.7 | 24.4 | 0.6 | 21.9 | 0.1 | 20.4 | 0.2 | 2.6 | 1.4 |
| 587738067260998978 | 109.5721 | 39.4395 | 25.3 | 0.9 | 25.7 | 0.6 | 24.6 | 0.7 | 22.1 | 0.2 | 20.0 | 0.1 | 2.5 | 2.1 |
| 587738066187126136 | 110.3269 | 38.8813 | 23.9 | 1.2 | 24.8 | 0.6 | 24.3 | 0.6 | 22.0 | 0.2 | 20.6 | 0.2 | 2.2 | 1.5 |
| 758884821194311430 | 111.7235 | 31.6748 | 23.3 | 0.5 | 24.9 | 0.5 | 23.8 | 0.4 | 21.4 | 0.1 | 20.0 | 0.1 | 2.4 | 1.4 |
| 758884803478619431 | 112.4325 | 31.0977 | 25.2 | 1.1 | 24.5 | 0.5 | 24.1 | 0.6 | 21.9 | 0.1 | 20.5 | 0.1 | 2.2 | 1.4 |
| 587737808490071190 | 112.6070 | 38.1797 | 25.4 | 1.0 | 25.2 | 0.6 | 24.8 | 0.8 | 22.2 | 0.2 | 20.7 | 0.2 | 2.6 | 1.6 |
| 587728906096674179 | 112.7248 | 27.9531 | 24.8 | 0.9 | 25.1 | 0.6 | 25.1 | 0.6 | 21.9 | 0.1 | 20.5 | 0.2 | 3.2 | 1.4 |
| 587725551190869074 | 113.3506 | 36.8066 | 23.7 | 0.7 | 24.8 | 0.3 | 25.1 | 0.8 | 21.9 | 0.1 | 20.4 | 0.1 | 3.3 | 1.5 |
| 587727866178372734 | 113.9236 | 31.5228 | 23.8 | 0.7 | 25.3 | 0.6 | 24.2 | 0.5 | 22.0 | 0.2 | 20.4 | 0.1 | 2.2 | 1.5 |
| 587725552265790733 | 114.2540 | 39.4958 | 23.7 | 0.7 | 24.7 | 0.6 | 25.0 | 0.7 | 22.1 | 0.2 | 20.8 | 0.2 | 2.9 | 1.4 |
| 587725775066563723 | 114.3135 | 39.3165 | 25.3 | 0.8 | 25.4 | 0.6 | 24.8 | 0.7 | 21.8 | 0.1 | 20.1 | 0.1 | 3.0 | 1.7 |
| 588013382718391798 | 115.5088 | 23.9862 | 25.6 | 0.6 | 25.1 | 0.5 | 24.2 | 0.5 | 22.0 | 0.1 | 20.5 | 0.1 | 2.2 | 1.4 |
| 587732152555078919 | 115.7199 | 22.3048 | 23.7 | 0.9 | 26.6 | 0.4 | 23.8 | 0.5 | 21.2 | 0.1 | 19.3 | 0.1 | 2.7 | 1.9 |
| 587725775067677784 | 115.9952 | 41.5387 | 25.5 | 0.8 | 25.3 | 0.6 | 24.0 | 0.5 | 21.6 | 0.1 | 20.3 | 0.1 | 2.3 | 1.3 |
| 587732054308947237 | 116.6473 | 26.0150 | 23.7 | 0.7 | 24.9 | 0.6 | 24.1 | 0.6 | 21.3 | 0.1 | 19.9 | 0.1 | 2.7 | 1.4 |
| 587725774530872383 | 116.6594 | 41.4087 | 24.1 | 0.8 | 23.9 | 0.4 | 24.0 | 0.6 | 21.8 | 0.1 | 20.4 | 0.1 | 2.3 | 1.3 |
| 588016878822295117 | 116.7229 | 18.5509 | 25.8 | 0.6 | 24.8 | 0.6 | 24.4 | 0.6 | 21.6 | 0.1 | 20.0 | 0.1 | 2.9 | 1.5 |
| 587737826210219010 | 116.7903 | 45.1563 | 24.7 | 1.0 | 24.7 | 0.6 | 24.8 | 0.7 | 21.9 | 0.1 | 20.5 | 0.2 | 3.0 | 1.3 |
| 587728906099623039 | 117.2504 | 33.4457 | 24.1 | 0.9 | 25.3 | 0.6 | 23.9 | 0.5 | 21.0 | 0.1 | 19.2 | 0.1 | 2.9 | 1.7 |

Table C.1 (cont'd)

| Object ID | RA | DEC | u | u err | g | g err | r | r err | i | i err | z | z err | r-i | i-z |
|---|---|---|---|---|---|---|---|---|---|---|---|---|---|---|
| 587738372742121166 | 117.5023 | 18.4613 | 24.8 | 0.8 | 25.5 | 0.5 | 24.9 | 0.5 | 22.7 | 0.3 | 20.8 | 0.2 | 2.2 | 1.9 |
| 588013383793771999 | 117.5227 | 27.3834 | 24.2 | 0.8 | 24.5 | 0.5 | 24.9 | 0.6 | 22.7 | 0.2 | 21.1 | 0.2 | 2.1 | 1.6 |
| 587728906636952618 | 117.5359 | 34.5913 | 24.9 | 0.9 | 24.5 | 0.5 | 24.3 | 0.6 | 21.6 | 0.1 | 20.2 | 0.1 | 2.7 | 1.4 |
| 587731679573509088 | 117.6023 | 27.9611 | 25.8 | 1.2 | 25.7 | 1.0 | 23.5 | 0.9 | 20.9 | 0.1 | 19.0 | 0.1 | 2.6 | 1.9 |
| 587735043069707709 | 117.7701 | 20.8646 | 24.7 | 0.9 | 25.2 | 0.6 | 25.6 | 0.5 | 22.4 | 0.2 | 20.9 | 0.2 | 3.3 | 1.4 |
| 587728931334653093 | 117.9390 | 33.6761 | 25.0 | 0.9 | 24.1 | 0.4 | 23.9 | 0.5 | 20.9 | 0.1 | 19.4 | 0.1 | 3.0 | 1.4 |
| 587735043069969790 | 118.3476 | 21.2348 | 25.0 | 0.8 | 25.2 | 0.6 | 24.5 | 0.6 | 22.3 | 0.2 | 20.9 | 0.2 | 2.2 | 1.4 |
| 587737809568531492 | 118.6204 | 48.1006 | 23.7 | 0.8 | 25.4 | 0.5 | 24.3 | 0.6 | 21.9 | 0.1 | 20.4 | 0.2 | 2.5 | 1.4 |
| 588016878286406831 | 118.8410 | 19.7030 | 25.0 | 1.4 | 25.0 | 0.8 | 25.1 | 0.7 | 22.0 | 0.2 | 20.5 | 0.2 | 3.2 | 1.4 |
| 587731873385481740 | 118.9846 | 32.3811 | 25.5 | 0.6 | 24.6 | 0.4 | 24.8 | 0.5 | 21.7 | 0.1 | 20.1 | 0.1 | 3.2 | 1.5 |
| 587735235806561437 | 118.9877 | 21.3134 | 23.5 | 0.8 | 24.9 | 0.6 | 24.7 | 0.7 | 21.4 | 0.1 | 20.0 | 0.1 | 3.3 | 1.4 |
| 587735236343759987 | 119.1972 | 22.2818 | 25.2 | 0.8 | 25.4 | 0.6 | 25.3 | 0.6 | 22.3 | 0.2 | 20.7 | 0.2 | 3.0 | 1.5 |
| 587738066730484820 | 119.4568 | 52.3041 | 24.7 | 0.9 | 24.7 | 0.5 | 23.9 | 0.4 | 21.6 | 0.1 | 20.2 | 0.1 | 2.3 | 1.4 |
| 758877528344757598 | 119.8005 | 65.7236 | 24.3 | 0.7 | 25.2 | 0.4 | 25.0 | 0.5 | 22.4 | 0.1 | 20.4 | 0.1 | 2.6 | 1.9 |
| 587739115234788850 | 119.8104 | 17.9973 | 24.0 | 0.8 | 24.7 | 0.4 | 24.0 | 0.4 | 21.6 | 0.1 | 20.1 | 0.1 | 2.4 | 1.5 |
| 587727867256243248 | 119.8520 | 39.6771 | 24.5 | 0.9 | 24.4 | 0.5 | 24.1 | 0.5 | 20.9 | 0.1 | 19.4 | 0.1 | 3.2 | 1.5 |
| 587742010042287707 | 120.2735 | 10.3882 | 23.7 | 1.0 | 24.7 | 0.6 | 24.8 | 0.7 | 22.1 | 0.2 | 20.4 | 0.2 | 2.7 | 1.6 |
| 588297863634682833 | 120.3658 | 24.4537 | 25.7 | 1.0 | 25.2 | 0.8 | 24.3 | 0.8 | 22.0 | 0.2 | 20.6 | 0.2 | 2.4 | 1.4 |
| 587725470665081929 | 120.4194 | 43.3815 | 23.5 | 0.6 | 25.6 | 0.5 | 24.2 | 0.4 | 21.5 | 0.1 | 19.9 | 0.1 | 2.7 | 1.6 |
| 587737826749645877 | 120.5762 | 50.4355 | 24.1 | 1.0 | 24.8 | 0.3 | 23.7 | 0.4 | 21.5 | 0.1 | 20.1 | 0.1 | 2.2 | 1.4 |
| 587741708859803246 | 120.6010 | 12.5824 | 25.5 | 0.6 | 25.1 | 0.5 | 23.5 | 0.3 | 21.3 | 0.1 | 19.9 | 0.1 | 2.2 | 1.4 |
| 587742010042549539 | 120.7911 | 10.6056 | 23.1 | 0.6 | 23.7 | 0.4 | 24.0 | 0.6 | 21.8 | 0.1 | 20.4 | 0.2 | 2.2 | 1.4 |
| 588013382184469831 | 120.8817 | 28.7355 | 23.8 | 0.4 | 25.0 | 0.6 | 25.7 | 0.4 | 22.9 | 0.2 | 21.1 | 0.2 | 2.8 | 1.8 |
| 587732469846377586 | 120.9695 | 26.5794 | 25.7 | 0.8 | 24.0 | 0.4 | 23.6 | 0.4 | 20.9 | 0.1 | 19.5 | 0.1 | 2.7 | 1.4 |
| 587745244689073605 | 121.0114 | 9.6150 | 24.5 | 0.8 | 24.5 | 0.4 | 23.7 | 0.3 | 21.1 | 0.1 | 19.8 | 0.1 | 2.5 | 1.3 |
| 587728669878912102 | 121.1313 | 40.8448 | 25.2 | 0.8 | 24.7 | 0.5 | 25.0 | 0.6 | 22.3 | 0.2 | 20.9 | 0.2 | 2.7 | 1.4 |
| 588023046933120424 | 121.1645 | 13.0654 | 24.1 | 0.8 | 24.5 | 0.4 | 24.9 | 0.6 | 22.0 | 0.2 | 20.7 | 0.2 | 2.8 | 1.3 |

Table C.1 (cont'd)

| Object ID | RA | DEC | u | u err | g | g err | r | r err | i | i err | z | z err | r-i | i-z |
|---|---|---|---|---|---|---|---|---|---|---|---|---|---|---|
| 587745243615266573 | 121.2201 | 8.7283 | 24.6 | 0.8 | 25.3 | 0.5 | 25.0 | 0.5 | 21.8 | 0.1 | 20.2 | 0.1 | 3.3 | 1.6 |
| 587739115235509353 | 121.2323 | 18.8467 | 25.1 | 0.9 | 24.7 | 0.5 | 25.2 | 0.6 | 21.9 | 0.1 | 20.2 | 0.1 | 3.2 | 1.8 |
| 587745403603453761 | 121.4298 | 8.4593 | 24.9 | 0.7 | 24.7 | 0.4 | 25.2 | 0.4 | 22.6 | 0.2 | 21.2 | 0.2 | 2.6 | 1.4 |
| 587745402529711807 | 121.5256 | 7.7839 | 25.0 | 0.7 | 24.8 | 0.4 | 24.2 | 0.4 | 22.0 | 0.1 | 20.4 | 0.1 | 2.2 | 1.6 |
| 587744637488596380 | 121.5423 | 11.1817 | 25.5 | 1.0 | 25.2 | 0.6 | 24.2 | 0.7 | 21.7 | 0.1 | 20.3 | 0.1 | 2.5 | 1.4 |
| 587731520662930498 | 121.5799 | 31.5473 | 25.4 | 1.0 | 25.3 | 0.7 | 24.0 | 0.6 | 21.3 | 0.1 | 19.6 | 0.1 | 2.7 | 1.7 |
| 587741387273275005 | 121.6111 | 16.0509 | 25.1 | 0.8 | 24.6 | 0.4 | 24.8 | 0.5 | 21.9 | 0.1 | 20.5 | 0.2 | 2.9 | 1.5 |
| 587734623238227199 | 121.6396 | 26.8599 | 25.5 | 0.7 | 24.7 | 0.5 | 23.9 | 0.5 | 21.3 | 0.1 | 19.8 | 0.1 | 2.6 | 1.4 |
| 587738066194465721 | 121.7083 | 53.7864 | 23.7 | 0.9 | 25.4 | 0.5 | 24.9 | 0.7 | 22.1 | 0.2 | 20.5 | 0.1 | 2.8 | 1.6 |
| 587738372744217890 | 121.7230 | 21.3338 | 24.3 | 0.8 | 26.0 | 0.5 | 24.9 | 0.6 | 22.3 | 0.2 | 20.9 | 0.2 | 2.6 | 1.4 |
| 587741532764898777 | 122.0871 | 14.6230 | 24.4 | 0.8 | 25.7 | 0.4 | 25.0 | 0.6 | 22.2 | 0.2 | 20.9 | 0.2 | 2.7 | 1.4 |
| 587731887346025354 | 122.1712 | 36.4783 | 25.4 | 0.7 | 25.1 | 0.6 | 24.5 | 0.5 | 22.2 | 0.2 | 20.8 | 0.1 | 2.4 | 1.4 |
| 587725550659240849 | 122.3177 | 46.7939 | 25.6 | 0.7 | 24.1 | 0.5 | 23.2 | 0.4 | 20.9 | 0.1 | 19.3 | 0.1 | 2.3 | 1.6 |
| 587728906102506800 | 122.3662 | 38.6413 | 24.7 | 0.9 | 25.3 | 0.5 | 24.1 | 0.5 | 21.0 | 0.1 | 19.6 | 0.1 | 3.1 | 1.4 |
| 587739377229628867 | 122.4993 | 18.3702 | 24.9 | 1.1 | 25.5 | 0.6 | 23.6 | 0.4 | 21.1 | 0.1 | 19.5 | 0.1 | 2.5 | 1.5 |
| 587745243615921560 | 122.5645 | 9.1305 | 25.5 | 0.6 | 24.6 | 0.4 | 24.8 | 0.5 | 22.7 | 0.2 | 21.0 | 0.2 | 2.1 | 1.7 |
| 587744874248799448 | 122.5791 | 9.5182 | 24.9 | 1.1 | 25.1 | 0.6 | 23.8 | 0.5 | 20.9 | 0.1 | 19.5 | 0.1 | 2.9 | 1.5 |
| 587734621627614164 | 122.5965 | 25.8422 | 24.8 | 1.1 | 24.6 | 0.5 | 24.7 | 0.7 | 22.2 | 0.2 | 20.7 | 0.2 | 2.4 | 1.5 |
| 587738565479368364 | 122.6182 | 7.3218 | 24.8 | 1.0 | 24.6 | 0.5 | 25.3 | 0.5 | 22.5 | 0.2 | 21.0 | 0.2 | 2.8 | 1.6 |
| 587742010043467053 | 122.8561 | 11.3085 | 25.9 | 0.6 | 25.8 | 0.5 | 25.2 | 0.6 | 22.3 | 0.2 | 20.9 | 0.3 | 2.9 | 1.4 |
| 588007005234004760 | 122.8710 | 45.4871 | 24.4 | 1.1 | 24.8 | 0.7 | 24.7 | 0.7 | 22.0 | 0.2 | 20.6 | 0.2 | 2.7 | 1.4 |
| 587739153354851262 | 123.2158 | 19.9350 | 25.5 | 0.9 | 25.4 | 0.7 | 24.0 | 0.6 | 21.5 | 0.1 | 19.9 | 0.1 | 2.5 | 1.6 |
| 587742008969790819 | 123.3029 | 10.5153 | 25.1 | 1.2 | 24.0 | 0.4 | 24.2 | 0.6 | 21.8 | 0.1 | 20.0 | 0.1 | 2.3 | 1.8 |
| 587732471458694255 | 123.3611 | 30.2143 | 24.3 | 1.0 | 25.6 | 0.6 | 25.1 | 0.7 | 22.6 | 0.3 | 20.9 | 0.2 | 2.5 | 1.7 |
| 587742009506792701 | 123.3705 | 11.1259 | 24.7 | 1.0 | 25.8 | 0.6 | 24.3 | 0.6 | 21.9 | 0.1 | 20.4 | 0.1 | 2.4 | 1.5 |
| 587739153354916942 | 123.4933 | 19.9022 | 23.5 | 0.9 | 25.7 | 0.6 | 24.9 | 0.7 | 22.3 | 0.2 | 20.6 | 0.2 | 2.6 | 1.8 |
| 587741386737255953 | 123.5510 | 16.6804 | 25.2 | 0.7 | 25.0 | 0.4 | 24.5 | 0.5 | 22.1 | 0.1 | 20.7 | 0.2 | 2.4 | 1.4 |

Table C.1 (cont'd)

| Object ID | RA | DEC | u | u err | g | g err | r | r err | i | i err | z | z err | r-i | i-z |
|---|---|---|---|---|---|---|---|---|---|---|---|---|---|---|
| 587745403067565543 | 123.6343 | 8.6650 | 24.6 | 0.9 | 24.2 | 0.3 | 23.9 | 0.4 | 21.2 | 0.1 | 19.9 | 0.1 | 2.7 | 1.3 |
| 587734949653120190 | 123.7966 | 6.6361 | 24.9 | 1.2 | 24.1 | 0.5 | 24.5 | 0.9 | 22.3 | 0.3 | 20.4 | 0.2 | 2.2 | 1.8 |
| 587731522275312616 | 123.8046 | 35.2063 | 24.6 | 1.1 | 25.7 | 0.5 | 25.4 | 0.7 | 22.2 | 0.2 | 20.6 | 0.2 | 3.2 | 1.6 |
| 587745244690384353 | 123.8545 | 10.4778 | 25.0 | 0.7 | 25.1 | 0.5 | 23.9 | 0.4 | 21.7 | 0.1 | 20.3 | 0.1 | 2.1 | 1.5 |
| 588016878825964493 | 123.8681 | 23.6659 | 25.1 | 1.2 | 23.9 | 0.4 | 23.9 | 0.6 | 21.2 | 0.1 | 19.6 | 0.1 | 2.7 | 1.7 |
| 587735236346315834 | 124.2462 | 25.9692 | 25.5 | 0.8 | 25.9 | 0.6 | 25.7 | 0.7 | 22.7 | 1.0 | 20.8 | 0.2 | 2.9 | 1.9 |
| 587734949653382475 | 124.4021 | 6.8419 | 23.4 | 0.7 | 24.4 | 0.6 | 24.0 | 0.7 | 21.8 | 0.2 | 20.2 | 0.2 | 2.2 | 1.6 |
| 587742008970380597 | 124.5343 | 11.0003 | 25.2 | 1.2 | 25.1 | 0.6 | 24.0 | 0.5 | 21.9 | 0.1 | 20.5 | 0.1 | 2.2 | 1.3 |
| 588016879363359634 | 124.5851 | 24.7195 | 23.2 | 0.6 | 25.5 | 0.6 | 23.8 | 0.5 | 21.5 | 0.1 | 20.1 | 0.1 | 2.3 | 1.4 |
| 588010358525134744 | 124.6703 | 1.9613 | 24.7 | 1.2 | 25.5 | 0.6 | 25.2 | 0.5 | 22.7 | 0.2 | 20.7 | 0.2 | 2.5 | 2.0 |
| 587735236883645397 | 124.8579 | 26.9178 | 25.4 | 0.9 | 25.3 | 0.6 | 25.3 | 0.7 | 22.0 | 0.2 | 20.4 | 0.2 | 3.2 | 1.7 |
| 587738948271473620 | 125.1085 | 23.5913 | 25.0 | 1.1 | 25.5 | 0.6 | 24.5 | 0.7 | 22.0 | 0.2 | 20.6 | 0.2 | 2.5 | 1.3 |
| 588016839634584912 | 125.2505 | 23.8631 | 25.8 | 0.7 | 25.3 | 0.6 | 23.5 | 0.3 | 21.3 | 0.1 | 19.7 | 0.1 | 2.2 | 1.6 |
| 587737808497673062 | 125.4675 | 53.0010 | 25.4 | 1.1 | 24.6 | 0.6 | 24.6 | 0.9 | 21.3 | 0.1 | 19.7 | 0.1 | 3.3 | 1.6 |
| 587735235809969032 | 125.5140 | 26.3690 | 23.9 | 1.1 | 25.9 | 0.5 | 23.9 | 0.6 | 21.7 | 0.1 | 19.9 | 0.1 | 2.3 | 1.7 |
| 587741816771773524 | 125.5536 | 13.5298 | 26.0 | 0.7 | 24.1 | 0.4 | 24.4 | 0.6 | 22.2 | 0.2 | 20.8 | 0.2 | 2.2 | 1.5 |
| 587739152819029103 | 125.7847 | 20.7065 | 25.9 | 1.0 | 26.5 | 0.9 | 24.8 | 0.7 | 22.3 | 0.2 | 20.9 | 0.2 | 2.5 | 1.4 |
| 587741532229731745 | 125.8905 | 16.0249 | 24.1 | 1.0 | 25.1 | 0.6 | 24.3 | 0.6 | 21.7 | 0.1 | 19.8 | 0.1 | 2.6 | 1.9 |
| 587731885736723588 | 125.9387 | 37.9468 | 24.1 | 1.0 | 25.3 | 0.6 | 25.0 | 0.6 | 22.1 | 0.1 | 20.8 | 0.1 | 2.9 | 1.4 |
| 588016879901017043 | 125.9927 | 26.2273 | 23.8 | 0.8 | 25.0 | 0.7 | 24.3 | 0.6 | 21.8 | 0.1 | 20.1 | 0.1 | 2.6 | 1.7 |
| 587741387812373747 | 126.0358 | 18.8876 | 25.2 | 0.6 | 25.3 | 0.4 | 24.4 | 0.5 | 21.9 | 0.1 | 20.0 | 0.1 | 2.5 | 1.9 |
| 587732701777364516 | 126.4451 | 3.4755 | 23.6 | 0.9 | 25.2 | 0.7 | 24.1 | 0.6 | 22.0 | 0.1 | 20.6 | 0.2 | 2.1 | 1.4 |
| 587739376157590638 | 126.4929 | 19.4975 | 23.4 | 0.7 | 24.7 | 0.6 | 24.1 | 0.5 | 21.7 | 0.1 | 20.3 | 0.1 | 2.4 | 1.4 |
| 587741817309234100 | 126.8135 | 14.3474 | 23.8 | 0.8 | 24.7 | 0.6 | 23.5 | 0.4 | 21.2 | 0.1 | 19.8 | 0.1 | 2.3 | 1.4 |
| 587734621629776894 | 126.9443 | 29.0573 | 25.3 | 1.0 | 24.1 | 0.4 | 23.5 | 0.4 | 21.0 | 0.1 | 19.7 | 0.1 | 2.5 | 1.4 |
| 588848899352561319 | 126.9608 | -0.5883 | 24.8 | 1.0 | 24.8 | 0.6 | 23.7 | 0.4 | 21.5 | 0.1 | 20.1 | 0.1 | 2.2 | 1.5 |
| 758877529419810240 | 127.3261 | 66.1607 | 24.4 | 0.7 | 25.3 | 0.4 | 23.5 | 0.3 | 20.9 | 0.1 | 19.1 | 0.0 | 2.5 | 1.8 |

Table C.1 (cont'd)

| Object ID | RA | DEC | u | u err | g | g err | r | r err | i | i err | z | z err | r-i | i-z |
|---|---|---|---|---|---|---|---|---|---|---|---|---|---|---|
| 588010358526444861 | 127.6105 | 2.2769 | 24.4 | 1.4 | 25.1 | 0.7 | 24.2 | 0.6 | 21.6 | 0.1 | 20.0 | 0.1 | 2.6 | 1.6 |
| 587742008971887729 | 127.7826 | 12.1561 | 23.8 | 1.0 | 25.5 | 0.6 | 24.7 | 0.6 | 22.0 | 0.1 | 20.5 | 0.1 | 2.7 | 1.6 |
| 588848900426761686 | 127.9468 | 0.2102 | 23.6 | 0.6 | 24.4 | 0.5 | 24.8 | 0.6 | 22.2 | 0.2 | 20.8 | 0.2 | 2.6 | 1.4 |
| 758885526635152958 | 128.0022 | -3.5678 | 24.2 | 1.0 | 24.4 | 0.4 | 24.3 | 0.6 | 21.1 | 0.1 | 19.5 | 0.1 | 3.2 | 1.6 |
| 587741709937149050 | 128.0561 | 16.6285 | 23.3 | 0.4 | 25.3 | 0.5 | 24.3 | 0.6 | 21.3 | 0.1 | 19.7 | 0.1 | 3.0 | 1.5 |
| 587739406759560244 | 128.1348 | 20.5569 | 24.8 | 1.0 | 24.2 | 0.4 | 24.8 | 0.8 | 21.5 | 0.1 | 20.1 | 0.1 | 3.3 | 1.5 |
| 588013382188270667 | 128.2241 | 34.6591 | 25.2 | 0.9 | 24.7 | 0.5 | 24.1 | 0.4 | 21.7 | 0.1 | 20.1 | 0.1 | 2.4 | 1.6 |
| 587735343181989199 | 128.2882 | 6.4828 | 24.2 | 1.0 | 25.7 | 0.4 | 24.9 | 0.5 | 22.3 | 0.2 | 20.8 | 0.1 | 2.7 | 1.5 |
| 587739115775985007 | 128.5542 | 23.6851 | 23.8 | 0.7 | 24.8 | 0.5 | 24.1 | 0.4 | 21.6 | 0.1 | 20.1 | 0.1 | 2.5 | 1.5 |
| 587739406222820115 | 128.5628 | 20.3347 | 24.2 | 1.2 | 25.9 | 0.5 | 23.6 | 0.5 | 21.0 | 0.1 | 19.5 | 0.1 | 2.5 | 1.6 |
| 587725552273458067 | 128.6043 | 54.1334 | 24.9 | 1.1 | 24.5 | 0.6 | 24.7 | 0.8 | 21.8 | 0.2 | 20.4 | 0.2 | 3.0 | 1.4 |
| 587727900001437041 | 128.7573 | 0.7449 | 24.4 | 1.1 | 24.6 | 0.6 | 24.3 | 0.5 | 22.0 | 0.1 | 20.1 | 0.1 | 2.3 | 1.9 |
| 588010136263263191 | 129.1525 | 47.2654 | 25.0 | 0.9 | 24.1 | 0.5 | 23.9 | 0.5 | 21.7 | 0.1 | 20.3 | 0.2 | 2.2 | 1.4 |
| 587735240099890134 | 129.1914 | 28.7956 | 24.4 | 1.3 | 24.1 | 0.6 | 24.6 | 0.7 | 22.1 | 0.2 | 20.8 | 0.2 | 2.5 | 1.3 |
| 587745243618936116 | 129.2938 | 11.3592 | 25.0 | 0.9 | 24.7 | 0.5 | 25.2 | 0.5 | 22.7 | 0.2 | 20.7 | 0.2 | 2.5 | 2.0 |
| 587732702315611255 | 129.5683 | 4.1795 | 24.8 | 1.1 | 25.7 | 0.8 | 23.8 | 0.5 | 21.0 | 0.1 | 19.2 | 0.1 | 2.7 | 1.8 |
| 588017979409171295 | 129.7783 | 26.2118 | 25.6 | 0.6 | 24.5 | 0.5 | 25.1 | 0.6 | 22.3 | 0.2 | 20.8 | 0.2 | 2.9 | 1.5 |
| 587744637492462684 | 130.0276 | 14.4030 | 23.2 | 0.7 | 25.7 | 0.5 | 24.1 | 0.7 | 22.0 | 0.1 | 20.6 | 0.2 | 2.1 | 1.5 |
| 587741532768634037 | 130.1910 | 18.3188 | 24.6 | 0.9 | 25.2 | 0.5 | 24.1 | 0.5 | 21.4 | 0.1 | 19.7 | 0.1 | 2.7 | 1.7 |
| 588023239936181347 | 130.8433 | 15.1661 | 24.7 | 0.9 | 24.9 | 0.6 | 23.5 | 0.3 | 21.2 | 0.1 | 19.9 | 0.1 | 2.2 | 1.4 |
| 588010360138499214 | 130.8541 | 3.6405 | 25.7 | 0.8 | 25.4 | 0.7 | 23.7 | 0.5 | 21.2 | 0.1 | 19.9 | 0.1 | 2.4 | 1.3 |
| 587735343183168623 | 130.9081 | 6.8343 | 25.5 | 0.8 | 24.2 | 0.4 | 24.6 | 0.6 | 22.2 | 0.2 | 20.2 | 0.1 | 2.5 | 2.0 |
| 587738947200287788 | 130.9399 | 26.1878 | 24.5 | 1.0 | 25.5 | 0.6 | 24.5 | 0.6 | 22.3 | 0.2 | 20.9 | 0.2 | 2.2 | 1.3 |
| 588023239130940550 | 131.1204 | 14.8844 | 24.3 | 1.1 | 25.2 | 0.6 | 23.6 | 0.9 | 21.4 | 0.1 | 19.5 | 0.1 | 2.2 | 1.9 |
| 587732048940958642 | 131.1430 | 41.9367 | 24.5 | 1.4 | 25.1 | 0.5 | 24.1 | 0.6 | 21.9 | 0.1 | 20.3 | 0.1 | 2.2 | 1.7 |
| 587732578297316598 | 131.4154 | 4.5721 | 23.5 | 0.6 | 25.5 | 0.4 | 24.9 | 0.5 | 22.6 | 0.2 | 20.5 | 0.1 | 2.3 | 2.1 |
| 587731885739410417 | 131.7574 | 42.1904 | 24.9 | 1.3 | 25.2 | 0.6 | 24.5 | 0.7 | 22.3 | 0.2 | 20.8 | 0.2 | 2.1 | 1.5 |

Table C.1 (cont'd)

| Object ID | RA | DEC | u | u err | g | g err | r | r err | i | i err | z | z err | r-i | i-z |
|---|---|---|---|---|---|---|---|---|---|---|---|---|---|---|
| 588016879367095353 | 132.6092 | 29.4826 | 23.6 | 0.8 | 25.2 | 0.6 | 24.6 | 0.6 | 21.9 | 0.1 | 20.6 | 0.2 | 2.7 | 1.3 |
| 587745243083638011 | 132.8636 | 11.8510 | 23.8 | 0.9 | 26.4 | 0.4 | 23.6 | 0.4 | 21.4 | 0.1 | 19.9 | 0.1 | 2.2 | 1.5 |
| 587745244157445136 | 132.8730 | 12.7470 | 24.2 | 1.0 | 25.3 | 0.5 | 24.3 | 0.6 | 22.2 | 0.2 | 20.8 | 0.3 | 2.2 | 1.4 |
| 587734623243994049 | 133.7811 | 35.0230 | 25.2 | 0.8 | 24.6 | 0.6 | 24.3 | 0.7 | 22.0 | 0.2 | 20.0 | 0.1 | 2.3 | 2.0 |
| 587741390494172383 | 133.7948 | 20.9534 | 24.7 | 1.0 | 25.3 | 0.5 | 25.2 | 0.5 | 22.2 | 0.1 | 20.7 | 0.2 | 3.0 | 1.5 |
| 587739115241407869 | 133.8194 | 25.8542 | 24.9 | 0.9 | 24.7 | 0.5 | 24.6 | 0.5 | 22.4 | 0.1 | 20.9 | 0.2 | 2.2 | 1.5 |
| 587738067810517573 | 134.0615 | 64.5391 | 25.2 | 0.9 | 24.8 | 0.5 | 23.5 | 0.3 | 21.4 | 0.1 | 20.0 | 0.1 | 2.2 | 1.4 |
| 587728880868459565 | 134.1800 | 3.7857 | 25.6 | 0.8 | 25.3 | 0.7 | 24.8 | 0.7 | 22.2 | 0.2 | 20.7 | 0.2 | 2.6 | 1.5 |
| 587728931879781318 | 134.3119 | 48.0796 | 24.0 | 0.9 | 25.9 | 0.5 | 24.2 | 0.6 | 22.0 | 0.1 | 20.5 | 0.2 | 2.3 | 1.5 |
| 587738065662444681 | 134.9270 | 62.3799 | 24.5 | 1.0 | 26.1 | 0.5 | 25.4 | 0.6 | 22.4 | 0.2 | 20.8 | 0.2 | 2.9 | 1.6 |
| 587725551201682191 | 135.0932 | 56.9195 | 23.9 | 1.0 | 25.2 | 0.7 | 24.3 | 0.7 | 21.3 | 0.1 | 20.0 | 0.1 | 3.0 | 1.4 |
| 588848900966974589 | 135.5404 | 0.7874 | 25.3 | 0.7 | 24.5 | 0.6 | 24.8 | 0.6 | 22.6 | 0.3 | 20.8 | 0.2 | 2.2 | 1.8 |
| 588010931370787667 | 136.2548 | -1.1901 | 25.9 | 0.9 | 25.9 | 0.8 | 23.9 | 0.8 | 21.1 | 0.1 | 19.6 | 0.1 | 2.8 | 1.5 |
| 587725074990892118 | 136.4803 | 0.0084 | 24.8 | 0.8 | 24.1 | 0.4 | 23.5 | 0.4 | 21.1 | 0.1 | 19.7 | 0.1 | 2.5 | 1.3 |
| 587739157111767895 | 136.4962 | 26.2652 | 23.1 | 0.7 | 24.9 | 0.6 | 23.4 | 0.4 | 21.1 | 0.1 | 19.5 | 0.1 | 2.3 | 1.6 |
| 587731887352513242 | 136.4992 | 46.7866 | 23.3 | 0.7 | 25.5 | 0.7 | 24.3 | 0.8 | 21.6 | 0.1 | 20.1 | 0.1 | 2.6 | 1.6 |
| 587735661006685535 | 136.6245 | 30.3807 | 25.2 | 0.8 | 24.9 | 0.5 | 24.6 | 0.6 | 22.1 | 0.1 | 20.7 | 0.1 | 2.5 | 1.5 |
| 587731521207075766 | 136.6842 | 43.0042 | 25.0 | 1.1 | 25.1 | 0.6 | 24.7 | 0.8 | 21.8 | 0.2 | 20.5 | 0.2 | 2.8 | 1.4 |
| 587737810113070028 | 137.0808 | 62.1737 | 25.4 | 0.7 | 24.5 | 0.4 | 25.0 | 0.7 | 21.9 | 0.1 | 20.4 | 0.1 | 3.1 | 1.5 |
| 588848899893953565 | 137.2123 | -0.1872 | 25.2 | 0.7 | 24.7 | 0.6 | 24.7 | 0.6 | 21.7 | 0.1 | 20.3 | 0.1 | 3.0 | 1.5 |
| 587726031692956510 | 137.2299 | 0.9463 | 24.0 | 1.4 | 25.7 | 0.7 | 24.2 | 0.6 | 22.0 | 0.2 | 20.5 | 0.2 | 2.2 | 1.5 |
| 587732771572941745 | 137.6327 | 6.8926 | 23.8 | 0.9 | 24.5 | 0.5 | 24.2 | 0.6 | 21.7 | 0.1 | 20.2 | 0.2 | 2.5 | 1.5 |
| 588010360141644747 | 137.9911 | 4.1146 | 25.6 | 0.7 | 25.9 | 0.5 | 23.2 | 0.3 | 20.9 | 0.1 | 19.4 | 0.1 | 2.3 | 1.5 |
| 587732578837267406 | 138.4298 | 5.7164 | 25.2 | 0.9 | 25.8 | 0.6 | 24.8 | 0.8 | 21.9 | 0.2 | 20.5 | 0.1 | 2.9 | 1.4 |
| 587745402000376763 | 138.6059 | 11.5764 | 25.0 | 1.2 | 25.4 | 0.6 | 24.9 | 0.6 | 22.3 | 0.2 | 20.5 | 0.1 | 2.6 | 1.8 |
| 587745403611120842 | 138.7042 | 12.7301 | 24.4 | 0.8 | 24.6 | 0.5 | 23.4 | 0.3 | 21.0 | 0.1 | 19.6 | 0.1 | 2.4 | 1.5 |
| 588010931372229514 | 139.5752 | -1.3058 | 24.8 | 1.4 | 24.7 | 0.8 | 25.0 | 0.9 | 21.9 | 0.2 | 20.5 | 0.2 | 3.2 | 1.3 |

Table C.1 (cont'd)

| Object ID | RA | DEC | u | u err | g | g err | r | r err | i | i err | z | z err | r-i | i-z |
|---|---|---|---|---|---|---|---|---|---|---|---|---|---|---|
| 587739116317901722 | 139.6774 | 29.3276 | 24.7 | 1.0 | 24.8 | 0.5 | 23.7 | 0.4 | 21.6 | 0.1 | 20.2 | 0.1 | 2.1 | 1.4 |
| 587739377237623666 | 139.9974 | 26.7931 | 25.1 | 1.0 | 24.0 | 0.4 | 25.0 | 0.6 | 21.8 | 0.1 | 20.4 | 0.2 | 3.2 | 1.4 |
| 588009366936683268 | 140.1298 | 53.4593 | 23.9 | 1.0 | 25.3 | 0.6 | 24.6 | 0.7 | 22.1 | 0.2 | 20.2 | 0.2 | 2.5 | 1.8 |
| 587741532236350353 | 140.7038 | 21.8742 | 25.0 | 1.0 | 25.3 | 0.5 | 24.8 | 0.6 | 22.1 | 0.1 | 20.3 | 0.1 | 2.7 | 1.7 |
| 588023046942032976 | 140.8789 | 20.6767 | 23.8 | 0.9 | 24.9 | 0.6 | 24.3 | 0.5 | 22.0 | 0.1 | 20.6 | 0.2 | 2.3 | 1.4 |
| 587742062128530595 | 141.0222 | 17.1453 | 25.0 | 0.8 | 26.0 | 0.4 | 24.8 | 0.6 | 22.5 | 0.2 | 21.0 | 0.2 | 2.3 | 1.5 |
| 587735661008782311 | 141.4131 | 32.7343 | 24.5 | 0.9 | 25.3 | 0.5 | 25.1 | 0.5 | 22.5 | 0.2 | 21.2 | 0.2 | 2.5 | 1.4 |
| 587725084112126989 | 141.8161 | -1.2311 | 24.9 | 0.9 | 23.9 | 0.3 | 24.7 | 0.7 | 21.8 | 0.1 | 20.2 | 0.1 | 2.9 | 1.6 |
| 587732048408216470 | 141.9283 | 47.6861 | 25.3 | 1.0 | 26.1 | 0.5 | 23.4 | 0.4 | 20.9 | 0.1 | 19.6 | 0.1 | 2.5 | 1.3 |
| 587741816779048079 | 142.0450 | 18.8744 | 24.1 | 0.9 | 25.2 | 0.4 | 23.6 | 0.3 | 20.8 | 0.0 | 19.3 | 0.1 | 2.8 | 1.6 |
| 587725082501710856 | 142.2355 | -2.5049 | 23.1 | 0.5 | 25.2 | 0.7 | 24.9 | 0.6 | 22.1 | 0.1 | 20.5 | 0.1 | 2.8 | 1.6 |
| 587742061055509536 | 142.9936 | 16.6777 | 23.6 | 0.6 | 25.3 | 0.5 | 23.4 | 0.3 | 21.3 | 0.1 | 19.6 | 0.1 | 2.1 | 1.7 |
| 587741490361992228 | 143.6895 | 23.6026 | 24.5 | 0.9 | 24.9 | 0.5 | 24.2 | 0.4 | 21.7 | 0.1 | 20.2 | 0.2 | 2.5 | 1.6 |
| 588009368548868956 | 143.8196 | 56.6921 | 25.0 | 1.2 | 24.5 | 0.5 | 25.1 | 0.8 | 22.0 | 0.2 | 20.3 | 0.2 | 3.1 | 1.8 |
| 587741821600007462 | 143.8346 | 20.0941 | 25.0 | 0.6 | 24.9 | 0.4 | 25.5 | 0.4 | 23.2 | 0.3 | 21.2 | 1.0 | 2.3 | 2.1 |
| 587745541052171128 | 143.8352 | 14.0716 | 24.0 | 0.7 | 25.2 | 0.5 | 25.1 | 0.7 | 22.3 | 0.2 | 21.0 | 0.2 | 2.7 | 1.3 |
| 587735239569244837 | 143.8536 | 35.9067 | 24.6 | 0.9 | 25.0 | 0.8 | 24.2 | 0.6 | 21.2 | 0.1 | 19.9 | 0.1 | 3.0 | 1.3 |
| 587735241717253077 | 144.2055 | 37.9672 | 24.1 | 0.7 | 25.3 | 0.5 | 24.9 | 0.6 | 22.7 | 0.3 | 21.1 | 0.2 | 2.2 | 1.5 |
| 587741532774990849 | 144.5733 | 23.6227 | 25.2 | 0.8 | 24.7 | 0.5 | 25.3 | 0.6 | 22.3 | 0.2 | 20.2 | 0.1 | 3.0 | 2.1 |
| 587725469600514982 | 144.7247 | 58.0650 | 23.3 | 0.5 | 24.1 | 0.4 | 24.7 | 0.7 | 22.1 | 0.2 | 20.6 | 0.2 | 2.6 | 1.5 |
| 588010135194960753 | 144.8458 | 54.8227 | 25.2 | 1.0 | 24.8 | 0.6 | 23.5 | 0.4 | 21.2 | 0.1 | 19.8 | 0.1 | 2.4 | 1.3 |
| 587746028521653096 | 145.0208 | 80.8068 | 24.9 | 1.7 | 25.6 | 0.9 | 25.1 | 1.0 | 22.0 | 0.2 | 20.3 | 0.2 | 3.1 | 1.7 |
| 587735347484492866 | 145.4473 | 11.0259 | 23.5 | 0.6 | 24.9 | 0.5 | 24.7 | 0.5 | 21.8 | 0.1 | 20.1 | 0.1 | 2.9 | 1.7 |
| 587745245236888254 | 145.6147 | 16.5869 | 23.9 | 0.9 | 24.3 | 0.4 | 24.3 | 0.6 | 20.9 | 0.1 | 19.6 | 0.1 | 3.3 | 1.4 |
| 587729149307519797 | 145.7727 | -2.8949 | 24.1 | 1.1 | 24.4 | 0.8 | 24.3 | 0.9 | 21.7 | 0.2 | 20.0 | 0.1 | 2.6 | 1.7 |
| 588010135732225093 | 145.8303 | 55.6668 | 23.0 | 0.4 | 24.6 | 0.6 | 24.2 | 0.5 | 21.7 | 0.1 | 20.2 | 0.1 | 2.4 | 1.6 |
| 587745964634277002 | 146.0568 | 80.7485 | 25.6 | 1.1 | 24.3 | 0.5 | 25.3 | 0.9 | 22.2 | 0.2 | 20.1 | 0.1 | 3.1 | 2.1 |

Table C.1 (cont'd)

| Object ID | RA | DEC | u | u err | g | g err | r | r err | i | i err | z | z err | r-i | i-z |
|---|---|---|---|---|---|---|---|---|---|---|---|---|---|---|
| 587742062130823973 | 146.4056 | 18.4595 | 25.1 | 0.8 | 25.1 | 0.7 | 24.0 | 0.4 | 21.6 | 0.1 | 20.2 | 0.1 | 2.4 | 1.4 |
| 587739114172974115 | 146.6519 | 30.3160 | 25.6 | 0.8 | 25.1 | 0.6 | 23.3 | 0.3 | 21.2 | 0.1 | 19.3 | 0.0 | 2.1 | 1.9 |
| 587745404151661507 | 147.1223 | 14.8640 | 25.0 | 0.9 | 25.4 | 0.5 | 24.0 | 0.5 | 21.4 | 0.1 | 19.9 | 0.1 | 2.6 | 1.5 |
| 587729387680760562 | 147.1262 | 54.4118 | 25.5 | 0.7 | 25.3 | 0.7 | 23.9 | 0.5 | 21.8 | 0.1 | 20.0 | 0.1 | 2.2 | 1.7 |
| 587725082503873175 | 147.1817 | -2.6797 | 24.0 | 1.3 | 25.6 | 0.9 | 23.6 | 0.5 | 21.2 | 0.1 | 19.5 | 0.1 | 2.4 | 1.7 |
| 587739407304885266 | 147.3420 | 29.0520 | 25.6 | 0.7 | 24.4 | 0.5 | 24.9 | 0.7 | 21.9 | 0.1 | 20.4 | 0.2 | 3.0 | 1.5 |
| 588016892783755943 | 148.5550 | 37.3050 | 25.6 | 0.7 | 25.1 | 0.6 | 23.9 | 0.6 | 21.7 | 0.1 | 20.2 | 0.1 | 2.2 | 1.5 |
| 587739377778164705 | 148.6406 | 30.2270 | 25.8 | 0.6 | 24.3 | 0.5 | 23.5 | 0.4 | 21.4 | 0.1 | 20.0 | 0.1 | 2.1 | 1.4 |
| 587731500257903502 | 149.5388 | 52.1156 | 25.5 | 0.8 | 24.4 | 0.4 | 23.5 | 0.3 | 21.0 | 0.1 | 19.4 | 0.1 | 2.6 | 1.6 |
| 587732771041313734 | 149.6479 | 7.8360 | 25.0 | 1.0 | 24.3 | 0.5 | 23.4 | 0.3 | 21.0 | 0.1 | 19.7 | 0.1 | 2.4 | 1.3 |
| 587734622176346991 | 149.6934 | 41.2482 | 24.1 | 1.0 | 24.3 | 0.4 | 24.0 | 0.7 | 21.8 | 0.2 | 20.5 | 0.2 | 2.2 | 1.4 |
| 587738410862183251 | 150.0329 | 12.6704 | 23.7 | 0.9 | 23.8 | 0.3 | 23.9 | 0.5 | 21.3 | 0.1 | 20.0 | 0.1 | 2.5 | 1.4 |
| 587732049484907326 | 150.0537 | 52.0423 | 24.2 | 0.9 | 24.8 | 0.6 | 24.2 | 0.6 | 21.6 | 0.1 | 20.0 | 0.1 | 2.6 | 1.6 |
| 588848900436788207 | 150.8812 | 0.2572 | 25.5 | 0.6 | 24.2 | 0.4 | 23.9 | 0.4 | 21.5 | 0.1 | 20.2 | 0.1 | 2.4 | 1.3 |
| 587741491438879653 | 151.0424 | 26.5829 | 25.1 | 0.9 | 25.0 | 0.5 | 23.8 | 0.4 | 21.6 | 0.1 | 20.1 | 0.1 | 2.2 | 1.5 |
| 587731500795429936 | 151.2333 | 53.2276 | 25.6 | 0.7 | 25.4 | 0.5 | 23.8 | 0.4 | 21.7 | 0.1 | 19.9 | 0.1 | 2.2 | 1.7 |
| 587735661012780068 | 151.5337 | 36.5869 | 24.5 | 1.0 | 25.1 | 0.5 | 23.4 | 0.3 | 21.1 | 0.0 | 19.3 | 0.0 | 2.3 | 1.8 |
| 587746028522308335 | 151.8511 | 79.8267 | 25.6 | 1.2 | 26.5 | 0.5 | 24.1 | 0.8 | 21.0 | 0.1 | 19.5 | 0.1 | 3.0 | 1.6 |
| 587735661012911027 | 152.0080 | 36.6516 | 25.0 | 0.9 | 24.7 | 0.5 | 24.7 | 0.5 | 22.0 | 0.1 | 20.6 | 0.1 | 2.7 | 1.4 |
| 587741815709762781 | 152.7671 | 20.7417 | 24.9 | 0.9 | 24.3 | 0.3 | 23.2 | 0.2 | 20.8 | 0.0 | 19.5 | 0.1 | 2.4 | 1.4 |
| 587745401469863009 | 153.3206 | 13.9345 | 22.9 | 0.3 | 25.3 | 0.7 | 23.7 | 0.4 | 21.2 | 0.1 | 19.7 | 0.1 | 2.5 | 1.5 |
| 587733079193813860 | 153.6774 | 49.4685 | 22.4 | 0.3 | 25.2 | 0.9 | 24.0 | 0.7 | 21.7 | 0.1 | 20.3 | 0.1 | 2.4 | 1.4 |
| 587739376706323289 | 153.8388 | 30.7842 | 25.3 | 0.9 | 24.2 | 0.4 | 24.4 | 0.7 | 22.0 | 0.1 | 20.6 | 0.2 | 2.4 | 1.4 |
| 587738618093962166 | 154.5962 | 34.5953 | 24.9 | 1.2 | 24.1 | 0.4 | 24.8 | 0.7 | 22.1 | 0.2 | 20.3 | 0.1 | 2.7 | 1.7 |
| 587734623788991419 | 154.6451 | 44.3487 | 25.3 | 0.9 | 24.9 | 0.5 | 23.5 | 0.3 | 21.3 | 0.1 | 20.0 | 0.1 | 2.2 | 1.3 |
| 587728879803827157 | 155.0198 | 3.9675 | 24.5 | 0.9 | 24.5 | 0.6 | 24.6 | 0.6 | 22.3 | 0.2 | 20.8 | 0.2 | 2.3 | 1.5 |
| 588023046411125759 | 155.0974 | 23.9575 | 25.5 | 0.6 | 24.4 | 0.4 | 23.9 | 0.4 | 21.6 | 0.1 | 20.1 | 0.1 | 2.3 | 1.5 |

Table C.1 (cont'd)

| Object ID | RA | DEC | u | u err | g | g err | r | r err | i | i err | z | z err | r-i | i-z |
|---|---|---|---|---|---|---|---|---|---|---|---|---|---|---|
| 587735661014287541 | 155.7114 | 37.7758 | 23.9 | 0.8 | 25.0 | 0.5 | 24.3 | 0.6 | 21.5 | 0.1 | 19.7 | 0.1 | 2.8 | 1.8 |
| 587731500260066168 | 157.0133 | 54.2306 | 23.8 | 0.8 | 25.6 | 0.5 | 23.5 | 0.4 | 20.9 | 0.1 | 19.3 | 0.1 | 2.7 | 1.6 |
| 587732482741568799 | 157.5530 | 46.1316 | 24.7 | 0.9 | 24.8 | 0.4 | 23.5 | 0.3 | 21.1 | 0.1 | 19.5 | 0.1 | 2.4 | 1.6 |
| 587734863221883710 | 157.9937 | 9.2045 | 25.9 | 0.6 | 25.2 | 0.6 | 24.3 | 0.6 | 21.6 | 0.1 | 19.9 | 0.1 | 2.7 | 1.7 |
| 588017605750096661 | 159.5751 | 42.8911 | 24.8 | 0.8 | 25.1 | 0.5 | 23.9 | 0.4 | 21.4 | 0.1 | 19.9 | 0.1 | 2.4 | 1.5 |
| 587745539985179956 | 159.6697 | 15.7868 | 25.4 | 0.5 | 24.9 | 0.6 | 23.8 | 0.3 | 21.5 | 0.1 | 20.1 | 0.1 | 2.3 | 1.4 |
| 587732578309702669 | 159.8156 | 7.0035 | 24.8 | 1.0 | 24.9 | 0.5 | 24.2 | 0.5 | 21.6 | 0.1 | 20.3 | 0.1 | 2.6 | 1.4 |
| 587739407846802324 | 160.0626 | 32.8519 | 25.1 | 0.8 | 24.6 | 0.5 | 23.8 | 0.4 | 21.0 | 0.1 | 19.6 | 0.1 | 2.8 | 1.3 |
| 587732578309833768 | 160.1011 | 6.8967 | 24.3 | 0.9 | 24.5 | 0.5 | 23.8 | 0.4 | 21.4 | 0.1 | 19.7 | 0.1 | 2.3 | 1.7 |
| 587735348564788049 | 160.5537 | 13.7753 | 24.0 | 0.8 | 25.3 | 0.5 | 24.4 | 0.4 | 22.1 | 0.1 | 20.2 | 0.1 | 2.3 | 1.9 |
| 587742863935997065 | 160.6133 | 15.4069 | 26.4 | 0.5 | 24.0 | 0.4 | 23.6 | 0.4 | 21.0 | 0.1 | 19.6 | 0.1 | 2.6 | 1.4 |
| 588009370149061217 | 160.6377 | 58.9619 | 25.1 | 0.9 | 25.6 | 0.7 | 23.8 | 0.5 | 21.1 | 0.1 | 19.8 | 0.1 | 2.7 | 1.3 |
| 588017978885014291 | 161.5637 | 37.6308 | 24.9 | 1.1 | 24.7 | 0.6 | 24.7 | 0.7 | 21.4 | 0.1 | 20.0 | 0.1 | 3.3 | 1.4 |
| 587731498650567700 | 161.8517 | 54.0201 | 24.4 | 1.0 | 24.3 | 0.5 | 25.0 | 0.7 | 22.4 | 0.2 | 20.9 | 0.2 | 2.6 | 1.5 |
| 588848900978770884 | 162.5416 | 0.7967 | 23.9 | 0.6 | 25.3 | 0.5 | 24.1 | 0.6 | 21.7 | 0.1 | 20.1 | 0.1 | 2.4 | 1.6 |
| 588017111826367362 | 162.7343 | 45.7594 | 25.1 | 0.9 | 25.4 | 0.6 | 23.5 | 0.3 | 21.2 | 0.1 | 19.6 | 0.1 | 2.3 | 1.6 |
| 587738615412360104 | 162.7542 | 34.2673 | 24.3 | 0.8 | 24.3 | 0.5 | 24.1 | 0.6 | 21.8 | 0.1 | 20.2 | 0.1 | 2.4 | 1.6 |
| 587745517955974092 | 163.6358 | -23.0362 | 23.9 | 1.6 | 25.6 | 0.7 | 24.5 | 0.8 | 22.1 | 0.2 | 20.2 | 0.1 | 2.5 | 1.8 |
| 587741531709309855 | 164.6244 | 27.4117 | 25.7 | 0.8 | 25.1 | 0.7 | 23.4 | 0.4 | 21.0 | 0.1 | 19.3 | 0.1 | 2.4 | 1.7 |
| 587726032241820432 | 164.6555 | 2.0157 | 23.1 | 0.6 | 24.3 | 0.5 | 24.7 | 0.7 | 22.5 | 0.3 | 20.4 | 0.2 | 2.2 | 2.1 |
| 588011098872087170 | 164.9986 | 61.8172 | 24.9 | 1.2 | 25.3 | 0.7 | 23.8 | 0.6 | 21.2 | 0.1 | 19.8 | 0.1 | 2.6 | 1.4 |
| 587739294550655835 | 165.0833 | 32.7535 | 24.4 | 1.2 | 25.5 | 0.5 | 24.8 | 0.6 | 22.1 | 0.2 | 20.7 | 0.2 | 2.7 | 1.4 |
| 588017110216475538 | 165.4542 | 45.0014 | 24.2 | 1.1 | 25.1 | 0.6 | 24.8 | 0.7 | 22.2 | 0.2 | 20.6 | 0.2 | 2.6 | 1.6 |
| 587745419172512941 | 165.5052 | -20.0161 | 24.6 | 1.3 | 24.7 | 0.5 | 24.9 | 0.6 | 22.2 | 0.2 | 20.9 | 0.2 | 2.7 | 1.3 |
| 587742949567759253 | 165.6178 | 62.9000 | 24.9 | 1.3 | 25.5 | 0.6 | 24.1 | 0.7 | 21.8 | 0.1 | 20.1 | 0.1 | 2.4 | 1.7 |
| 588017720101962625 | 166.1909 | 40.1517 | 25.5 | 0.9 | 24.8 | 0.6 | 25.2 | 0.6 | 22.3 | 0.2 | 20.5 | 0.1 | 2.9 | 1.8 |
| 587742061065405423 | 166.4210 | 21.0518 | 25.3 | 0.7 | 25.1 | 0.6 | 23.9 | 0.4 | 21.7 | 0.1 | 20.3 | 0.1 | 2.2 | 1.5 |

Table C.1 (cont'd)

| Object ID | RA | DEC | u | u err | g | g err | r | r err | i | i err | z | z err | r-i | i-z |
|---|---|---|---|---|---|---|---|---|---|---|---|---|---|---|
| 587745419173299268 | 166.4666 | -18.4174 | 24.4 | 1.6 | 24.9 | 0.6 | 23.9 | 0.4 | 21.5 | 0.1 | 20.0 | 0.1 | 2.4 | 1.5 |
| 587739097519883343 | 166.5179 | 36.0247 | 25.0 | 1.0 | 25.1 | 0.6 | 23.5 | 0.9 | 20.8 | 0.0 | 19.4 | 0.1 | 2.7 | 1.4 |
| 587745517421659160 | 167.3495 | -18.3025 | 25.4 | 1.1 | 25.2 | 0.9 | 23.9 | 0.5 | 21.7 | 0.1 | 20.4 | 0.2 | 2.2 | 1.4 |
| 588017702388368164 | 167.7542 | 10.9681 | 25.0 | 1.2 | 25.7 | 0.8 | 24.7 | 1.0 | 22.2 | 0.3 | 20.4 | 0.2 | 2.5 | 1.8 |
| 588017627224015847 | 168.5089 | 44.2847 | 25.1 | 0.7 | 24.5 | 0.5 | 24.0 | 0.5 | 21.8 | 0.1 | 20.1 | 0.1 | 2.2 | 1.7 |
| 587745421325763640 | 170.8485 | -7.7415 | 24.5 | 0.9 | 24.5 | 0.4 | 23.9 | 0.4 | 21.7 | 0.1 | 20.0 | 0.1 | 2.2 | 1.8 |
| 588010358008710228 | 171.3568 | 3.8177 | 23.3 | 0.5 | 24.7 | 0.6 | 23.2 | 0.2 | 21.0 | 0.1 | 19.3 | 0.0 | 2.2 | 1.7 |
| 587726032781706246 | 171.5645 | 2.4977 | 24.1 | 1.2 | 23.5 | 0.3 | 23.9 | 0.5 | 21.7 | 0.1 | 20.2 | 0.2 | 2.2 | 1.5 |
| 588017110755509046 | 172.2477 | 46.4072 | 23.9 | 0.8 | 24.6 | 0.5 | 23.7 | 0.4 | 21.2 | 0.1 | 19.6 | 0.1 | 2.5 | 1.6 |
| 587748878767293348 | 172.4064 | -4.6113 | 25.1 | 1.0 | 24.4 | 0.4 | 24.0 | 0.6 | 21.7 | 0.2 | 20.3 | 0.1 | 2.3 | 1.5 |
| 588010878755930812 | 172.6794 | 4.6231 | 25.1 | 1.0 | 23.6 | 0.4 | 24.4 | 0.8 | 21.0 | 0.1 | 19.6 | 0.1 | 3.4 | 1.5 |
| 587732772662215483 | 173.3376 | 10.7932 | 25.1 | 1.1 | 24.6 | 0.5 | 25.0 | 0.7 | 22.6 | 0.3 | 20.8 | 0.2 | 2.4 | 1.7 |
| 587732483283551295 | 174.1708 | 49.3591 | 24.4 | 0.7 | 24.4 | 0.3 | 24.4 | 0.4 | 22.0 | 0.1 | 20.3 | 0.1 | 2.4 | 1.7 |
| 587741709419676538 | 174.5612 | 27.4629 | 23.9 | 0.8 | 24.7 | 0.4 | 23.5 | 0.3 | 21.3 | 0.1 | 19.8 | 0.1 | 2.2 | 1.5 |
| 587735349376451646 | 175.4564 | 15.3323 | 24.5 | 0.8 | 24.1 | 0.3 | 24.3 | 0.5 | 21.8 | 0.1 | 19.9 | 0.1 | 2.6 | 1.9 |
| 587734894361904010 | 175.8093 | 10.9364 | 23.1 | 0.6 | 24.0 | 0.5 | 23.8 | 0.7 | 20.9 | 0.1 | 19.6 | 0.1 | 2.9 | 1.3 |
| 588023668631536741 | 175.8511 | 19.2520 | 25.4 | 1.0 | 25.0 | 0.6 | 24.3 | 0.4 | 22.0 | 0.1 | 20.7 | 0.1 | 2.3 | 1.3 |
| 587732771589850177 | 176.5640 | 9.9435 | 25.2 | 1.0 | 23.9 | 0.4 | 23.5 | 0.4 | 20.9 | 0.1 | 19.6 | 0.1 | 2.6 | 1.3 |
| 587731869096477517 | 177.0183 | 54.6310 | 25.6 | 0.8 | 25.0 | 0.6 | 24.6 | 0.7 | 21.7 | 0.1 | 20.3 | 0.1 | 2.9 | 1.4 |
| 587742572151440523 | 177.3201 | 19.6050 | 24.5 | 0.9 | 24.7 | 0.5 | 23.5 | 0.3 | 20.9 | 0.0 | 19.3 | 0.1 | 2.6 | 1.5 |
| 588013381668373442 | 177.6184 | 51.0420 | 25.4 | 0.8 | 25.0 | 0.7 | 24.2 | 0.5 | 21.1 | 0.1 | 19.4 | 0.1 | 3.1 | 1.7 |
| 587729386077750152 | 178.0388 | 59.0900 | 24.8 | 1.1 | 24.1 | 0.5 | 24.0 | 0.7 | 21.8 | 0.1 | 20.3 | 0.1 | 2.3 | 1.4 |
| 587741602029831217 | 179.2004 | 27.5228 | 25.5 | 0.8 | 26.2 | 0.3 | 24.4 | 0.6 | 22.3 | 0.2 | 20.7 | 0.2 | 2.2 | 1.5 |
| 588848900449436610 | 179.6998 | 0.2298 | 25.3 | 0.7 | 23.7 | 0.3 | 23.6 | 0.3 | 21.2 | 0.1 | 19.9 | 0.1 | 2.4 | 1.4 |
| 588017979428438734 | 180.6327 | 40.3433 | 24.9 | 1.0 | 24.3 | 0.6 | 24.7 | 0.7 | 22.1 | 0.2 | 20.8 | 0.2 | 2.6 | 1.3 |
| 587742189366609038 | 180.7011 | 24.2325 | 24.5 | 1.1 | 24.8 | 0.5 | 23.4 | 0.3 | 21.2 | 0.1 | 19.6 | 0.1 | 2.2 | 1.6 |
| 587728676856660277 | 180.7489 | 63.7893 | 22.3 | 0.2 | 24.9 | 0.6 | 25.5 | 0.5 | 23.2 | 0.9 | 21.7 | 0.4 | 2.2 | 1.5 |

Table C.1 (cont'd)

| Object ID | RA | DEC | u | u err | g | g err | r | r err | i | i err | z | z err | r-i | i-z |
|---|---|---|---|---|---|---|---|---|---|---|---|---|---|---|
| 588017949350822800 | 181.0926 | 43.1136 | 26.1 | 0.9 | 24.3 | 0.3 | 23.7 | 0.4 | 21.5 | 0.1 | 19.7 | 0.1 | 2.1 | 1.8 |
| 587742863676605501 | 182.0668 | 16.8712 | 25.2 | 1.1 | 25.0 | 0.5 | 23.6 | 0.4 | 21.0 | 0.1 | 19.5 | 0.1 | 2.6 | 1.5 |
| 587732702875419575 | 182.1231 | 7.8887 | 25.6 | 1.0 | 24.5 | 0.5 | 24.0 | 0.5 | 21.3 | 0.1 | 19.9 | 0.1 | 2.8 | 1.4 |
| 587741602031862746 | 184.3958 | 27.6086 | 24.3 | 1.0 | 24.9 | 0.5 | 23.4 | 0.3 | 21.3 | 0.1 | 19.9 | 0.1 | 2.1 | 1.4 |
| 588013381670405094 | 185.0387 | 51.4017 | 24.9 | 0.9 | 25.2 | 0.6 | 23.8 | 0.4 | 20.8 | 0.1 | 19.0 | 0.0 | 3.0 | 1.9 |
| 587741601495319326 | 185.2366 | 27.2104 | 25.5 | 0.6 | 24.8 | 0.5 | 23.3 | 0.3 | 20.9 | 0.1 | 19.6 | 0.1 | 2.4 | 1.3 |
| 588017109685896049 | 185.9750 | 46.4380 | 25.3 | 0.9 | 25.7 | 0.6 | 25.2 | 0.6 | 21.8 | 0.1 | 19.9 | 0.1 | 3.3 | 1.9 |
| 587725039557936262 | 186.5731 | -3.2575 | 25.7 | 0.8 | 25.6 | 0.5 | 24.0 | 0.5 | 21.8 | 0.1 | 20.4 | 0.2 | 2.1 | 1.4 |
| 587741602032976873 | 187.2962 | 27.6403 | 24.1 | 1.1 | 25.7 | 0.4 | 23.7 | 0.4 | 21.4 | 0.1 | 19.9 | 0.1 | 2.2 | 1.5 |
| 587725040632071125 | 187.5061 | -2.3313 | 25.1 | 0.8 | 24.1 | 0.4 | 23.4 | 0.3 | 21.0 | 0.1 | 19.5 | 0.1 | 2.3 | 1.5 |
| 588017720645911348 | 187.5605 | 42.1361 | 24.8 | 1.1 | 25.2 | 0.5 | 24.3 | 0.6 | 21.8 | 0.1 | 20.3 | 0.1 | 2.5 | 1.5 |
| 587731869099492352 | 189.0408 | 54.8202 | 23.6 | 0.9 | 24.5 | 0.7 | 23.3 | 0.3 | 21.1 | 0.1 | 19.7 | 0.1 | 2.3 | 1.4 |
| 587732483287942155 | 189.8179 | 49.8006 | 23.7 | 0.6 | 25.4 | 0.5 | 24.4 | 0.6 | 21.2 | 0.1 | 19.7 | 0.1 | 3.2 | 1.6 |
| 587742904474141884 | 190.4263 | 18.6385 | 25.8 | 0.5 | 25.0 | 0.5 | 24.6 | 0.6 | 21.9 | 0.2 | 20.2 | 0.1 | 2.6 | 1.8 |
| 587732772132750451 | 190.6511 | 10.5235 | 26.0 | 0.9 | 25.0 | 0.6 | 25.3 | 0.6 | 22.3 | 0.2 | 21.0 | 0.2 | 3.0 | 1.4 |
| 588017991220789974 | 190.9165 | 9.9436 | 25.5 | 0.9 | 24.1 | 0.4 | 24.1 | 0.6 | 21.7 | 0.1 | 20.3 | 0.1 | 2.4 | 1.4 |
| 587738575141209378 | 190.9666 | 40.9319 | 23.6 | 0.5 | 25.1 | 0.4 | 25.0 | 0.4 | 22.4 | 0.2 | 20.9 | 0.2 | 2.6 | 1.4 |
| 587745543729120325 | 191.7133 | -13.2505 | 23.8 | 1.3 | 25.7 | 0.6 | 24.5 | 0.7 | 22.1 | 0.2 | 20.6 | 0.2 | 2.4 | 1.5 |
| 587746041410552832 | 192.0253 | -8.3185 | 24.0 | 1.0 | 25.4 | 0.7 | 24.9 | 0.7 | 22.3 | 0.2 | 20.9 | 0.2 | 2.6 | 1.4 |
| 587742902327510145 | 192.3695 | 16.7756 | 25.2 | 0.8 | 24.5 | 0.4 | 24.9 | 0.5 | 22.4 | 0.2 | 20.9 | 0.2 | 2.6 | 1.5 |
| 587742575908619510 | 192.6829 | 19.1709 | 24.9 | 1.1 | 23.7 | 0.3 | 23.5 | 0.3 | 20.9 | 0.0 | 19.5 | 0.1 | 2.6 | 1.4 |
| 587732771596993679 | 193.1921 | 9.9646 | 25.9 | 0.6 | 24.9 | 0.6 | 23.3 | 0.3 | 21.1 | 0.1 | 19.7 | 0.1 | 2.2 | 1.4 |
| 588023668639007562 | 193.9799 | 19.3382 | 24.7 | 1.3 | 24.3 | 0.4 | 24.4 | 0.5 | 21.3 | 0.1 | 19.9 | 0.1 | 3.0 | 1.5 |
| 587741724971762568 | 194.2034 | 23.7828 | 24.5 | 0.8 | 25.1 | 0.6 | 24.9 | 0.6 | 21.7 | 0.1 | 20.2 | 0.1 | 3.3 | 1.5 |
| 587739720291189639 | 195.6271 | 29.1829 | 24.9 | 1.1 | 25.2 | 0.6 | 24.4 | 0.6 | 21.4 | 0.1 | 19.4 | 0.1 | 3.0 | 2.0 |
| 587733195697226654 | 195.8201 | 54.0262 | 25.5 | 0.9 | 25.1 | 0.6 | 24.8 | 0.7 | 22.1 | 0.2 | 20.3 | 0.1 | 2.7 | 1.8 |
| 587728678470157331 | 196.2246 | 64.6864 | 23.7 | 0.8 | 24.3 | 0.5 | 24.3 | 0.6 | 21.6 | 0.1 | 20.1 | 0.1 | 2.8 | 1.5 |

Table C.1 (cont'd)

| Object ID | RA | DEC | u | u err | g | g err | r | r err | i | i err | z | z err | r-i | i-z |
|---|---|---|---|---|---|---|---|---|---|---|---|---|---|---|
| 587742062151271483 | 196.3262 | 22.5705 | 24.6 | 1.1 | 25.4 | 0.6 | 25.2 | 0.5 | 21.8 | 0.1 | 20.5 | 0.1 | 3.3 | 1.4 |
| 588017722260062969 | 198.7887 | 42.6726 | 25.4 | 1.2 | 24.8 | 0.6 | 24.1 | 0.6 | 21.7 | 0.1 | 20.3 | 0.1 | 2.4 | 1.4 |
| 588018055645299778 | 199.3085 | 51.5645 | 24.6 | 0.8 | 24.3 | 0.3 | 24.8 | 0.5 | 21.8 | 0.1 | 20.4 | 0.1 | 3.0 | 1.4 |
| 587736807225361346 | 201.7009 | 13.2873 | 24.3 | 1.0 | 25.0 | 0.7 | 24.2 | 0.5 | 21.9 | 0.1 | 20.6 | 0.2 | 2.2 | 1.3 |
| 587725816953439053 | 201.7913 | 66.0372 | 23.6 | 0.8 | 24.1 | 0.3 | 24.2 | 0.7 | 21.1 | 0.1 | 19.3 | 0.1 | 3.2 | 1.7 |
| 587729773680264258 | 202.0138 | -2.3744 | 24.3 | 1.2 | 25.3 | 0.7 | 23.9 | 0.6 | 21.7 | 0.1 | 20.1 | 0.2 | 2.3 | 1.5 |
| 588017991225574380 | 202.0260 | 9.4413 | 23.7 | 0.9 | 24.5 | 0.5 | 24.9 | 0.7 | 22.5 | 0.2 | 20.9 | 0.2 | 2.4 | 1.6 |
| 587739504476357411 | 202.0431 | 30.4375 | 25.3 | 0.9 | 24.9 | 0.8 | 24.8 | 0.7 | 21.9 | 0.1 | 20.2 | 0.1 | 2.9 | 1.7 |
| 587729776902079384 | 202.2706 | -2.9269 | 25.7 | 1.0 | 23.6 | 0.4 | 24.2 | 0.7 | 21.9 | 0.1 | 20.5 | 0.2 | 2.3 | 1.4 |
| 587741721216156530 | 202.4198 | 25.8089 | 25.3 | 0.9 | 25.2 | 0.6 | 23.6 | 0.4 | 21.3 | 0.1 | 19.4 | 0.1 | 2.3 | 1.9 |
| 587726014005445549 | 203.3734 | 1.3577 | 25.2 | 1.0 | 24.5 | 0.7 | 23.4 | 0.3 | 21.1 | 0.1 | 19.6 | 0.1 | 2.3 | 1.5 |
| 588017726019208408 | 203.7106 | 7.6235 | 25.4 | 0.7 | 25.3 | 0.5 | 25.0 | 0.6 | 22.5 | 0.2 | 20.7 | 0.1 | 2.4 | 1.8 |
| 588017570317075482 | 204.1004 | 11.4837 | 25.1 | 0.8 | 25.1 | 0.6 | 24.6 | 0.6 | 22.4 | 0.2 | 21.0 | 0.2 | 2.2 | 1.4 |
| 587739132951987468 | 204.4014 | 36.6419 | 25.2 | 0.6 | 25.0 | 0.4 | 24.1 | 0.4 | 21.9 | 0.1 | 20.3 | 0.1 | 2.2 | 1.6 |
| 587729773681574984 | 204.9153 | -2.1625 | 23.8 | 0.9 | 25.5 | 0.6 | 24.2 | 0.5 | 22.0 | 0.2 | 20.6 | 0.2 | 2.2 | 1.4 |
| 587738574072317507 | 205.2519 | 38.5611 | 24.9 | 0.7 | 24.9 | 0.4 | 24.4 | 0.4 | 21.9 | 0.1 | 20.6 | 0.1 | 2.5 | 1.3 |
| 588011219135431601 | 205.9093 | 61.4749 | 25.2 | 0.7 | 24.0 | 0.3 | 23.6 | 0.3 | 21.3 | 0.1 | 19.8 | 0.1 | 2.4 | 1.5 |
| 587739707943027687 | 206.4155 | 28.6515 | 25.5 | 0.9 | 25.1 | 0.5 | 24.0 | 0.5 | 21.5 | 0.1 | 19.9 | 0.1 | 2.5 | 1.6 |
| 587742060544918633 | 206.5629 | 20.3468 | 25.9 | 0.9 | 24.7 | 0.6 | 24.8 | 0.6 | 22.5 | 0.2 | 21.1 | 0.2 | 2.3 | 1.4 |
| 587738574609647082 | 206.5928 | 38.7391 | 24.7 | 0.6 | 25.2 | 0.3 | 25.3 | 0.4 | 23.0 | 0.3 | 21.2 | 0.2 | 2.4 | 1.7 |
| 587722981751915681 | 206.9856 | -1.0598 | 24.3 | 0.8 | 25.1 | 0.6 | 24.0 | 0.4 | 21.8 | 0.1 | 20.0 | 0.1 | 2.2 | 1.8 |
| 587746269582001411 | 207.0844 | -3.5539 | 23.6 | 1.0 | 24.4 | 0.5 | 24.5 | 0.6 | 21.4 | 0.1 | 20.0 | 0.1 | 3.1 | 1.4 |
| 587735696449209285 | 207.2544 | 55.4942 | 24.2 | 1.0 | 25.4 | 0.5 | 24.6 | 0.6 | 22.2 | 0.2 | 20.5 | 0.2 | 2.4 | 1.7 |
| 587729774756561829 | 207.8376 | -1.3271 | 25.6 | 0.8 | 24.4 | 0.6 | 23.9 | 0.5 | 21.4 | 0.1 | 20.0 | 0.1 | 2.5 | 1.4 |
| 588017625089115043 | 207.9801 | 41.4142 | 25.0 | 0.9 | 24.9 | 0.7 | 24.3 | 0.5 | 21.6 | 0.1 | 20.2 | 0.1 | 2.7 | 1.4 |
| 587746236297905182 | 209.0299 | -6.4122 | 25.7 | 0.9 | 25.6 | 0.5 | 24.7 | 0.7 | 21.8 | 0.1 | 19.9 | 0.1 | 2.9 | 1.9 |
| 587739406254277723 | 209.2927 | 31.8219 | 23.7 | 0.8 | 25.2 | 0.4 | 24.3 | 0.5 | 21.9 | 0.1 | 20.4 | 0.1 | 2.4 | 1.5 |

Table C.1 (cont'd)

| Object ID | RA | DEC | u | u err | g | g err | r | r err | i | i err | z | z err | r-i | i-z |
|---|---|---|---|---|---|---|---|---|---|---|---|---|---|---|
| 587729159509705539 | 209.4048 | 4.8979 | 25.7 | 0.9 | 24.5 | 0.6 | 23.6 | 0.4 | 21.5 | 0.1 | 20.2 | 0.2 | 2.1 | 1.3 |
| 587736586573120665 | 209.4356 | 40.8209 | 24.0 | 0.7 | 24.7 | 0.4 | 24.0 | 0.4 | 21.6 | 0.1 | 19.7 | 0.1 | 2.4 | 1.9 |
| 588298664117994712 | 209.4619 | 45.5971 | 24.4 | 0.6 | 25.1 | 0.4 | 23.8 | 0.3 | 21.0 | 0.1 | 19.4 | 0.0 | 2.8 | 1.6 |
| 587742594695693110 | 209.6562 | 16.8099 | 23.3 | 0.5 | 24.4 | 0.5 | 23.6 | 0.4 | 21.1 | 0.1 | 19.7 | 0.1 | 2.5 | 1.4 |
| 587742592548537313 | 210.3118 | 15.0032 | 25.4 | 0.9 | 25.1 | 0.8 | 24.3 | 0.6 | 21.1 | 0.1 | 19.6 | 0.1 | 3.3 | 1.4 |
| 588017991229244610 | 210.5254 | 8.9233 | 23.7 | 0.8 | 24.9 | 0.6 | 25.4 | 0.6 | 22.3 | 0.2 | 20.9 | 0.2 | 3.1 | 1.4 |
| 588017991229310016 | 210.6635 | 8.9254 | 25.5 | 0.9 | 25.2 | 0.6 | 23.4 | 0.3 | 21.0 | 0.1 | 19.6 | 0.1 | 2.4 | 1.3 |
| 587735695913321470 | 210.8686 | 54.3749 | 26.0 | 0.6 | 27.4 | 0.2 | 24.0 | 0.7 | 21.8 | 0.1 | 20.5 | 0.2 | 2.1 | 1.4 |
| 588017992303838071 | 212.4217 | 9.5701 | 25.1 | 0.8 | 25.1 | 0.6 | 24.2 | 0.6 | 21.4 | 0.1 | 19.9 | 0.1 | 2.8 | 1.5 |
| 587736478662656905 | 212.5009 | 11.6189 | 25.0 | 0.8 | 24.3 | 0.5 | 24.5 | 0.6 | 22.3 | 0.2 | 20.7 | 0.2 | 2.2 | 1.6 |
| 588011219137004633 | 212.6382 | 60.1345 | 24.3 | 0.8 | 24.9 | 0.5 | 24.6 | 0.5 | 22.2 | 0.2 | 20.8 | 0.2 | 2.4 | 1.4 |
| 587739380985562078 | 213.0207 | 31.6272 | 26.1 | 0.6 | 25.3 | 0.5 | 25.0 | 0.6 | 22.0 | 0.2 | 20.3 | 0.1 | 3.0 | 1.7 |
| 587746278167282738 | 213.5916 | -18.0786 | 23.1 | 0.9 | 25.6 | 0.7 | 23.9 | 0.7 | 21.7 | 0.1 | 20.1 | 0.1 | 2.2 | 1.7 |
| 587739609175163770 | 213.6255 | 29.3398 | 24.7 | 1.2 | 25.2 | 0.5 | 24.3 | 0.6 | 21.9 | 0.1 | 20.1 | 0.1 | 2.4 | 1.9 |
| 588848899927442575 | 213.6762 | -0.1211 | 25.5 | 0.6 | 25.8 | 0.5 | 23.8 | 0.5 | 21.5 | 0.1 | 20.1 | 0.1 | 2.3 | 1.4 |
| 587736542017750200 | 213.9824 | 8.3750 | 24.6 | 0.9 | 26.3 | 0.3 | 23.8 | 0.4 | 21.4 | 0.1 | 19.8 | 0.1 | 2.4 | 1.7 |
| 588011123583091390 | 214.1712 | 59.0976 | 25.4 | 0.8 | 24.4 | 0.6 | 24.4 | 0.8 | 21.9 | 0.2 | 20.6 | 0.2 | 2.5 | 1.3 |
| 587746278167938208 | 214.2849 | -19.4582 | 23.9 | 1.8 | 26.3 | 0.5 | 25.4 | 0.8 | 22.0 | 0.2 | 20.7 | 0.2 | 3.4 | 1.4 |
| 587736585501410737 | 214.8308 | 38.5935 | 23.8 | 0.6 | 24.5 | 0.3 | 24.1 | 0.3 | 21.8 | 0.1 | 20.0 | 0.1 | 2.3 | 1.8 |
| 587742190454244421 | 215.2578 | 22.1226 | 25.3 | 1.0 | 25.2 | 0.5 | 25.0 | 0.5 | 22.3 | 0.2 | 20.6 | 0.2 | 2.6 | 1.7 |
| 587736914602951670 | 215.2992 | 12.1341 | 23.2 | 0.5 | 25.5 | 0.6 | 23.3 | 0.3 | 21.0 | 0.1 | 19.7 | 0.1 | 2.3 | 1.3 |
| 587736584428062095 | 215.5006 | 37.3992 | 24.1 | 0.6 | 24.1 | 0.3 | 23.6 | 0.3 | 20.9 | 0.0 | 19.5 | 0.1 | 2.7 | 1.4 |
| 587730022789809162 | 215.5008 | 6.5153 | 24.9 | 1.3 | 25.5 | 0.6 | 23.9 | 0.5 | 21.7 | 0.1 | 20.2 | 0.2 | 2.2 | 1.5 |
| 588017606304989959 | 216.2809 | 41.6769 | 25.8 | 0.8 | 24.5 | 0.5 | 23.5 | 0.3 | 21.0 | 0.1 | 19.6 | 0.1 | 2.5 | 1.4 |
| 587736541481927841 | 216.3328 | 7.8922 | 23.4 | 0.7 | 24.5 | 0.4 | 23.4 | 0.3 | 21.0 | 0.1 | 19.7 | 0.1 | 2.4 | 1.3 |
| 588017713661412643 | 216.6573 | 49.0901 | 25.6 | 0.7 | 25.1 | 0.4 | 23.7 | 0.3 | 20.8 | 0.1 | 19.1 | 0.0 | 2.8 | 1.7 |
| 587733410984231821 | 218.0394 | 49.9561 | 23.6 | 0.7 | 25.2 | 0.6 | 23.8 | 0.5 | 20.8 | 0.1 | 19.1 | 0.0 | 2.9 | 1.7 |

Table C.1 (cont'd)

| Object ID | RA | DEC | u | u err | g | g err | r | r err | i | i err | z | z err | r-i | i-z |
|---|---|---|---|---|---|---|---|---|---|---|---|---|---|---|
| 587733397562262461 | 218.1495 | 49.2996 | 24.0 | 1.2 | 24.1 | 0.4 | 24.2 | 0.7 | 21.5 | 0.1 | 20.0 | 0.1 | 2.8 | 1.5 |
| 587739827129484142 | 218.6243 | 22.7365 | 25.4 | 1.2 | 25.6 | 0.5 | 24.1 | 0.5 | 21.3 | 0.1 | 20.0 | 0.1 | 2.7 | 1.3 |
| 588298662510789880 | 218.8043 | 41.5426 | 23.8 | 0.6 | 25.0 | 0.3 | 24.6 | 0.4 | 22.5 | 0.2 | 20.4 | 0.1 | 2.1 | 2.1 |
| 587736962922316671 | 219.5107 | 31.8622 | 24.7 | 0.9 | 24.9 | 0.5 | 24.5 | 0.6 | 22.3 | 0.2 | 21.0 | 0.2 | 2.2 | 1.3 |
| 588017711515370532 | 220.0139 | 46.1570 | 24.8 | 1.0 | 25.3 | 0.5 | 24.2 | 0.4 | 22.0 | 0.1 | 20.3 | 0.1 | 2.2 | 1.6 |
| 587739630630863931 | 220.8132 | 27.5135 | 25.3 | 0.9 | 24.7 | 0.5 | 23.7 | 0.4 | 21.5 | 0.1 | 20.1 | 0.1 | 2.3 | 1.3 |
| 587742629061329898 | 221.6043 | 14.8235 | 25.1 | 0.9 | 24.2 | 0.4 | 24.3 | 0.6 | 22.1 | 0.2 | 20.6 | 0.1 | 2.1 | 1.5 |
| 587722982295340447 | 221.9858 | -0.7504 | 24.9 | 0.9 | 25.2 | 0.5 | 24.5 | 0.5 | 21.4 | 0.1 | 19.7 | 0.1 | 3.1 | 1.7 |
| 587726032267052136 | 222.3068 | 1.6773 | 24.4 | 1.2 | 24.4 | 0.6 | 23.4 | 0.4 | 21.2 | 0.1 | 19.9 | 0.1 | 2.2 | 1.4 |
| 588018055115703409 | 222.6902 | 45.3658 | 25.0 | 1.0 | 24.2 | 0.4 | 24.6 | 0.5 | 22.3 | 0.2 | 20.9 | 0.2 | 2.3 | 1.4 |
| 587729776911123462 | 223.0024 | -2.4566 | 24.6 | 1.5 | 25.7 | 0.6 | 24.0 | 0.5 | 21.9 | 0.1 | 20.4 | 0.2 | 2.2 | 1.5 |
| 587735490821751827 | 223.3052 | 43.5829 | 23.6 | 0.5 | 24.4 | 0.4 | 23.3 | 0.2 | 20.9 | 0.1 | 19.5 | 0.1 | 2.3 | 1.4 |
| 587736585504622197 | 223.3183 | 35.7665 | 23.7 | 0.5 | 25.2 | 0.3 | 23.8 | 0.3 | 21.1 | 0.1 | 19.2 | 0.0 | 2.6 | 2.0 |
| 587729776911385690 | 223.6075 | -2.4566 | 26.0 | 0.8 | 25.2 | 0.7 | 24.0 | 0.5 | 21.8 | 0.1 | 19.9 | 0.1 | 2.2 | 1.8 |
| 587739827131974679 | 224.4462 | 21.0559 | 25.6 | 1.0 | 24.7 | 0.5 | 24.3 | 0.5 | 21.9 | 0.1 | 20.4 | 0.1 | 2.4 | 1.5 |
| 588017979980907639 | 224.8475 | 33.7420 | 24.5 | 0.9 | 25.0 | 0.4 | 24.3 | 0.5 | 22.0 | 0.1 | 20.4 | 0.1 | 2.3 | 1.6 |
| 588017702949880900 | 224.9550 | 9.1385 | 24.8 | 1.1 | 24.9 | 0.5 | 24.4 | 0.5 | 21.8 | 0.1 | 20.4 | 0.1 | 2.6 | 1.3 |
| 588848899932554225 | 225.4619 | -0.0569 | 25.3 | 0.7 | 24.9 | 0.4 | 24.9 | 0.6 | 22.3 | 0.2 | 20.8 | 0.2 | 2.6 | 1.5 |
| 587739131349632328 | 225.6101 | 29.7374 | 25.9 | 0.5 | 24.8 | 0.4 | 23.9 | 0.3 | 20.9 | 0.0 | 19.3 | 0.0 | 3.0 | 1.6 |
| 587739382064350410 | 225.8459 | 28.7320 | 23.8 | 0.7 | 25.0 | 0.4 | 24.9 | 0.5 | 21.8 | 0.1 | 20.1 | 0.1 | 3.1 | 1.7 |
| 587739707950957500 | 225.9034 | 23.8605 | 24.9 | 1.1 | 25.3 | 0.5 | 24.6 | 0.6 | 22.2 | 0.2 | 20.5 | 0.2 | 2.4 | 1.7 |
| 587742061090112393 | 226.3155 | 16.9165 | 24.6 | 1.0 | 25.0 | 0.5 | 23.9 | 0.4 | 21.8 | 0.1 | 20.5 | 0.1 | 2.1 | 1.3 |
| 587742782061151186 | 226.3166 | 66.5927 | 24.7 | 1.5 | 25.3 | 0.6 | 25.0 | 0.7 | 22.1 | 0.2 | 20.7 | 0.2 | 2.8 | 1.4 |
| 587739810492187739 | 226.4236 | 21.1685 | 25.3 | 0.7 | 23.9 | 0.3 | 24.2 | 0.4 | 21.5 | 0.1 | 20.1 | 0.1 | 2.6 | 1.4 |
| 587729228758057768 | 226.4657 | 61.8045 | 25.3 | 0.9 | 24.8 | 0.6 | 24.7 | 0.7 | 22.1 | 0.2 | 20.5 | 0.1 | 2.5 | 1.6 |
| 587736975270610131 | 226.9655 | 28.8498 | 25.3 | 0.9 | 24.8 | 0.5 | 23.3 | 0.2 | 21.1 | 0.1 | 19.8 | 0.1 | 2.2 | 1.3 |
| 588017605772248021 | 227.2607 | 37.3744 | 24.1 | 0.9 | 25.9 | 0.4 | 24.6 | 0.6 | 22.2 | 0.2 | 20.9 | 0.2 | 2.4 | 1.3 |

Table C.1 (cont'd)

| Object ID | RA | DEC | u | u err | g | g err | r | r err | i | i err | z | z err | r-i | i-z |
|---|---|---|---|---|---|---|---|---|---|---|---|---|---|---|
| 587726100415775772 | 227.5137 | 2.9317 | 24.5 | 1.7 | 24.9 | 0.8 | 23.7 | 0.5 | 21.2 | 0.1 | 19.8 | 0.1 | 2.5 | 1.4 |
| 587742610269472024 | 227.7051 | 12.5743 | 25.2 | 0.9 | 24.3 | 0.4 | 23.5 | 0.3 | 21.1 | 0.1 | 19.4 | 0.1 | 2.4 | 1.8 |
| 587733412061119193 | 228.1641 | 47.1411 | 24.4 | 1.1 | 25.5 | 0.6 | 24.7 | 0.7 | 21.8 | 0.2 | 20.4 | 0.1 | 2.9 | 1.4 |
| 588017990700303528 | 228.5661 | 6.7330 | 23.7 | 0.9 | 24.6 | 0.6 | 24.6 | 0.6 | 21.9 | 0.1 | 20.4 | 0.1 | 2.8 | 1.4 |
| 587739720304493641 | 228.7774 | 22.4037 | 25.5 | 0.8 | 24.6 | 0.5 | 23.5 | 0.4 | 21.3 | 0.1 | 19.9 | 0.1 | 2.3 | 1.4 |
| 588017626707199080 | 228.8637 | 35.9400 | 25.0 | 0.9 | 25.1 | 0.4 | 23.8 | 0.3 | 21.6 | 0.1 | 19.9 | 0.1 | 2.2 | 1.7 |
| 587729227148624895 | 229.2771 | 59.1033 | 25.3 | 1.1 | 24.3 | 0.5 | 24.4 | 0.7 | 21.4 | 0.1 | 20.0 | 0.1 | 2.9 | 1.4 |
| 587735667458310997 | 229.2816 | 49.6756 | 25.8 | 0.8 | 25.2 | 0.6 | 23.5 | 0.3 | 21.2 | 0.1 | 19.8 | 0.1 | 2.3 | 1.4 |
| 587739720304886838 | 229.6108 | 21.9413 | 23.9 | 0.9 | 25.1 | 0.5 | 24.1 | 0.4 | 21.3 | 0.1 | 19.7 | 0.1 | 2.9 | 1.5 |
| 587729746838029514 | 230.4316 | 1.0337 | 24.6 | 1.4 | 24.6 | 0.6 | 23.3 | 0.3 | 21.0 | 0.1 | 19.6 | 0.1 | 2.3 | 1.3 |
| 587736478670521399 | 230.5734 | 9.3747 | 24.6 | 0.7 | 24.9 | 0.5 | 25.0 | 0.6 | 22.1 | 0.2 | 20.6 | 0.1 | 2.9 | 1.5 |
| 587733411525559181 | 231.3260 | 45.0889 | 26.0 | 0.7 | 24.6 | 0.5 | 24.9 | 0.6 | 22.1 | 0.1 | 20.7 | 0.2 | 2.8 | 1.4 |
| 587733427626967884 | 231.5140 | 49.0118 | 23.8 | 1.0 | 24.8 | 0.6 | 23.6 | 0.3 | 21.5 | 0.1 | 20.0 | 0.1 | 2.1 | 1.5 |
| 587739811568026947 | 231.6018 | 20.3935 | 25.2 | 0.6 | 25.2 | 0.4 | 24.5 | 0.4 | 22.1 | 0.1 | 20.8 | 0.2 | 2.4 | 1.3 |
| 587739845389386773 | 231.6261 | 18.0976 | 25.1 | 0.9 | 24.1 | 0.3 | 24.3 | 0.4 | 21.5 | 0.1 | 19.9 | 0.1 | 2.7 | 1.6 |
| 587742629065851966 | 231.9400 | 12.6672 | 24.9 | 1.0 | 25.2 | 0.5 | 25.3 | 0.6 | 22.3 | 0.2 | 20.8 | 0.2 | 3.0 | 1.5 |
| 587729159519601807 | 232.0062 | 3.6837 | 24.1 | 1.0 | 25.1 | 0.7 | 24.4 | 0.6 | 22.0 | 0.2 | 20.5 | 0.2 | 2.4 | 1.5 |
| 587742628529374488 | 232.8739 | 12.0835 | 22.7 | 0.4 | 25.2 | 0.5 | 24.9 | 0.6 | 22.0 | 0.1 | 20.5 | 0.2 | 2.9 | 1.5 |
| 588017703490356395 | 233.2395 | 8.2607 | 23.8 | 0.9 | 25.3 | 0.6 | 24.2 | 0.5 | 21.9 | 0.1 | 20.5 | 0.1 | 2.3 | 1.4 |
| 587735489215398938 | 233.4104 | 37.4698 | 24.6 | 1.2 | 24.8 | 0.5 | 25.1 | 0.7 | 22.0 | 0.2 | 20.7 | 0.2 | 3.1 | 1.3 |
| 587736584972141961 | 233.8093 | 30.7206 | 24.8 | 0.7 | 24.9 | 0.4 | 25.0 | 0.4 | 22.4 | 0.1 | 21.0 | 0.2 | 2.6 | 1.4 |
| 588011217533076244 | 233.9039 | 50.5680 | 26.2 | 0.5 | 25.3 | 0.6 | 24.4 | 0.6 | 21.8 | 0.1 | 20.4 | 0.1 | 2.6 | 1.3 |
| 587739131353236873 | 233.9560 | 26.2114 | 25.1 | 0.9 | 24.9 | 0.5 | 23.3 | 0.2 | 21.0 | 0.0 | 19.7 | 0.1 | 2.3 | 1.3 |
| 587729229296894714 | 234.0202 | 59.1885 | 23.7 | 1.0 | 24.9 | 0.7 | 24.4 | 0.7 | 21.2 | 0.1 | 19.9 | 0.1 | 3.2 | 1.3 |
| 587736542026532135 | 234.0643 | 6.1930 | 24.9 | 0.9 | 25.3 | 0.5 | 23.3 | 0.3 | 21.1 | 0.1 | 19.6 | 0.1 | 2.2 | 1.5 |
| 588017991239533745 | 234.0934 | 6.3800 | 24.9 | 1.4 | 24.9 | 0.7 | 24.2 | 0.7 | 21.9 | 0.1 | 20.5 | 0.2 | 2.3 | 1.4 |
| 588011219679904764 | 234.0954 | 52.7817 | 22.6 | 0.3 | 24.4 | 0.4 | 24.3 | 0.5 | 21.9 | 0.1 | 20.5 | 0.2 | 2.4 | 1.4 |

Table C.1 (cont'd)

| Object ID | RA | DEC | u | u err | g | g err | r | r err | i | i err | z | z err | r-i | i-z |
|---|---|---|---|---|---|---|---|---|---|---|---|---|---|---|
| 587739849672885314 | 234.2626 | 61.2775 | 25.3 | 1.0 | 24.7 | 0.5 | 25.0 | 0.6 | 22.3 | 0.2 | 21.0 | 0.3 | 2.7 | 1.3 |
| 587729407535023060 | 234.7772 | 53.2424 | 24.0 | 1.3 | 25.2 | 0.6 | 24.1 | 0.6 | 21.4 | 0.1 | 19.8 | 0.1 | 2.7 | 1.6 |
| 587733604262217093 | 234.9250 | 48.0162 | 25.0 | 0.8 | 25.4 | 0.4 | 25.3 | 0.4 | 23.0 | 0.2 | 20.9 | 0.2 | 2.4 | 2.0 |
| 587729748450608329 | 234.9880 | 2.0907 | 24.5 | 1.0 | 24.6 | 0.5 | 23.5 | 0.4 | 20.9 | 0.1 | 19.4 | 0.1 | 2.6 | 1.5 |
| 588018090541581454 | 235.0644 | 35.0280 | 24.2 | 1.0 | 25.1 | 0.5 | 23.7 | 0.4 | 21.0 | 0.1 | 19.6 | 0.1 | 2.7 | 1.4 |
| 587736543100798537 | 235.4796 | 6.8844 | 23.6 | 0.5 | 25.0 | 0.5 | 23.7 | 0.3 | 21.4 | 0.1 | 20.0 | 0.1 | 2.2 | 1.4 |
| 587736752465708166 | 235.5902 | 36.6984 | 25.1 | 1.0 | 24.9 | 0.6 | 24.6 | 0.6 | 22.2 | 0.2 | 20.9 | 0.2 | 2.4 | 1.3 |
| 588011217533731867 | 235.6902 | 49.4629 | 24.6 | 1.3 | 24.6 | 0.5 | 24.7 | 0.7 | 22.3 | 0.2 | 20.5 | 0.2 | 2.3 | 1.8 |
| 587729158984303831 | 235.6940 | 3.1472 | 23.9 | 0.9 | 24.5 | 0.7 | 23.6 | 0.4 | 21.2 | 0.1 | 19.8 | 0.1 | 2.4 | 1.4 |
| 587739815314785389 | 235.9708 | 22.2438 | 26.0 | 0.6 | 25.1 | 0.5 | 24.0 | 0.4 | 21.3 | 0.1 | 19.9 | 0.1 | 2.8 | 1.4 |
| 588848900474078591 | 236.0793 | 0.2772 | 23.9 | 0.7 | 25.3 | 0.5 | 24.0 | 0.5 | 21.2 | 0.1 | 19.6 | 0.1 | 2.7 | 1.6 |
| 588017991777322253 | 236.1821 | 6.6733 | 24.7 | 1.4 | 24.2 | 0.5 | 24.1 | 0.6 | 21.9 | 0.1 | 20.5 | 0.2 | 2.2 | 1.4 |
| 587742611346949395 | 236.4521 | 11.5199 | 25.2 | 1.0 | 25.4 | 0.5 | 23.4 | 0.3 | 21.1 | 0.1 | 19.4 | 0.1 | 2.3 | 1.6 |
| 587736478673405157 | 237.1816 | 8.2832 | 25.9 | 0.4 | 24.7 | 0.5 | 23.9 | 0.4 | 21.6 | 0.1 | 20.3 | 0.1 | 2.3 | 1.4 |
| 588017992314717506 | 237.4281 | 6.8918 | 23.6 | 0.8 | 25.6 | 0.6 | 24.4 | 0.6 | 21.9 | 0.1 | 20.3 | 0.1 | 2.4 | 1.7 |
| 587742782064231497 | 237.8862 | 61.7237 | 25.8 | 0.9 | 24.4 | 0.5 | 24.0 | 0.5 | 21.8 | 0.1 | 20.5 | 0.2 | 2.2 | 1.4 |
| 587736584437237083 | 237.8977 | 27.9870 | 24.7 | 1.0 | 25.3 | 0.4 | 23.7 | 0.3 | 21.3 | 0.1 | 19.4 | 0.0 | 2.4 | 1.9 |
| 587739845392270485 | 238.1536 | 15.9378 | 24.3 | 1.0 | 25.8 | 0.4 | 23.2 | 0.2 | 21.1 | 0.1 | 19.6 | 0.1 | 2.2 | 1.4 |
| 587736751930147927 | 238.1548 | 34.5144 | 25.7 | 0.8 | 25.2 | 0.6 | 24.8 | 0.6 | 22.1 | 0.1 | 20.6 | 0.1 | 2.7 | 1.5 |
| 587736478137124342 | 238.4324 | 7.6701 | 24.8 | 0.9 | 25.2 | 0.5 | 24.7 | 0.6 | 21.9 | 0.1 | 20.3 | 0.1 | 2.8 | 1.6 |
| 587733609086452775 | 238.5687 | 46.0634 | 26.0 | 0.8 | 25.0 | 0.7 | 25.1 | 0.7 | 22.3 | 0.2 | 21.0 | 0.3 | 2.7 | 1.4 |
| 587739652644734147 | 238.8518 | 21.2850 | 24.3 | 0.9 | 25.2 | 0.5 | 24.2 | 0.5 | 21.9 | 0.2 | 20.6 | 0.2 | 2.2 | 1.4 |
| 587736478137386319 | 238.9851 | 7.4959 | 24.3 | 0.9 | 25.0 | 0.5 | 23.5 | 0.3 | 21.0 | 0.1 | 19.2 | 0.1 | 2.5 | 1.8 |
| 588018253757678463 | 239.0767 | 37.5630 | 25.3 | 1.1 | 25.2 | 0.7 | 23.8 | 0.5 | 21.3 | 0.1 | 19.8 | 0.1 | 2.5 | 1.4 |
| 587739651034514532 | 239.1066 | 19.7811 | 23.7 | 1.0 | 25.2 | 0.6 | 23.3 | 0.3 | 21.0 | 0.1 | 19.3 | 0.1 | 2.3 | 1.7 |
| 587735665851958247 | 239.1080 | 42.5534 | 23.6 | 0.7 | 25.2 | 0.7 | 24.5 | 0.7 | 22.2 | 0.2 | 20.7 | 0.2 | 2.3 | 1.5 |
| 587736915687245537 | 239.6342 | 8.7628 | 25.2 | 0.6 | 24.7 | 0.4 | 23.3 | 0.2 | 21.1 | 0.1 | 19.7 | 0.1 | 2.2 | 1.4 |

Table C.1 (cont'd)

| Object ID | RA | DEC | u | u err | g | g err | r | r err | i | i err | z | z err | r-i | i-z |
|---|---|---|---|---|---|---|---|---|---|---|---|---|---|---|
| 587739720309343534 | 239.6798 | 18.1405 | 25.0 | 1.1 | 25.6 | 0.5 | 24.1 | 0.5 | 21.8 | 0.1 | 20.5 | 0.2 | 2.3 | 1.4 |
| 587736921042388393 | 240.0317 | 30.7710 | 25.6 | 0.5 | 24.7 | 0.4 | 25.1 | 0.5 | 22.5 | 0.2 | 20.8 | 0.1 | 2.6 | 1.7 |
| 587736545780958737 | 240.4654 | 3.7250 | 24.6 | 1.0 | 25.0 | 0.5 | 23.6 | 0.3 | 21.0 | 0.1 | 19.7 | 0.1 | 2.5 | 1.4 |
| 588011218609374239 | 241.1320 | 47.0361 | 23.6 | 0.6 | 23.9 | 0.3 | 25.1 | 0.6 | 21.9 | 0.1 | 20.5 | 0.2 | 3.2 | 1.4 |
| 587736619325261027 | 241.3784 | 26.7038 | 25.0 | 0.7 | 25.3 | 0.5 | 23.7 | 0.4 | 21.4 | 0.1 | 19.8 | 0.1 | 2.3 | 1.6 |
| 588018056733459669 | 241.4014 | 36.8108 | 24.2 | 0.8 | 24.3 | 0.4 | 24.1 | 0.4 | 21.9 | 0.1 | 20.4 | 0.1 | 2.2 | 1.5 |
| 587739382071231978 | 241.6125 | 21.9298 | 25.2 | 0.8 | 24.3 | 0.4 | 25.1 | 0.5 | 22.9 | 0.3 | 21.1 | 0.2 | 2.3 | 1.8 |
| 587736543103616588 | 241.8496 | 6.0972 | 24.7 | 0.8 | 24.6 | 0.5 | 24.3 | 0.4 | 22.0 | 0.1 | 20.6 | 0.2 | 2.2 | 1.4 |
| 587742610275763654 | 241.9947 | 9.2120 | 25.9 | 0.7 | 25.6 | 0.5 | 25.0 | 0.7 | 22.6 | 0.2 | 20.6 | 0.2 | 2.4 | 2.0 |
| 587742615099475377 | 242.0435 | 13.8276 | 25.8 | 0.6 | 25.3 | 0.6 | 23.7 | 0.4 | 21.3 | 0.1 | 19.8 | 0.1 | 2.4 | 1.5 |
| 587736478675633759 | 242.1584 | 7.3265 | 24.6 | 0.8 | 25.4 | 0.5 | 24.6 | 0.6 | 22.4 | 0.2 | 21.1 | 0.2 | 2.2 | 1.3 |
| 588018055660438849 | 242.1775 | 35.0422 | 25.1 | 0.9 | 25.4 | 0.5 | 24.3 | 0.5 | 22.1 | 0.1 | 20.5 | 0.1 | 2.3 | 1.6 |
| 587745969465197834 | 242.2062 | 18.6575 | 25.7 | 0.6 | 25.4 | 0.4 | 24.3 | 0.6 | 21.6 | 0.1 | 20.0 | 0.1 | 2.7 | 1.6 |
| 587735743153964425 | 242.3917 | 30.4111 | 24.6 | 0.8 | 25.1 | 0.4 | 24.9 | 0.5 | 22.2 | 0.1 | 20.8 | 0.2 | 2.7 | 1.4 |
| 587742062170867072 | 242.4613 | 13.0901 | 24.2 | 0.9 | 24.7 | 0.5 | 24.7 | 0.6 | 21.8 | 0.1 | 20.3 | 0.1 | 2.9 | 1.5 |
| 588017991780140686 | 242.5729 | 5.7330 | 25.3 | 1.1 | 25.5 | 0.6 | 25.1 | 0.6 | 22.7 | 0.3 | 20.7 | 0.2 | 2.4 | 2.0 |
| 587733398108570644 | 242.7150 | 36.9276 | 23.4 | 0.7 | 25.6 | 0.6 | 24.7 | 0.8 | 21.8 | 0.1 | 20.3 | 0.2 | 2.9 | 1.5 |
| 587733411530540062 | 242.8266 | 37.5447 | 25.2 | 1.1 | 25.7 | 0.6 | 24.7 | 0.7 | 21.6 | 0.1 | 20.3 | 0.2 | 3.1 | 1.3 |
| 587736975277753681 | 243.0262 | 21.3412 | 25.0 | 0.9 | 25.3 | 0.5 | 25.0 | 0.4 | 22.8 | 0.2 | 20.9 | 0.2 | 2.3 | 1.9 |
| 587735665853990030 | 243.3169 | 39.3194 | 24.5 | 0.9 | 24.4 | 0.4 | 23.4 | 0.3 | 21.2 | 0.1 | 19.9 | 0.1 | 2.1 | 1.4 |
| 588017704031618682 | 243.3674 | 6.9732 | 23.6 | 0.9 | 24.4 | 0.4 | 24.9 | 0.7 | 21.8 | 0.1 | 19.9 | 0.1 | 3.1 | 1.9 |
| 588017990706922819 | 243.6486 | 4.6922 | 25.3 | 1.2 | 25.3 | 0.6 | 24.3 | 0.7 | 22.0 | 0.2 | 20.7 | 0.2 | 2.3 | 1.4 |
| 587733410457519145 | 243.7203 | 35.9499 | 25.3 | 1.2 | 24.7 | 0.6 | 25.1 | 0.6 | 21.9 | 0.1 | 20.5 | 0.1 | 3.2 | 1.4 |
| 587742610276550453 | 243.7307 | 8.7167 | 24.5 | 1.2 | 25.5 | 0.5 | 23.9 | 0.5 | 21.3 | 0.1 | 19.7 | 0.1 | 2.6 | 1.6 |
| 587729227154129885 | 243.9273 | 49.8892 | 26.2 | 1.0 | 26.1 | 0.5 | 24.0 | 0.7 | 21.8 | 0.1 | 19.8 | 0.1 | 2.2 | 2.0 |
| 588017990707054071 | 244.0028 | 4.6171 | 24.9 | 1.5 | 23.8 | 0.3 | 24.7 | 0.7 | 22.1 | 0.1 | 20.5 | 0.1 | 2.6 | 1.6 |
| 587733603729540496 | 244.0163 | 40.8852 | 24.5 | 1.1 | 24.4 | 0.4 | 24.2 | 0.3 | 21.8 | 0.1 | 20.2 | 0.1 | 2.4 | 1.5 |

Table C.1 (cont'd)

| Object ID | RA | DEC | u | u err | g | g err | r | r err | i | i err | z | z err | r-i | i-z |
|---|---|---|---|---|---|---|---|---|---|---|---|---|---|---|
| 588017978915816840 | 244.0491 | 23.3466 | 24.1 | 0.7 | 25.2 | 0.4 | 23.7 | 0.8 | 21.1 | 0.1 | 19.6 | 0.1 | 2.6 | 1.5 |
| 587742645701707491 | 244.1075 | 12.2334 | 25.1 | 0.9 | 25.1 | 0.5 | 24.0 | 0.4 | 21.6 | 0.1 | 20.2 | 0.1 | 2.3 | 1.4 |
| 587739384742544637 | 244.2294 | 19.1452 | 23.6 | 0.9 | 25.0 | 0.6 | 23.6 | 0.4 | 21.5 | 0.1 | 19.5 | 0.1 | 2.1 | 2.0 |
| 587742628534551977 | 244.5379 | 9.2653 | 24.6 | 1.6 | 24.9 | 0.7 | 24.1 | 0.6 | 21.2 | 0.1 | 19.8 | 0.1 | 2.9 | 1.5 |
| 587733604266476986 | 244.6289 | 41.1774 | 24.8 | 0.8 | 24.8 | 0.4 | 23.3 | 0.2 | 21.1 | 0.1 | 19.7 | 0.1 | 2.2 | 1.4 |
| 587736542031251048 | 244.7886 | 4.7700 | 26.1 | 0.4 | 24.5 | 0.4 | 24.3 | 0.5 | 22.1 | 0.1 | 20.6 | 0.2 | 2.2 | 1.5 |
| 587739815318848801 | 244.9110 | 18.0632 | 26.0 | 0.6 | 24.9 | 0.5 | 24.0 | 0.4 | 21.7 | 0.1 | 19.8 | 0.1 | 2.3 | 1.9 |
| 587736477603203007 | 245.1129 | 6.0467 | 25.1 | 0.8 | 24.8 | 0.5 | 25.1 | 0.5 | 22.0 | 0.1 | 20.2 | 0.1 | 3.1 | 1.8 |
| 587742550692071086 | 245.3298 | 10.1221 | 24.0 | 0.8 | 25.2 | 0.4 | 24.2 | 0.4 | 22.0 | 0.1 | 20.4 | 0.1 | 2.2 | 1.6 |
| 587739720848770485 | 245.3571 | 15.9546 | 24.6 | 1.3 | 25.0 | 0.6 | 23.6 | 0.4 | 21.5 | 0.1 | 20.0 | 0.1 | 2.2 | 1.4 |
| 588017978916472499 | 245.5021 | 22.5628 | 23.6 | 0.5 | 24.7 | 0.3 | 24.0 | 0.3 | 21.8 | 0.1 | 20.4 | 0.1 | 2.2 | 1.3 |
| 587733411531981933 | 245.7252 | 35.3316 | 23.1 | 0.6 | 24.8 | 0.6 | 24.8 | 0.6 | 21.9 | 0.1 | 20.5 | 0.2 | 2.8 | 1.4 |
| 587733441588954429 | 246.0699 | 37.4823 | 25.0 | 0.8 | 25.1 | 0.4 | 23.3 | 0.2 | 20.8 | 0.0 | 19.4 | 0.1 | 2.5 | 1.5 |
| 587739827678545312 | 246.3828 | 13.6807 | 23.1 | 0.6 | 24.9 | 0.6 | 24.5 | 0.7 | 21.5 | 0.1 | 20.1 | 0.1 | 3.0 | 1.4 |
| 587736981712339898 | 246.5739 | 54.2199 | 22.8 | 0.6 | 25.1 | 0.7 | 24.7 | 0.7 | 22.4 | 0.3 | 20.5 | 0.2 | 2.3 | 1.8 |
| 587729652884440235 | 246.7736 | 42.0935 | 25.3 | 0.9 | 24.4 | 0.5 | 24.4 | 0.6 | 21.4 | 0.1 | 20.0 | 0.1 | 3.0 | 1.4 |
| 587729653957723430 | 246.8709 | 43.4958 | 24.6 | 1.0 | 24.8 | 0.6 | 23.5 | 0.3 | 21.3 | 0.1 | 20.0 | 0.1 | 2.1 | 1.3 |
| 587729751668950320 | 247.0348 | 41.4821 | 23.3 | 0.5 | 25.1 | 0.5 | 24.0 | 0.4 | 21.3 | 0.1 | 19.9 | 0.1 | 2.7 | 1.4 |
| 587739166239753205 | 247.2699 | 19.6234 | 24.7 | 1.5 | 25.1 | 0.8 | 24.4 | 0.9 | 21.8 | 0.2 | 20.4 | 0.2 | 2.6 | 1.4 |
| 587736813139854969 | 247.5860 | 7.0929 | 24.3 | 1.3 | 25.4 | 0.6 | 24.8 | 0.6 | 22.1 | 0.1 | 20.6 | 0.2 | 2.8 | 1.5 |
| 587729751669278024 | 247.7063 | 40.8164 | 24.6 | 0.9 | 24.8 | 0.5 | 23.4 | 0.3 | 21.0 | 0.1 | 19.7 | 0.1 | 2.3 | 1.3 |
| 587735743156717021 | 247.9481 | 26.3187 | 23.8 | 0.6 | 25.2 | 0.5 | 24.8 | 0.5 | 22.4 | 0.2 | 21.0 | 0.2 | 2.4 | 1.4 |
| 587736919436166489 | 248.1066 | 23.6474 | 25.3 | 1.1 | 24.7 | 0.5 | 24.5 | 0.5 | 22.3 | 0.2 | 20.6 | 0.1 | 2.2 | 1.7 |
| 587733440516916637 | 248.3485 | 33.9695 | 24.6 | 0.9 | 25.3 | 0.4 | 24.8 | 0.5 | 22.5 | 0.2 | 20.9 | 0.2 | 2.3 | 1.7 |
| 587736751935325329 | 248.6440 | 26.9571 | 24.6 | 1.3 | 25.5 | 0.6 | 24.4 | 0.6 | 22.1 | 0.2 | 20.6 | 0.2 | 2.3 | 1.5 |
| 587736782000162004 | 248.9315 | 26.9147 | 23.7 | 1.0 | 25.5 | 0.7 | 23.8 | 0.5 | 21.0 | 0.1 | 19.1 | 0.1 | 2.8 | 1.9 |
| 758879715545319438 | 248.9442 | -5.1978 | 23.5 | 0.8 | 23.8 | 0.4 | 23.3 | 0.3 | 20.9 | 0.1 | 19.3 | 0.1 | 2.4 | 1.6 |

Table C.1 (cont'd)

| Object ID | RA | DEC | u | u err | g | g err | r | r err | i | i err | z | z err | r-i | i-z |
|---|---|---|---|---|---|---|---|---|---|---|---|---|---|---|
| 587733441590724022 | 249.3206 | 34.4546 | 24.8 | 0.8 | 24.9 | 0.4 | 23.5 | 0.3 | 21.0 | 0.0 | 19.1 | 0.0 | 2.6 | 1.9 |
| 587729652885816245 | 249.4168 | 39.6499 | 24.7 | 1.0 | 25.1 | 0.5 | 25.2 | 0.6 | 22.1 | 0.2 | 20.8 | 0.2 | 3.2 | 1.3 |
| 587742782068950343 | 249.4335 | 52.7792 | 25.3 | 1.0 | 24.4 | 0.4 | 24.3 | 0.5 | 21.3 | 0.1 | 19.9 | 0.1 | 3.0 | 1.4 |
| 587736751935718633 | 249.4523 | 26.2625 | 24.3 | 1.2 | 24.5 | 0.5 | 25.0 | 0.6 | 22.6 | 0.2 | 20.8 | 0.2 | 2.4 | 1.8 |
| 758879663465040338 | 249.4910 | -6.4353 | 24.5 | 1.3 | 24.5 | 0.5 | 24.7 | 0.6 | 21.7 | 0.1 | 20.1 | 0.1 | 3.0 | 1.5 |
| 587736946812651159 | 249.5874 | 23.8315 | 25.3 | 0.6 | 25.7 | 0.4 | 25.1 | 0.5 | 22.9 | 0.3 | 21.0 | 0.2 | 2.2 | 1.9 |
| 587733431921345875 | 249.6904 | 30.5633 | 25.4 | 0.9 | 24.5 | 0.4 | 24.0 | 0.5 | 21.7 | 0.1 | 20.3 | 0.1 | 2.2 | 1.4 |
| 587739845397514242 | 249.7283 | 11.5006 | 25.3 | 0.8 | 24.6 | 0.5 | 25.1 | 0.5 | 22.0 | 0.1 | 20.4 | 0.2 | 3.1 | 1.6 |
| 587739707961902675 | 250.2695 | 13.8930 | 23.9 | 1.2 | 25.0 | 0.7 | 24.0 | 0.5 | 21.7 | 0.1 | 20.2 | 0.2 | 2.2 | 1.5 |
| 758879662928890205 | 250.6202 | -7.6837 | 24.6 | 1.3 | 24.5 | 0.5 | 24.9 | 0.7 | 22.4 | 0.2 | 20.8 | 0.2 | 2.5 | 1.6 |
| 587736976891774814 | 250.6440 | 18.2724 | 25.0 | 0.7 | 24.5 | 0.4 | 23.5 | 0.2 | 21.1 | 0.1 | 19.4 | 0.0 | 2.4 | 1.7 |
| 587729231979742631 | 250.7657 | 44.0368 | 25.2 | 0.7 | 25.2 | 0.5 | 24.8 | 0.6 | 22.1 | 0.1 | 20.3 | 0.1 | 2.7 | 1.8 |
| 588017978382681775 | 251.3875 | 18.0645 | 24.6 | 0.7 | 25.0 | 0.4 | 24.7 | 0.5 | 22.2 | 0.2 | 20.7 | 0.2 | 2.5 | 1.5 |
| 758879663466088597 | 251.4277 | -7.8792 | 24.8 | 1.3 | 25.1 | 0.6 | 25.6 | 0.5 | 22.3 | 0.2 | 20.4 | 0.2 | 3.2 | 1.9 |
| 588018056202028389 | 251.5395 | 27.8247 | 25.5 | 0.8 | 25.5 | 0.4 | 24.9 | 0.5 | 22.2 | 0.1 | 20.5 | 0.2 | 2.7 | 1.7 |
| 587736753546986772 | 251.6243 | 26.1073 | 24.1 | 0.9 | 24.7 | 0.5 | 24.2 | 0.5 | 21.9 | 0.1 | 20.5 | 0.1 | 2.3 | 1.4 |
| 587739706889012739 | 251.6538 | 12.3188 | 23.1 | 0.8 | 24.1 | 0.5 | 24.1 | 0.7 | 21.7 | 0.1 | 20.3 | 0.2 | 2.3 | 1.4 |
| 587736619330438661 | 251.7312 | 19.8500 | 24.9 | 0.8 | 25.1 | 0.5 | 25.0 | 0.5 | 22.3 | 0.2 | 20.6 | 0.1 | 2.7 | 1.7 |
| 587739720851982082 | 252.0974 | 12.7373 | 25.4 | 1.0 | 24.5 | 0.5 | 24.3 | 0.5 | 22.0 | 0.2 | 20.6 | 0.2 | 2.3 | 1.5 |
| 587736586054468875 | 252.2020 | 20.3096 | 25.3 | 0.7 | 24.9 | 0.6 | 23.6 | 0.4 | 21.0 | 0.1 | 19.7 | 0.1 | 2.5 | 1.4 |
| 587736980105659250 | 252.4118 | 45.8986 | 24.4 | 1.0 | 24.5 | 0.5 | 24.2 | 0.4 | 22.1 | 0.1 | 20.3 | 0.1 | 2.1 | 1.8 |
| 587725993039037495 | 252.4292 | 41.6562 | 25.7 | 0.8 | 24.6 | 0.5 | 24.2 | 0.6 | 21.1 | 0.1 | 19.7 | 0.1 | 3.1 | 1.4 |
| 587733603734193524 | 252.4306 | 32.8219 | 23.8 | 0.9 | 25.7 | 0.5 | 23.7 | 0.3 | 21.5 | 0.1 | 20.1 | 0.1 | 2.1 | 1.4 |
| 587735743695947666 | 252.6627 | 23.0738 | 25.2 | 0.8 | 25.0 | 0.4 | 25.1 | 0.5 | 22.1 | 0.1 | 20.7 | 0.2 | 2.9 | 1.4 |
| 587735665322427744 | 252.6977 | 29.8417 | 23.9 | 0.7 | 24.9 | 0.5 | 24.4 | 0.6 | 21.2 | 0.1 | 19.8 | 0.1 | 3.2 | 1.4 |
| 588007004197422275 | 252.7092 | 38.3522 | 25.1 | 0.8 | 25.5 | 0.5 | 23.7 | 0.4 | 21.3 | 0.1 | 20.0 | 0.1 | 2.4 | 1.3 |
| 587733603734521243 | 252.9105 | 32.0392 | 25.5 | 0.9 | 24.1 | 0.4 | 23.4 | 0.3 | 20.8 | 0.1 | 19.2 | 0.1 | 2.6 | 1.6 |

Table C.1 (cont'd)

| Object ID | RA | DEC | u | u err | g | g err | r | r err | i | i err | z | z err | r-i | i-z |
|---|---|---|---|---|---|---|---|---|---|---|---|---|---|---|
| 587739863639262265 | 252.9721 | 52.0506 | 25.5 | 0.8 | 24.8 | 0.5 | 23.9 | 0.4 | 21.4 | 0.1 | 20.0 | 0.1 | 2.5 | 1.4 |
| 587736976356214727 | 253.0261 | 16.0940 | 24.9 | 0.9 | 26.1 | 0.3 | 24.4 | 0.4 | 22.0 | 0.1 | 20.4 | 0.1 | 2.3 | 1.6 |
| 587725994112648394 | 253.2654 | 42.3323 | 24.9 | 1.1 | 25.6 | 0.5 | 24.6 | 0.7 | 21.8 | 0.2 | 20.4 | 0.2 | 2.8 | 1.4 |
| 587742783680611670 | 253.2765 | 51.3818 | 25.1 | 0.7 | 25.1 | 0.4 | 24.7 | 0.6 | 22.3 | 0.2 | 20.9 | 0.2 | 2.3 | 1.5 |
| 587725489986733093 | 253.2858 | 62.1073 | 25.4 | 0.8 | 24.8 | 0.7 | 23.5 | 0.4 | 20.9 | 0.1 | 19.5 | 0.1 | 2.6 | 1.4 |
| 587736919439181090 | 253.8167 | 19.2425 | 25.5 | 1.2 | 25.7 | 0.7 | 25.0 | 0.9 | 22.8 | 0.3 | 20.6 | 0.2 | 2.2 | 2.2 |
| 587736919439312192 | 253.9703 | 19.0003 | 24.1 | 1.7 | 23.8 | 0.3 | 24.9 | 0.9 | 21.9 | 0.1 | 20.4 | 0.1 | 3.1 | 1.5 |
| 588018090551084753 | 254.0996 | 21.3105 | 23.2 | 0.5 | 25.0 | 0.5 | 25.1 | 0.5 | 22.0 | 0.1 | 20.5 | 0.2 | 3.1 | 1.5 |
| 587729752746427740 | 254.2227 | 35.0509 | 25.4 | 0.6 | 24.8 | 0.5 | 24.8 | 0.5 | 22.5 | 0.2 | 20.9 | 0.2 | 2.4 | 1.6 |
| 588007005271754255 | 254.4336 | 37.5274 | 25.2 | 0.7 | 24.7 | 0.4 | 24.9 | 0.5 | 22.6 | 0.2 | 21.3 | 0.3 | 2.2 | 1.4 |
| 588018055130384012 | 254.4947 | 23.8064 | 25.4 | 0.8 | 24.6 | 0.4 | 25.0 | 0.5 | 22.4 | 0.1 | 20.8 | 0.2 | 2.7 | 1.5 |
| 587736586055714227 | 254.5579 | 18.4856 | 25.0 | 0.8 | 25.3 | 0.5 | 24.0 | 0.5 | 21.0 | 0.1 | 19.5 | 0.1 | 3.0 | 1.5 |
| 588007005271819804 | 254.5623 | 37.4297 | 24.0 | 0.7 | 24.9 | 0.5 | 24.9 | 0.5 | 22.0 | 0.1 | 20.5 | 0.2 | 3.0 | 1.4 |
| 587739848072365482 | 254.7056 | 41.8400 | 25.1 | 1.1 | 24.5 | 0.6 | 24.5 | 0.5 | 22.2 | 0.2 | 20.3 | 0.1 | 2.3 | 1.9 |
| 587742781535684101 | 254.9394 | 45.4067 | 25.3 | 0.8 | 24.9 | 0.6 | 24.2 | 0.5 | 21.9 | 0.1 | 20.2 | 0.1 | 2.3 | 1.7 |
| 587736618795468652 | 255.0328 | 16.8106 | 23.9 | 0.9 | 24.8 | 0.6 | 24.2 | 0.4 | 22.0 | 0.1 | 20.5 | 0.1 | 2.2 | 1.5 |
| 587736945742382695 | 255.3519 | 18.0737 | 24.5 | 1.0 | 24.3 | 0.4 | 24.1 | 0.5 | 21.1 | 0.1 | 19.7 | 0.1 | 3.0 | 1.4 |
| 587730842593919931 | 255.4256 | 75.2287 | 25.6 | 0.7 | 25.3 | 0.6 | 24.8 | 0.6 | 22.1 | 0.1 | 20.5 | 0.1 | 2.7 | 1.6 |
| 758882760135739040 | 255.5078 | 11.5037 | 23.1 | 0.8 | 25.5 | 0.6 | 25.3 | 0.7 | 21.9 | 0.2 | 20.6 | 0.3 | 3.4 | 1.4 |
| 587742837363049620 | 255.5588 | 44.5236 | 26.1 | 0.5 | 24.3 | 0.6 | 23.5 | 0.4 | 20.9 | 0.1 | 19.1 | 0.1 | 2.6 | 1.8 |
| 588018090015262523 | 255.7956 | 19.2954 | 24.5 | 0.9 | 25.4 | 0.5 | 25.0 | 0.6 | 22.5 | 0.2 | 21.1 | 0.3 | 2.4 | 1.4 |
| 587733604809508269 | 255.8353 | 30.3520 | 26.4 | 0.4 | 25.7 | 0.4 | 24.1 | 0.5 | 21.9 | 0.1 | 20.4 | 0.2 | 2.2 | 1.5 |
| 587736980644496959 | 255.8479 | 42.1073 | 24.6 | 1.0 | 24.9 | 0.5 | 24.1 | 0.4 | 21.9 | 0.1 | 20.5 | 0.2 | 2.2 | 1.3 |
| 588018253229852213 | 255.8540 | 22.7398 | 24.8 | 1.2 | 25.2 | 0.6 | 25.0 | 0.7 | 22.0 | 0.2 | 20.5 | 0.2 | 2.9 | 1.5 |
| 587736945742710257 | 255.9018 | 17.5926 | 24.9 | 1.0 | 24.4 | 0.4 | 24.3 | 0.5 | 22.0 | 0.1 | 20.4 | 0.1 | 2.3 | 1.6 |
| 587729751137716155 | 255.9747 | 30.7506 | 24.4 | 0.9 | 25.2 | 0.5 | 24.0 | 0.4 | 21.9 | 0.1 | 20.5 | 0.1 | 2.1 | 1.4 |
| 587739862031861165 | 256.1489 | 44.8678 | 25.3 | 0.9 | 25.3 | 0.4 | 24.5 | 0.5 | 21.9 | 0.1 | 20.6 | 0.2 | 2.6 | 1.4 |

Table C.1 (cont'd)

| Object ID | RA | DEC | u | u err | g | g err | r | r err | i | i err | z | z err | r-i | i-z |
|---|---|---|---|---|---|---|---|---|---|---|---|---|---|---|
| 587729781199799884 | 256.1800 | 33.6150 | 23.7 | 0.8 | 25.6 | 0.4 | 24.7 | 0.5 | 21.9 | 0.1 | 20.5 | 0.1 | 2.8 | 1.4 |
| 587729409155925388 | 256.5650 | 35.3264 | 23.8 | 0.7 | 24.6 | 0.5 | 24.4 | 0.6 | 22.3 | 0.2 | 20.9 | 0.2 | 2.2 | 1.4 |
| 758879771378845842 | 256.6357 | 11.7766 | 26.0 | 0.5 | 25.6 | 0.5 | 24.8 | 0.6 | 21.9 | 0.1 | 20.5 | 0.1 | 2.9 | 1.5 |
| 588018253766985235 | 256.6869 | 22.5763 | 24.9 | 1.3 | 24.0 | 0.4 | 24.4 | 0.7 | 21.4 | 0.1 | 19.6 | 0.1 | 3.0 | 1.8 |
| 587739850219849059 | 256.6912 | 42.5799 | 26.2 | 0.4 | 24.8 | 0.5 | 24.2 | 0.5 | 21.8 | 0.1 | 20.2 | 0.1 | 2.5 | 1.5 |
| 587736752476587872 | 256.7066 | 20.0545 | 25.2 | 0.9 | 25.6 | 0.5 | 24.6 | 0.6 | 22.3 | 0.2 | 21.0 | 0.2 | 2.2 | 1.4 |
| 758879771915716733 | 256.7997 | 12.0263 | 25.9 | 0.8 | 25.0 | 0.5 | 24.8 | 0.6 | 22.3 | 0.2 | 20.9 | 0.2 | 2.5 | 1.4 |
| 587725491597870175 | 256.8440 | 61.5855 | 25.4 | 0.9 | 24.6 | 0.5 | 24.0 | 0.5 | 21.8 | 0.2 | 20.5 | 0.2 | 2.2 | 1.4 |
| 587729409156253046 | 256.9946 | 34.7249 | 24.3 | 0.8 | 24.5 | 0.5 | 23.6 | 0.4 | 20.9 | 0.1 | 19.5 | 0.1 | 2.7 | 1.4 |
| 587725489989026939 | 257.1205 | 57.2346 | 25.9 | 0.5 | 24.3 | 0.6 | 25.1 | 0.7 | 22.1 | 0.2 | 20.5 | 0.2 | 3.0 | 1.6 |
| 587730842058425492 | 257.2105 | 72.1206 | 24.6 | 1.2 | 24.7 | 0.5 | 24.6 | 0.6 | 22.3 | 0.2 | 21.0 | 0.2 | 2.3 | 1.4 |
| 587733398653502709 | 257.3226 | 23.5716 | 25.9 | 1.1 | 25.6 | 0.7 | 24.3 | 0.9 | 22.0 | 0.2 | 20.2 | 0.2 | 2.3 | 1.8 |
| 587729781200717393 | 257.4297 | 31.7636 | 25.0 | 1.0 | 24.4 | 0.4 | 24.9 | 0.5 | 22.0 | 0.1 | 20.6 | 0.1 | 2.9 | 1.4 |
| 758882760673462010 | 257.4823 | 11.0434 | 25.2 | 1.2 | 25.0 | 0.8 | 24.3 | 0.7 | 22.0 | 0.2 | 20.7 | 0.2 | 2.3 | 1.4 |
| 758882759599916688 | 257.5127 | 10.2060 | 25.9 | 0.8 | 24.7 | 0.7 | 24.2 | 0.7 | 21.7 | 0.2 | 20.2 | 0.2 | 2.5 | 1.5 |
| 587739850220438969 | 257.5187 | 41.2803 | 25.9 | 0.5 | 24.8 | 0.5 | 24.4 | 0.5 | 22.3 | 0.2 | 20.6 | 0.1 | 2.1 | 1.7 |
| 758882758526371526 | 257.5470 | 9.1500 | 25.1 | 1.4 | 25.5 | 0.9 | 24.6 | 0.9 | 21.6 | 0.2 | 20.1 | 0.1 | 3.0 | 1.5 |
| 587733431926130522 | 257.6034 | 22.1850 | 23.9 | 0.5 | 25.2 | 0.5 | 23.9 | 0.4 | 21.1 | 0.1 | 19.6 | 0.1 | 2.8 | 1.5 |
| 587746214818612526 | 257.7310 | 36.2683 | 25.8 | 1.0 | 24.3 | 0.5 | 23.6 | 0.4 | 21.0 | 0.1 | 19.7 | 0.1 | 2.6 | 1.3 |
| 587736980109329796 | 257.7816 | 38.6284 | 24.6 | 0.9 | 25.2 | 0.5 | 23.7 | 0.4 | 21.5 | 0.1 | 20.2 | 0.1 | 2.2 | 1.4 |
| 587725491598591049 | 257.9375 | 59.9488 | 24.9 | 1.1 | 25.1 | 0.6 | 24.5 | 0.6 | 21.7 | 0.1 | 20.3 | 0.2 | 2.8 | 1.4 |
| 587742632274429117 | 258.1832 | 42.0965 | 26.1 | 0.6 | 24.5 | 0.5 | 24.9 | 0.7 | 22.5 | 0.2 | 21.0 | 0.2 | 2.4 | 1.5 |
| 587746214282396851 | 258.1880 | 34.6982 | 25.1 | 1.3 | 24.6 | 0.6 | 23.9 | 0.6 | 21.1 | 0.1 | 19.8 | 0.1 | 2.8 | 1.4 |
| 587729409157236396 | 258.2269 | 32.7377 | 25.8 | 0.5 | 25.2 | 0.5 | 24.7 | 0.6 | 22.5 | 0.2 | 21.0 | 0.2 | 2.3 | 1.4 |
| 758882759063504941 | 258.3772 | 9.3276 | 25.6 | 1.2 | 25.5 | 0.7 | 24.5 | 0.9 | 22.1 | 0.2 | 20.6 | 0.2 | 2.5 | 1.4 |
| 587733604811409067 | 258.5882 | 26.7106 | 25.3 | 1.1 | 23.6 | 0.3 | 23.8 | 0.4 | 21.6 | 0.1 | 20.2 | 0.1 | 2.2 | 1.4 |
| 587729652355368489 | 258.6758 | 27.2485 | 26.0 | 0.6 | 24.7 | 0.6 | 23.6 | 0.4 | 21.4 | 0.1 | 19.8 | 0.1 | 2.3 | 1.5 |

Table C.1 (cont'd)

| Object ID | RA | DEC | u | u err | g | g err | r | r err | i | i err | z | z err | r-i | i-z |
|---|---|---|---|---|---|---|---|---|---|---|---|---|---|---|
| 758882760674183086 | 258.9452 | 10.2856 | 25.1 | 1.2 | 24.6 | 0.7 | 24.5 | 0.8 | 21.9 | 0.2 | 20.3 | 0.1 | 2.5 | 1.6 |
| 587729782275049006 | 259.1334 | 31.0371 | 25.4 | 0.8 | 24.3 | 0.4 | 24.6 | 0.5 | 22.5 | 0.2 | 21.0 | 0.3 | 2.1 | 1.4 |
| 758882758527092812 | 259.1883 | 8.4838 | 26.8 | 0.3 | 25.3 | 0.9 | 24.9 | 0.8 | 22.1 | 0.2 | 20.6 | 0.2 | 2.8 | 1.5 |
| 587739849149187654 | 259.5068 | 35.7880 | 23.0 | 0.5 | 25.6 | 0.5 | 24.4 | 0.5 | 22.1 | 0.1 | 20.8 | 0.2 | 2.3 | 1.3 |
| 587742632275412364 | 259.5289 | 40.0295 | 24.9 | 1.1 | 24.4 | 0.5 | 25.6 | 0.5 | 22.5 | 0.2 | 21.1 | 0.2 | 3.1 | 1.4 |
| 587742633348367682 | 259.6630 | 42.0777 | 25.4 | 0.8 | 25.6 | 0.5 | 24.8 | 0.7 | 22.4 | 0.2 | 21.0 | 0.2 | 2.4 | 1.4 |
| 587742632275608757 | 259.7201 | 39.6730 | 23.3 | 0.6 | 24.7 | 0.5 | 23.9 | 0.5 | 21.0 | 0.1 | 19.4 | 0.1 | 2.9 | 1.5 |
| 587729751677143147 | 259.7740 | 26.0275 | 24.9 | 0.8 | 24.8 | 0.4 | 24.3 | 0.4 | 21.9 | 0.1 | 20.6 | 0.1 | 2.4 | 1.3 |
| 587739850222536105 | 259.9737 | 36.9954 | 25.4 | 0.7 | 25.8 | 0.4 | 24.4 | 0.5 | 22.2 | 0.2 | 20.7 | 0.2 | 2.2 | 1.5 |
| 587729652892829434 | 259.9849 | 26.2638 | 23.3 | 0.6 | 25.3 | 0.6 | 23.8 | 0.5 | 21.5 | 0.1 | 20.1 | 0.1 | 2.4 | 1.4 |
| 758882761211381701 | 259.9916 | 10.4703 | 22.9 | 0.7 | 25.6 | 0.7 | 24.3 | 0.7 | 21.4 | 0.1 | 20.0 | 0.1 | 2.9 | 1.4 |
| 758879770843744759 | 260.1522 | 9.6868 | 22.4 | 0.3 | 25.4 | 0.6 | 24.9 | 0.6 | 21.9 | 0.1 | 20.5 | 0.2 | 3.0 | 1.4 |
| 758879770307005127 | 260.2121 | 9.0591 | 26.0 | 0.7 | 24.5 | 0.5 | 25.0 | 0.6 | 22.2 | 0.2 | 20.2 | 0.1 | 2.9 | 2.0 |
| 587729408622397293 | 260.3897 | 28.4186 | 24.8 | 0.9 | 25.3 | 0.5 | 23.6 | 0.4 | 21.0 | 0.1 | 19.4 | 0.1 | 2.6 | 1.6 |
| 587739863108355554 | 260.6001 | 39.5375 | 25.3 | 0.8 | 25.0 | 0.5 | 23.9 | 0.4 | 21.5 | 0.1 | 20.0 | 0.1 | 2.4 | 1.5 |
| 588011502062404545 | 260.7412 | 70.5535 | 24.1 | 1.4 | 23.6 | 0.4 | 24.1 | 0.6 | 21.5 | 0.1 | 20.2 | 0.2 | 2.6 | 1.3 |
| 587729781203208138 | 260.7426 | 26.8782 | 23.4 | 0.6 | 24.9 | 0.6 | 23.8 | 0.4 | 21.3 | 0.1 | 19.8 | 0.1 | 2.5 | 1.5 |
| 758882758527879636 | 260.7825 | 7.6438 | 23.6 | 0.9 | 25.4 | 0.8 | 25.2 | 0.7 | 22.3 | 0.2 | 20.5 | 0.2 | 2.9 | 1.8 |
| 758882760675035440 | 260.7964 | 9.5815 | 25.1 | 1.1 | 25.4 | 0.6 | 25.3 | 0.7 | 22.1 | 0.2 | 20.7 | 0.2 | 3.3 | 1.4 |
| 587729408086182141 | 260.8324 | 26.8894 | 24.4 | 0.7 | 24.6 | 0.5 | 24.7 | 0.6 | 22.1 | 0.1 | 20.6 | 0.1 | 2.6 | 1.5 |
| 758879769233853381 | 261.1184 | 7.7240 | 26.1 | 0.6 | 25.5 | 0.8 | 24.1 | 0.6 | 21.9 | 0.1 | 20.4 | 0.1 | 2.2 | 1.5 |
| 587729408086378539 | 261.2006 | 26.5870 | 24.2 | 0.7 | 24.7 | 0.5 | 24.5 | 0.6 | 22.2 | 0.2 | 20.5 | 0.1 | 2.3 | 1.7 |
| 587729781740144448 | 261.2399 | 26.9407 | 23.9 | 0.8 | 24.0 | 0.4 | 24.6 | 0.6 | 22.0 | 0.1 | 20.6 | 0.2 | 2.6 | 1.3 |
| 587725491064931490 | 261.2604 | 52.8318 | 24.5 | 0.9 | 26.0 | 0.4 | 24.1 | 0.6 | 21.9 | 0.2 | 20.4 | 0.2 | 2.2 | 1.5 |
| 587729408086837186 | 261.7103 | 25.7472 | 23.7 | 0.6 | 25.1 | 0.5 | 24.5 | 0.6 | 21.7 | 0.1 | 20.3 | 0.1 | 2.8 | 1.4 |
| 587746215358432840 | 261.7363 | 30.4520 | 24.1 | 1.1 | 25.3 | 0.6 | 25.8 | 0.8 | 22.5 | 0.3 | 20.8 | 0.2 | 3.3 | 1.7 |
| 587742632277640802 | 261.9570 | 35.2503 | 25.5 | 0.8 | 24.0 | 0.3 | 25.0 | 0.6 | 22.3 | 0.2 | 20.8 | 0.2 | 2.8 | 1.5 |

Table C.1 (cont'd)

| Object ID | RA | DEC | u | u err | g | g err | r | r err | i | i err | z | z err | r-i | i-z |
|---|---|---|---|---|---|---|---|---|---|---|---|---|---|---|
| 587746214285739793 | 262.2928 | 27.8783 | 25.9 | 0.6 | 25.5 | 0.5 | 25.1 | 0.6 | 22.4 | 0.2 | 20.9 | 0.2 | 2.7 | 1.5 |
| 587739850224633642 | 262.3707 | 32.6224 | 22.8 | 0.4 | 24.5 | 0.4 | 24.2 | 0.4 | 21.3 | 0.1 | 19.8 | 0.1 | 2.9 | 1.5 |
| 587725577499116558 | 262.3744 | 59.8877 | 24.4 | 1.4 | 24.5 | 0.6 | 24.2 | 0.4 | 22.0 | 0.2 | 20.5 | 0.2 | 2.3 | 1.5 |
| 758877291036084359 | 262.9636 | 25.3941 | 25.3 | 0.7 | 25.4 | 0.7 | 23.8 | 0.4 | 21.4 | 0.1 | 19.9 | 0.1 | 2.4 | 1.5 |
| 758882760139344771 | 263.1063 | 7.9430 | 24.2 | 1.4 | 25.0 | 0.7 | 24.6 | 0.7 | 21.6 | 0.1 | 20.1 | 0.2 | 3.1 | 1.5 |
| 758882758529125574 | 263.3234 | 6.3313 | 25.4 | 1.1 | 25.6 | 0.9 | 23.6 | 0.4 | 21.2 | 0.1 | 19.7 | 0.1 | 2.4 | 1.5 |
| 587739862038087456 | 263.3453 | 31.8399 | 24.7 | 1.0 | 24.7 | 0.5 | 24.5 | 0.5 | 22.1 | 0.1 | 20.7 | 0.2 | 2.4 | 1.4 |
| 758882761213086475 | 263.5151 | 8.7344 | 25.1 | 1.4 | 25.9 | 0.6 | 24.8 | 0.7 | 22.5 | 0.3 | 20.5 | 0.2 | 2.3 | 2.1 |
| 587742633352103738 | 263.5610 | 34.1023 | 23.6 | 0.6 | 24.6 | 0.5 | 25.1 | 0.5 | 22.6 | 0.2 | 21.1 | 0.2 | 2.6 | 1.4 |
| 758877273857657029 | 263.6971 | 25.2289 | 25.3 | 0.8 | 25.1 | 0.7 | 25.5 | 0.5 | 22.5 | 0.2 | 20.9 | 0.2 | 3.0 | 1.7 |
| 587742633352300273 | 263.6975 | 33.6899 | 23.7 | 0.7 | 24.5 | 0.5 | 25.0 | 0.6 | 22.4 | 0.2 | 21.0 | 0.2 | 2.6 | 1.4 |
| 758877292110088500 | 263.8506 | 25.8400 | 24.6 | 0.9 | 25.2 | 0.5 | 23.4 | 0.3 | 21.0 | 0.1 | 19.5 | 0.1 | 2.4 | 1.5 |
| 587742632279541546 | 263.9289 | 31.3187 | 24.2 | 0.8 | 25.5 | 0.5 | 24.8 | 0.5 | 21.8 | 0.1 | 20.3 | 0.1 | 2.9 | 1.6 |
| 758877275468532229 | 264.8312 | 26.2702 | 25.5 | 0.7 | 25.1 | 0.5 | 24.5 | 0.6 | 22.3 | 0.2 | 20.9 | 0.3 | 2.2 | 1.4 |
| 758877276542208313 | 264.9979 | 27.2111 | 25.3 | 0.8 | 25.1 | 0.5 | 23.7 | 0.4 | 21.2 | 0.1 | 19.8 | 0.1 | 2.5 | 1.4 |
| 587734174952326699 | 265.1735 | 49.7183 | 24.9 | 1.2 | 25.1 | 0.6 | 24.6 | 0.3 | 22.1 | 0.1 | 20.4 | 0.1 | 2.5 | 1.7 |
| 758877291037002069 | 265.2069 | 24.7046 | 25.2 | 0.8 | 25.9 | 0.6 | 23.6 | 0.3 | 21.1 | 0.1 | 19.6 | 0.1 | 2.6 | 1.5 |
| 587734175489459584 | 266.0173 | 49.1882 | 24.5 | 0.9 | 25.0 | 0.5 | 23.8 | 0.4 | 20.8 | 0.0 | 19.2 | 0.0 | 3.0 | 1.7 |
| 587730842601129417 | 266.3485 | 59.3150 | 24.0 | 0.8 | 24.5 | 0.5 | 24.1 | 0.4 | 21.4 | 0.1 | 20.1 | 0.1 | 2.7 | 1.3 |
| 587734176026527402 | 266.9295 | 48.8554 | 25.1 | 0.9 | 25.4 | 0.5 | 25.1 | 0.6 | 22.5 | 0.2 | 21.1 | 0.3 | 2.7 | 1.4 |
| 587734174955341054 | 267.1264 | 42.9341 | 25.5 | 1.1 | 25.5 | 0.9 | 24.0 | 0.6 | 21.3 | 0.1 | 19.8 | 0.1 | 2.7 | 1.5 |
| 587730807702357170 | 267.3163 | 41.1764 | 24.4 | 1.7 | 26.0 | 0.6 | 23.8 | 0.7 | 21.6 | 0.1 | 20.1 | 0.1 | 2.2 | 1.6 |
| 758877293185140800 | 267.3254 | 25.7639 | 24.9 | 0.9 | 25.0 | 0.5 | 24.6 | 0.6 | 21.9 | 0.1 | 20.5 | 0.1 | 2.6 | 1.5 |
| 588011502068368684 | 267.4633 | 57.2745 | 23.3 | 0.6 | 25.3 | 0.6 | 24.3 | 0.6 | 22.2 | 0.2 | 20.6 | 0.2 | 2.2 | 1.5 |
| 758883006032184816 | 267.8302 | 65.6736 | 23.4 | 0.8 | 25.3 | 0.5 | 24.7 | 0.6 | 21.6 | 0.1 | 20.2 | 0.1 | 3.1 | 1.3 |
| 587734176564249664 | 267.9171 | 46.9716 | 25.2 | 0.9 | 24.1 | 0.5 | 23.6 | 0.4 | 21.1 | 0.1 | 19.7 | 0.1 | 2.6 | 1.4 |
| 587730809846891561 | 267.9193 | 48.0153 | 25.6 | 1.1 | 24.9 | 0.8 | 23.7 | 0.6 | 21.1 | 0.1 | 19.7 | 0.1 | 2.6 | 1.4 |

Table C.1 (cont'd)

| Object ID | RA | DEC | u | u err | g | g err | r | r err | i | i err | z | z err | r-i | i-z |
|---|---|---|---|---|---|---|---|---|---|---|---|---|---|---|
| 758877291575052929 | 267.9698 | 24.1137 | 25.1 | 1.1 | 25.8 | 0.5 | 25.0 | 0.6 | 22.7 | 0.2 | 20.7 | 0.2 | 2.3 | 2.0 |
| 588011502069810430 | 268.1147 | 54.0275 | 25.1 | 1.2 | 25.6 | 0.5 | 24.1 | 0.5 | 21.6 | 0.1 | 19.9 | 0.1 | 2.5 | 1.7 |
| 758874294221145127 | 268.2962 | 78.2125 | 23.4 | 0.9 | 24.7 | 0.6 | 24.1 | 0.6 | 21.8 | 0.1 | 20.3 | 0.1 | 2.3 | 1.4 |
| 588011503140930769 | 268.3149 | 59.9652 | 25.1 | 1.3 | 24.9 | 0.7 | 24.3 | 0.7 | 21.8 | 0.2 | 20.4 | 0.2 | 2.6 | 1.4 |
| 758883003347961142 | 268.4961 | 63.6166 | 24.8 | 1.0 | 24.8 | 0.6 | 24.5 | 0.5 | 22.2 | 0.2 | 20.7 | 0.2 | 2.3 | 1.5 |
| 587734176029869411 | 268.6625 | 41.3388 | 25.5 | 1.2 | 25.4 | 0.7 | 24.1 | 0.8 | 21.9 | 0.2 | 20.5 | 0.2 | 2.2 | 1.4 |
| 758877291038575154 | 268.7399 | 23.4486 | 24.4 | 1.0 | 25.5 | 0.7 | 25.5 | 0.5 | 22.1 | 0.2 | 20.5 | 0.1 | 3.4 | 1.6 |
| 587730808777082334 | 268.8786 | 39.0188 | 24.3 | 1.5 | 25.6 | 0.7 | 24.6 | 0.8 | 21.9 | 0.2 | 20.5 | 0.3 | 2.7 | 1.5 |
| 588011503142372743 | 268.9401 | 56.7506 | 25.8 | 0.8 | 24.2 | 0.4 | 23.3 | 0.3 | 21.0 | 0.1 | 19.6 | 0.1 | 2.2 | 1.5 |
| 587734176030459448 | 269.0289 | 39.8995 | 25.4 | 1.1 | 24.5 | 0.6 | 24.3 | 0.7 | 22.2 | 0.2 | 20.5 | 0.3 | 2.1 | 1.6 |
| 758879801444206165 | 269.0647 | 44.1647 | 24.6 | 1.1 | 25.0 | 0.6 | 25.2 | 0.5 | 22.5 | 0.2 | 21.0 | 0.2 | 2.7 | 1.5 |
| 758877274933562048 | 269.1480 | 24.3495 | 25.2 | 0.8 | 24.8 | 0.5 | 23.7 | 0.4 | 21.3 | 0.1 | 19.9 | 0.1 | 2.4 | 1.4 |
| 588011502071776366 | 269.3381 | 49.6072 | 23.1 | 0.7 | 24.7 | 0.7 | 24.0 | 0.6 | 21.2 | 0.1 | 19.8 | 0.1 | 2.8 | 1.4 |
| 758879800370595475 | 269.3537 | 43.1697 | 23.8 | 0.9 | 24.5 | 0.5 | 25.2 | 0.6 | 22.2 | 0.2 | 20.2 | 0.1 | 2.9 | 2.1 |
| 587734176566937094 | 269.4759 | 40.9627 | 24.8 | 1.2 | 25.2 | 0.7 | 25.5 | 0.8 | 22.7 | 0.4 | 20.6 | 0.2 | 2.8 | 2.0 |
| 588011503143290028 | 269.5050 | 54.7412 | 24.6 | 1.2 | 25.3 | 0.7 | 23.3 | 0.3 | 21.1 | 0.1 | 19.7 | 0.1 | 2.2 | 1.4 |
| 758877274933758866 | 269.6641 | 24.2277 | 24.8 | 0.9 | 25.6 | 0.5 | 24.4 | 0.4 | 21.8 | 0.1 | 20.5 | 0.1 | 2.5 | 1.4 |
| 758877292649450148 | 269.9273 | 24.4050 | 24.5 | 1.0 | 24.2 | 0.4 | 24.2 | 0.5 | 21.8 | 0.1 | 20.5 | 0.2 | 2.4 | 1.4 |
| 758877274934086491 | 270.3753 | 24.0512 | 23.9 | 0.8 | 25.0 | 0.6 | 24.7 | 0.6 | 21.5 | 0.1 | 19.7 | 0.1 | 3.3 | 1.8 |
| 588011503145452721 | 270.5323 | 49.7575 | 25.2 | 1.3 | 25.9 | 0.6 | 25.1 | 0.8 | 21.9 | 0.2 | 20.2 | 0.2 | 3.2 | 1.7 |
| 758879743999608647 | 270.5526 | 42.5107 | 24.8 | 1.1 | 25.1 | 0.5 | 24.1 | 0.4 | 21.7 | 0.1 | 20.3 | 0.1 | 2.4 | 1.4 |
| 758877274934217530 | 270.7269 | 23.9671 | 25.4 | 0.8 | 25.2 | 0.6 | 24.7 | 0.6 | 21.6 | 0.1 | 20.2 | 0.1 | 3.0 | 1.4 |
| 588011503146042364 | 270.7437 | 48.5025 | 23.8 | 1.3 | 26.2 | 0.6 | 24.1 | 0.7 | 22.0 | 0.2 | 20.3 | 0.2 | 2.2 | 1.6 |
| 758877276007959231 | 270.9368 | 24.6711 | 25.7 | 0.6 | 24.5 | 0.5 | 24.1 | 0.5 | 21.5 | 0.1 | 19.9 | 0.1 | 2.5 | 1.6 |
| 758882837984248917 | 271.6909 | 64.9125 | 25.4 | 1.0 | 25.2 | 0.7 | 23.8 | 0.5 | 21.6 | 0.1 | 20.3 | 0.1 | 2.2 | 1.3 |
| 758879799834708180 | 272.1941 | 42.3734 | 24.3 | 1.1 | 24.6 | 0.4 | 24.5 | 0.5 | 21.8 | 0.1 | 20.4 | 0.1 | 2.7 | 1.4 |
| 758882836910703914 | 272.5915 | 64.0585 | 25.6 | 0.9 | 25.5 | 0.5 | 24.2 | 0.6 | 22.0 | 0.2 | 20.4 | 0.2 | 2.3 | 1.5 |

Table C.1 (cont'd)

| Object ID | RA | DEC | u | u err | g | g err | r | r err | i | i err | z | z err | r-i | i-z |
|---|---|---|---|---|---|---|---|---|---|---|---|---|---|---|
| 758879800371906760 | 273.3558 | 42.5621 | 25.2 | 0.8 | 25.1 | 0.5 | 24.1 | 0.5 | 21.9 | 0.1 | 20.5 | 0.1 | 2.2 | 1.4 |
| 758879745611073714 | 273.6150 | 43.1534 | 23.9 | 0.7 | 25.2 | 0.4 | 23.8 | 0.3 | 21.4 | 0.1 | 19.5 | 0.1 | 2.3 | 1.9 |
| 758879800372299970 | 274.5077 | 42.2531 | 25.4 | 0.8 | 24.5 | 0.5 | 24.4 | 0.5 | 21.6 | 0.1 | 19.6 | 0.1 | 2.8 | 2.0 |
| 758879800372365338 | 274.6957 | 42.3814 | 25.6 | 0.7 | 25.1 | 0.6 | 23.9 | 0.4 | 21.3 | 0.1 | 19.8 | 0.1 | 2.6 | 1.5 |
| 758882835837617362 | 275.8669 | 63.1277 | 26.0 | 0.7 | 25.2 | 0.8 | 25.0 | 0.8 | 22.2 | 0.2 | 20.7 | 0.2 | 2.8 | 1.5 |
| 758879800372824046 | 276.0684 | 41.8951 | 23.3 | 0.6 | 24.8 | 0.5 | 24.8 | 0.6 | 22.2 | 0.2 | 20.7 | 0.2 | 2.6 | 1.5 |
| 758879801983436639 | 276.4392 | 43.1702 | 25.8 | 0.9 | 25.3 | 0.5 | 24.5 | 0.6 | 22.0 | 0.2 | 20.6 | 0.2 | 2.5 | 1.3 |
| 758883003886470770 | 276.9034 | 63.6557 | 24.5 | 1.2 | 24.5 | 0.5 | 24.2 | 0.5 | 21.7 | 0.1 | 20.3 | 0.1 | 2.5 | 1.4 |
| 758879745075448276 | 276.9994 | 41.9097 | 25.2 | 0.8 | 25.2 | 0.4 | 24.1 | 0.4 | 21.4 | 0.1 | 19.8 | 0.1 | 2.8 | 1.5 |
| 758879801983633403 | 277.1004 | 43.0152 | 23.6 | 0.9 | 25.3 | 0.5 | 23.9 | 0.5 | 20.9 | 0.1 | 19.2 | 0.0 | 3.0 | 1.7 |
| 758879745075776134 | 278.0546 | 41.7461 | 25.4 | 0.7 | 25.3 | 0.4 | 24.1 | 0.4 | 21.5 | 0.1 | 19.7 | 0.1 | 2.6 | 1.8 |
| 758879799299934602 | 278.2223 | 40.5655 | 23.8 | 0.9 | 24.4 | 0.6 | 24.4 | 0.6 | 21.7 | 0.1 | 20.3 | 0.1 | 2.7 | 1.4 |
| 758879799300000074 | 278.3825 | 40.4587 | 24.6 | 1.2 | 26.0 | 0.6 | 25.6 | 0.5 | 22.6 | 0.3 | 20.5 | 0.1 | 3.1 | 2.1 |
| 758879801447483544 | 278.9912 | 42.1108 | 24.9 | 1.1 | 25.1 | 0.6 | 24.9 | 0.6 | 22.5 | 0.2 | 20.9 | 0.2 | 2.5 | 1.5 |
| 758879801984551053 | 279.8073 | 42.3506 | 24.5 | 1.4 | 24.9 | 0.6 | 25.1 | 0.6 | 22.1 | 0.2 | 20.7 | 0.2 | 3.0 | 1.4 |
| 758882836376455142 | 285.5722 | 62.6958 | 25.0 | 1.5 | 24.8 | 0.5 | 24.3 | 0.6 | 22.1 | 0.2 | 20.5 | 0.1 | 2.2 | 1.6 |
| 758883004961916696 | 285.9520 | 63.8609 | 26.2 | 0.6 | 25.1 | 0.5 | 24.8 | 0.5 | 21.5 | 0.1 | 20.1 | 0.1 | 3.3 | 1.5 |
| 758883006035724115 | 286.5770 | 64.5230 | 25.7 | 0.9 | 25.7 | 0.4 | 25.2 | 0.6 | 22.8 | 0.3 | 21.0 | 0.2 | 2.3 | 1.9 |
| 758882837987198851 | 287.0166 | 63.8325 | 25.3 | 0.8 | 24.2 | 0.4 | 23.6 | 0.3 | 21.2 | 0.1 | 19.6 | 0.1 | 2.4 | 1.6 |
| 758874337169704032 | 288.4135 | 77.8720 | 25.7 | 1.0 | 24.7 | 0.7 | 24.0 | 0.7 | 21.8 | 0.2 | 20.4 | 0.2 | 2.1 | 1.5 |
| 758874337706574831 | 288.6738 | 78.3016 | 25.6 | 1.1 | 24.5 | 0.7 | 23.8 | 0.6 | 21.6 | 0.1 | 20.2 | 0.2 | 2.2 | 1.4 |
| 758883034478347963 | 289.1602 | 62.7378 | 24.3 | 1.3 | 25.3 | 0.6 | 24.0 | 0.5 | 20.9 | 0.1 | 19.5 | 0.1 | 3.1 | 1.3 |
| 758874294759851155 | 289.4078 | 78.5075 | 25.7 | 1.2 | 25.2 | 0.7 | 24.0 | 0.7 | 21.2 | 0.1 | 19.8 | 0.1 | 2.8 | 1.4 |
| 758883004425832388 | 289.4148 | 62.8697 | 25.4 | 0.9 | 24.5 | 0.5 | 24.5 | 0.5 | 21.4 | 0.1 | 19.9 | 0.1 | 3.1 | 1.5 |
| 758874293686305978 | 289.9318 | 77.5889 | 24.1 | 1.4 | 24.5 | 0.6 | 25.2 | 0.9 | 22.2 | 0.2 | 20.5 | 0.2 | 3.0 | 1.6 |
| 758883033404999281 | 290.2589 | 61.6931 | 23.9 | 1.0 | 24.5 | 0.7 | 25.1 | 0.6 | 22.1 | 0.2 | 20.8 | 0.2 | 3.0 | 1.3 |
| 758874293149500612 | 290.7478 | 77.2522 | 26.5 | 1.0 | 25.1 | 0.8 | 25.1 | 0.9 | 21.9 | 0.2 | 20.3 | 0.2 | 3.2 | 1.6 |

Table C.1 (cont'd)

| Object ID | RA | DEC | u | u err | g | g err | r | r err | i | i err | z | z err | r-i | i-z |
|---|---|---|---|---|---|---|---|---|---|---|---|---|---|---|
| 758874293149828414 | 293.8706 | 76.9509 | 24.8 | 1.2 | 24.9 | 0.7 | 25.4 | 0.7 | 22.5 | 0.3 | 20.6 | 0.2 | 2.9 | 1.9 |
| 758874294760899955 | 300.5010 | 77.8988 | 25.7 | 0.8 | 25.4 | 0.6 | 25.1 | 0.7 | 22.0 | 0.2 | 20.6 | 0.2 | 3.0 | 1.5 |

# Appendix D

## EXPANSION ON THE EXPECTED HVS CALCULATIONS.

Here we expand on the calculations outlined in section 3.6.4, determining the expected number of HVSs originating from an interaction with a central SMBH assuming varying initial mass functions.

We start with the Salpeter IMF, given by the equation:

$$\frac{dN}{dM} = \int_{M_1}^{M_2} M^{-2.35} \tag{4.1}$$

where $\frac{dN}{dM}$ is the number of stars in a small mass range and $M_1$ is the lower mass limit and $M_2$ is the upper mass limit. If we follow exactly the prediction from Section 3.6.4, considering the $0.6 - 1.2$ solar mass range for G/K-type stars and the $3 - 4$ solar mass range for the known B-type HVS, we find:

$$\frac{N_B}{N_{G/K}} = \frac{\int_3^4 M^{-2.35}}{\int_{0.6}^{1.2} M^{-2.35}} = \frac{3^{-1.35} - 4^{-1.35}}{0.6^{-1.35} - 1.2^{-1.35}} = \frac{0.7}{1.2} \tag{4.2}$$

Once scaled for the 14 known B-type HVS that were also detected by SDSS, we get that the expected number of G/K-type HVS is roughly 240.

However, since we were uncertain of the exact masses for the confirmed high mass HVS, we instead assumed an average mass of 3.5 $M_\odot$ to determine $\frac{dN}{dM}$, the number of stars in a 1 dex mass bin around this average, and to be more in line with the approach of Kollmeier et al. (2010). Similarly, at the low mass end of the IMF low mass stars dominate significantly, and we assume that the contribution from 1.2 $M_\odot$ stars is negligible. In this case, we find:

$$\frac{N_B}{N_{G/K}} = \frac{3.5^{-1.35}}{0.6^{-1.35}} \tag{4.3}$$

Scaling for the 14 known B-type HVSs, yields the predicted ∼150 G/K-type HVSs stated in Section 3.6.4.

We make similar assumptions for the top-heavy IMF (Figer et al., 1999):

$$\frac{dN}{dM} = \int_{M_1}^{M_2} M^{-1.6} = \frac{3.5^{-0.6}}{0.6^{-0.6}} \tag{4.4}$$

Assuming an average B-type mass of 3.5 $M_\odot$ and a dominating contribution from 0.6 $M_\odot$ stars, we get the expected 40 G/K-type HVSs.

## References


Abadi, M. G., Navarro, J. F., & Steinmetz, M. 2006, MNRAS, 365, 747

—. 2009, ApJ, 691, L63

Abadi, M. G., Navarro, J. F., Steinmetz, M., & Eke, V. R. 2003, ApJ, 597, 21

Abt, H. A. 1983, ARA&A, 21, 343

Aguerri, J. A. L., Gerhard, O. E., Arnaboldi, M., Napolitano, N. R., Castro-Rodriguez, N., & Freeman, K. C. 2005, AJ, 129, 2585

Aihara, H., et al. 2011a, ApJS, 195, 26

—. 2011b, ApJS, 193, 29

Allende Prieto, C., Beers, T. C., Wilhelm, R., Newberg, H. J., Rockosi, C. M., Yanny, B., & Lee, Y. S. 2006, ApJ, 636, 804

Allende Prieto, C., et al. 2008, AJ, 136, 2070

—. 2014, A&A, 568, A7

Alves-Brito, A., Meléndez, J., Asplund, M., Ramírez, I., & Yong, D. 2010, A&A, 513, A35+

An, D., et al. 2009, ApJ, 700, 523

—. 2013, ApJ, 763, 65

Bahcall, J. N., & Wolf, R. A. 1976, ApJ, 209, 214

Bartko, H., et al. 2010, ApJ, 708, 834

Belokurov, V., et al. 2006a, ApJ, 642, L137

—. 2006b, ApJ, 642, L137

Bensby, T., Alves-Brito, A., Oey, M. S., Yong, D., & Meléndez, J. 2011, ApJ, 735, L46

Bessell, M. S., & Brett, J. M. 1988, PASP, 100, 1134

Binney, J., & Merrifield, M. 1998, Galactic Astronomy, ed. J. Binney & M. Merrifield

Bird, J. C., Kazantzidis, S., & Weinberg, D. H. 2011, ArXiv e-prints

Bird, J. C., Kazantzidis, S., Weinberg, D. H., Guedes, J., Callegari, S., Mayer, L., & Madau, P. 2013, ApJ, 773, 43

Blaauw, A. 1961, Bull. Astron. Inst. Netherlands, 15, 265

Blanton, M. R., et al. 2003, AJ, 125, 2348

Bond, H. E. 1970, ApJS, 22, 117

Bond, N. A., et al. 2010, ApJ, 716, 1

Bournaud, F., Elmegreen, B. G., & Elmegreen, D. M. 2007, ApJ, 670, 237

Bovy, J., Rix, H.-W., & Hogg, D. W. 2012a, ApJ, 751, 131

Bovy, J., Rix, H.-W., Liu, C., Hogg, D. W., Beers, T. C., & Lee, Y. S. 2012b, ApJ, 753, 148

Brown, W. R., Geller, M. J., & Kenyon, S. J. 2009, ApJ, 690, 1639

—. 2012, ApJ, 751, 55

Brown, W. R., Geller, M. J., Kenyon, S. J., & Kurtz, M. J. 2005, ApJ, 622, L33

Burgasser, A. J., Cruz, K. L., Cushing, M., Gelino, C. R., Looper, D. L., Faherty, J. K., Kirkpatrick, J. D., & Reid, I. N. 2010, ApJ, 710, 1142

Byrd, G., & Valtonen, M. 1990, The Astrophysical Journal, 350, 89

Caldwell, N., Morrison, H., Kenyon, S. J., Schiavon, R., Harding, P., & Rose, J. A. 2010, AJ, 139, 372

Carollo, D., et al. 2007, Nature, 450, 1020

—. 2010, ApJ, 712, 692

Chandar, R., Fall, S. M., & Whitmore, B. C. 2010, ApJ, 711, 1263

Cheng, J. Y., et al. 2012, ApJ, 752, 51

Chernoff, D. F., & Weinberg, M. D. 1990, ApJ, 351, 121

Chou, M., et al. 2007, ApJ, 670, 346

Cohen, J. G. 1978, ApJ, 221, 788

Conroy, C., Wechsler, R. H., & Kravtsov, A. V. 2007, ApJ, 668, 826

Covey, K. R., et al. 2007, AJ, 134, 2398 de Vaucouleurs, G. 1964, in IAU Symposium, Vol. 20, The Galaxy and the Magellanic Clouds, ed. F. J. Kerr, 195–+

Do, T., Ghez, A. M., Morris, M. R., Lu, J. R., Matthews, K., Yelda, S., & Larkin, J. 2009, ApJ, 703, 1323

Dong, R., Gunn, J., Knapp, G., Rockosi, C., & Blanton, M. 2011, AJ, 142, 116

Durrell, P. R., Ciardullo, R., Feldmeier, J. J., Jacoby, G. H., & Sigurdsson, S. 2002, ApJ, 570, 119

Edelmann, H., Napiwotzki, R., Heber, U., Christlieb, N., & Reimers, D. 2005, ApJ, 634, L181

Eggen, O. J., Lynden-Bell, D., & Sandage, A. R. 1962, ApJ, 136, 748

Eisenstein, D. J., et al. 2011, AJ, 142, 72

Fan, X., et al. 2001, AJ, 121, 31

Feldmeier, J. J., Ciardullo, R., Jacoby, G. H., & Durrell, P. R. 2004a, ApJ, 615, 196

Feldmeier, J. J., Mihos, J. C., Morrison, H. L., Harding, P., & Kaib, N. 2004b

Feldmeier, J. J., Mihos, J. C., Morrison, H. L., Rodney, S. A., & Harding, P. 2002, ApJ, 575, 779

Figer, D. F., Morris, M., Geballe, T. R., Rich, R. M., Serabyn, E., McLean, I. S., Puetter, R. C., & Yahil, A. 1999, ApJ, 525, 759

Fouquet, S., Hammer, F., Yang, Y., Puech, M., & Flores, H. 2012, MNRAS, 427, 1769

Freeman, K., & Bland-Hawthorn, J. 2002, ARA&A, 40, 487

Freeman, K. C. 1987, ARA&A, 25, 603

Fukugita, M., Ichikawa, T., Gunn, J. E., Doi, M., Shimasaku, K., & Schneider, D. P. 1996a, AJ, 111, 1748

—. 1996b, AJ, 111, 1748

Ghez, A. M., et al. 2008, ApJ, 689, 1044

Gilmore, G. 1984, MNRAS, 207, 223

Gilmore, G., & Reid, N. 1983, MNRAS, 202, 1025

Gnedin, O. Y., & Ostriker, J. P. 1997, ApJ, 474, 223

Gould, A. 2003, AJ, 126, 472

Gould, A., & Kollmeier, J. A. 2004, ApJS, 152, 103

Gould, A., & Quillen, A. C. 2003, ApJ, 592, 935

Gould, A., & Salim, S. 2003, ApJ, 582, 1001

Gunn, J. E., et al. 1998, AJ, 116, 3040

—. 2006, AJ, 131, 2332

Gvaramadze, V. V., Gualandris, A., & Portegies Zwart, S. 2009, MNRAS, 396, 570

Harding, P., Morrison, H. L., Olszewski, E. W., Arabadjis, J., Mateo, M., Dohm-Palmer, R. C., Freeman, K. C., & Norris, J. E. 2001, AJ, 122, 1397

Harris, W. E. 1997, VizieR Online Data Catalog, 7202, 0

Hawley, S. L., et al. 2002, AJ, 123, 3409

Hernquist, L. 1990, ApJ, 356, 359

Hills, J. G. 1988, Nature, 331, 687

Hirsch, H. A., Heber, U., O'Toole, S. J., & Bresolin, F. 2005, A&A, 444, L61

Hogg, D. W., Finkbeiner, D. P., Schlegel, D. J., & Gunn, J. E. 2001, AJ, 122, 2129

Holley-Bockelmann, K., Sigurdsson, S., Mihos, J. C., Feldmeier, J. J., Ciardullo, R., & McBride, C. 2005, ArXiv Astrophysics e-prints

Ibata, R., Lewis, G. F., Irwin, M., Totten, E., & Quinn, T. 2001, ApJ, 551, 294

Ibata, R., Martin, N. F., Irwin, M., Chapman, S., Ferguson, A. M. N., Lewis, G. F., & McConnachie, A. W. 2007, ApJ, 671, 1591

Ivezić, Ž., et al. 2004, Astronomische Nachrichten, 325, 583

—. 2007, AJ, 134, 973

—. 2008, ApJ, 684, 287

Jacoby, G. H., & Ciardullo, R. 1999a, ApJ, 515, 169

—. 1999b, ApJ, 515, 169

Kauffmann, G., White, S. D. M., & Guiderdoni, B. 1993, MNRAS, 264, 201

Kilic, M., et al. 2006, AJ, 131, 582

King, III, C., Brown, W. R., Geller, M. J., & Kenyon, S. J. 2012, ApJ, 750, 81

Kirby, E. N., Simon, J. D., Geha, M., Guhathakurta, P., & Frebel, A. 2008, ApJ, 685, L43

Kirkpatrick, D. in prep.

Kollmeier, J. A., Gould, A., Knapp, G., & Beers, T. C. 2009, ApJ, 697, 1543

Kollmeier, J. A., et al. 2010, ApJ, 723, 812

Krick, J. E., & Bernstein, R. A. 2007, AJ, 134, 466

Laidler, V. et al, Synphot User's Guide, Version 5.0 (Baltimore STScI). 2005

Lang, M., Holley-Bockelmann, K., Bogdanovic, T., Amaro-Seoane, P., & Sesana, A. 2011, ArXiv e-prints

Larson, R. B. 1969, MNRAS, 145, 405

—. 1976, MNRAS, 176, 31

Law, D. R., & Majewski, S. R. 2010, ApJ, 718, 1128

Lawrence, A., et al. 2007, MNRAS, 379, 1599

Lee, M. G., Park, H. S., & Hwang, H. S. 2010, Science, 328, 334

Lee, Y. S., et al. 2008a, AJ, 136, 2022

—. 2008b, AJ, 136, 2050

—. 2011, AJ, 141, 90

Leonard, P. J. T., & Dewey, R. J. 1993, in Astronomical Society of the Pacific Conference Series, Vol. 45, Luminous High-Latitude Stars, ed. D. D. Sasselov, 239

Łokas, E. L., & Mamon, G. A. 2001, MNRAS, 321, 155

López-Corredoira, M., Cabrera-Lavers, A., Mahoney, T. J., Hammersley, P. L., Garzón, F., & González-Fernández, C. 2007, AJ, 133, 154

Magorrian, J., & Tremaine, S. 1999, MNRAS, 309, 447

Majewski, S. R. 1993, ARA&A, 31, 575

Majewski, S. R., Skrutskie, M. F., Weinberg, M. D., & Ostheimer, J. C. 2003, ApJ, 599, 1082

Manukian, H., Guillochon, J., Ramirez-Ruiz, E., & O'Leary, R. M. 2013, ApJ, 771, L28

Mateo, M., Olszewski, E. W., & Walker, M. G. 2008, ApJ, 675, 201

McConnachie, A. W., et al. 2009, Nature, 461, 66

McLaughlin, D. E., & Fall, S. M. 2008, ApJ, 679, 1272

Merritt, D. 1984, ApJ, 276, 26

Mihalas, D., & Binney, J. 1981, Galactic astronomy: Structure and kinematics /2nd edition/, ed. Mihalas, D. & Binney, J.

Mihos, C. 2003, ArXiv Astrophysics e-prints

Mihos, J. C. 2004, 217, 390

Mihos, J. C., Harding, P., Feldmeier, J., & Morrison, H. 2005, ApJ, 631, L41

Miyamoto, M., & Nagai, R. 1975, PASJ, 27, 533

Moore, B., Katz, N., Lake, G., Dressler, A., & Oemler, A. 1996, Nature, 379, 613

Morris, M., & Serabyn, E. 1996, ARA&A, 34, 645

Morrison, H. L. 1993, AJ, 106, 578

Morrison, H. L., Mateo, M., Olszewski, E. W., Harding, P., Dohm-Palmer, R. C., Freeman, K. C., Norris, J. E., & Morita, M. 2000, AJ, 119, 2254

Munn, J. A., et al. 2004, AJ, 127, 3034

—. 2008, AJ, 136, 895

Murante, G., Giovalli, M., Gerhard, O., Arnaboldi, M., Borgani, S., & Dolag, K. 2007, MNRAS, 377, 2

Murante, G., et al. 2004, ApJ, 607, L83

Napiwotzki, R., & Silva, M. D. V. 2012, Mem. Soc. Astron. Italiana, 83, 272

Napolitano, N. R., et al. 2003, ApJ, 594, 172

Navarro, J. F., Frenk, C. S., & White, S. D. M. 1997, ApJ, 490, 493

Oke, J. B., et al. 1995, PASP, 107, 375

Oort, J. H. 1958, Ricerche Astronomiche, Vol. 5, Specola Vaticana, Proceedings of a Conference at Vatican Observatory, Castel Gandolfo, May 20-28, 1957, Amsterdam:

North-Holland, and New York: Interscience, 1958, edited by D.J.K. O'Connell., p.415, 5, 415

Palladino, L. E., Schlesinger, K. J., Holley-Bockelmann, K., Allende Prieto, C., Beers, T. C., Lee, Y. S., & Schneider, D. P. 2014, ApJ, 780, 7

Palladino, L. E., et al. 2012, AJ, 143, 128

Peng, E. W., et al. 2011, ApJ, 730, 23

Pickles, A. J. 1998, PASP, 110, 863

Pier, J. R., Munn, J. A., Hindsley, R. B., Hennessy, G. S., Kent, S. M., Lupton, R. H., & Ivezić, Ž. 2003, AJ, 125, 1559

Piffl, T., Williams, M., & Steinmetz, M. 2011, A&A, 535, A70

Poveda, A., Ruiz, J., & Allen, C. 1967, Boletin de los Observatorios Tonantzintla y Tacubaya, 4, 86

Przybilla, N., Nieva, M. F., Heber, U., & Butler, K. 2008, ApJ, 684, L103

Quinlan, G. D. 1996, New Astronomy, 1, 35

Reid, I. N., & Hawley, S. L. 2005, New light on dark stars : red dwarfs, low-mass stars, brown dwarfs, ed. I. N. Reid & S. L. Hawley

Reid, M. J., & Brunthaler, A. 2004, ApJ, 616, 872

Richards, G. T., et al. 2002, AJ, 123, 2945

Rockosi, C., Beers, T. C., Majewski, S., Schiavon, R., & Eisenstein, D. 2009, in ArXiv Astrophysics e-prints, Vol. 2010, astro2010: The Astronomy and Astrophysics Decadal Survey, 14–+

Rougoor, G. W., & Oort, J. H. 1960, Proceedings of the National Academy of Science, 46, 1

Rudick, C. S., Mihos, J. C., Frey, L. H., & McBride, C. K. 2009, ApJ, 699, 1518

Sadler, E. M., Rich, R. M., & Terndrup, D. M. 1996, AJ, 112, 171

Sales, L. V., Navarro, J. F., Abadi, M. G., & Steinmetz, M. 2007, MNRAS, 379, 1475

Sato, K., Tokoi, K., Matsushita, K., Ishisaki, Y., Yamasaki, N. Y., Ishida, M., & Ohashi, T. 2007, ApJ, 667, L41

Schlegel, D. J., Finkbeiner, D. P., & Davis, M. 1998, ApJ, 500, 525

Schlesinger, K. J., et al. 2012, ApJ, 761, 160

Schmidt, S. J., West, A. A., Hawley, S. L., & Pineda, J. S. 2010, AJ, 139, 1808

Schödel, R., et al. 2007, A&A, 469, 125

Schönrich, R. 2012, MNRAS, 427, 274

Schönrich, R., & Binney, J. 2009, MNRAS, 399, 1145

Schönrich, R., Binney, J., & Dehnen, W. 2010, MNRAS, 403, 1829

SDSS-III. 2008, Massive Spectroscopic Surveys of the Distant Universe, the Milky Way Galaxy, and Extra-Solar Planetary Systems, abstracted from an NSF proposal

SDSS-III Collaboration et al. 2012, ArXiv e-prints

Searle, L., & Zinn, R. 1978, ApJ, 225, 357

Sesana, A., Haardt, F., & Madau, P. 2006, ApJ, 651, 392

Sherwin, B. D., Loeb, A., & O'Leary, R. M. 2008, MNRAS, 386, 1179

Simon, J. D., & Geha, M. 2007, ApJ, 670, 313

Skiff, B. A. 2010, VizieR Online Data Catalog, 1, 2023

Smee, S. A., et al. 2013, AJ, 146, 32

Smith, M. C., et al. 2007, MNRAS, 379, 755

Smolinski, J. P., et al. 2011, AJ, 141, 89

Sohn, S. T., Anderson, J., & van der Marel, R. P. 2012, ApJ, 753, 7

Tauris, T. M. 2015, MNRAS, 448, L6

Tinsley, B. M., & Larson, R. B. 1979, MNRAS, 186, 503

`http://www.sdss.org`. ????

Villalobos, Á., & Helmi, A. 2008, MNRAS, 391, 1806

von Weizsäcker, C. F. 1951, ApJ, 114, 165

Williams, B. F., et al. 2007, ApJ, 656, 756

Worthey, G., & Lee, H. 2006, ArXiv Astrophysics e-prints

Yanny, B., et al. 2000, ApJ, 540, 825

—. 2009, AJ, 137, 4377

York, D. G., et al. 2000a, AJ, 120, 1579

—. 2000b, AJ, 120, 1579

Yoshii, Y., & Saio, H. 1979, PASJ, 31, 339

Yu, Q., & Tremaine, S. 2003, ApJ, 599, 1129

Zhang, F., Lu, Y., & Yu, Q. 2013, ApJ, 768, 153

Zucker, D. B., et al. 2007, ApJ, 659, L21